PB81-120792

Application of Fourier Transform Spectroscopy to Air Pollution Problems

Ohio State Univ. Research Foundation
Columbus

Prepared for

Environmental Sciences Research Lab.
Research Triangle Park, NC

Nov 80

U.S. Department of Commerce
National Technical Information Service
NTIS

TECHNICAL REPORT DATA
(Please read Instructions on the reverse before completing)

1. REPORT NO. EPA-600/3-80-093	2.	3. RECIPIENT'S ACCESSION NO. PB81 120792
4. TITLE AND SUBTITLE APPLICATION OF FOURIER TRANSFORM SPECTROSCOPY TO AIR POLLUTION PROBLEMS Final Report		5. REPORT DATE November 1980 Issuing Date. 6. PERFORMING ORGANIZATION CODE
7. AUTHOR(S) John H. Shaw and Jack G. Calvert		8. PERFORMING ORGANIZATION REPORT NO.
9. PERFORMING ORGANIZATION NAME AND ADDRESS The Ohio State University Research Foundation 1314 Kinnear Road Columbus, Ohio 43212		10. PROGRAM ELEMENT NO. 1AA603A AF-07 (FY-79) 11. CONTRACT/GRANT NO. R 803868
12. SPONSORING AGENCY NAME AND ADDRESS Environmental Sciences Research Laboratory-RTP,NC Office of Research and Development U.S. Environmental Protection Agency Research Triangle Park, N.C. 27711		13. TYPE OF REPORT AND PERIOD COVERED Final 7/75-7/79 14. SPONSORING AGENCY CODE EPA/600/09
15. SUPPLEMENTARY NOTES Interim Report: EPA-600/3-78-057, June 1978		

16. ABSTRACT

The nature of information that can be retrieved from spectra obtained with Fourier transform spectroscopy is discussed. Nonlinear, least-squares analysis of spectra is capable of retrieving information that is beyond the reach of conventional methods and has improved precision and accuracy. These studies have allowed the approval of experimental design to the analysis of spectra to be placed on a quantitative basis.

Fourier transform infrared spectroscopy was used to study quantitatively the kinetics and mechanisms of several chemical reactions that are of interest to atmospheric chemists and are important in the development of air pollution control strategies. The systems studied include the metastable, reactive, gaseous, species, peroxynitric acid, hypochlorous acid, and dimethylnitrosamine. Rate constants related to the formation and decay of these species and infrared extinction data necessary for the quantitative analyses of these compounds were determined.

17. KEY WORDS AND DOCUMENT ANALYSIS

a. DESCRIPTORS	b. IDENTIFIERS/OPEN ENDED TERMS	c. COSATI Field/Group
Air pollution Infrared spectroscopy Optical equipment Solar spectrum Reaction kinetics Photochemical reactions	Fourier transform spectroscopy	13B 14B 20F 03B 07D 07E

18. DISTRIBUTION STATEMENT RELEASE TO PUBLIC	19. SECURITY CLASS *(This Report)* UNCLASSIFIED	21. NO. OF PAGES
	20. SECURITY CLASS *(This page)* UNCLASSIFIED	22. PRICE

EPA Form 2220-1 (9-73)

PB81-120792

EPA-600/3-80-093
November 1980

APPLICATION OF FOURIER TRANSFORM SPECTROSCOPY TO AIR POLLUTION PROBLEMS

by

John H. Shaw and Jack G. Calvert
The Ohio State University Research Foundation
1314 Kinnear Road
Columbus, Ohio 43212

Grant No. R803868

Project Officer

John W. Spence
Atmospheric Chemistry & Physics Division
Environmental Sciences Research Laboratory
Research Triangle Park, N.C. 27711

ENVIRONMENTAL SCIENCES RESEARCH LABORATORY
OFFICE OF RESEARCH AND DEVELOPMENT
U.S. ENVIRONMENTAL PROTECTION AGENCY
RESEARCH TRIANGLE PARK, NORTH CAROLINA 27711

REPRODUCED BY
NATIONAL TECHNICAL
INFORMATION SERVICE
U.S. DEPARTMENT OF COMMERCE
SPRINGFIELD, VA 22161

DISCLAIMER

This report has been reviewed by the Environmental Sciences Research Laboratory, U.S. Environmental Protection Agency, and approved for publication. Approval does not signify that the contents necessarily reflect the views and policies of the U.S. Environmental Protection Agency, nor does mention of trade names or commercial products constitute endorsement or recommendation for use.

ABSTRACT

In the first phase of this work the results of investigations of the nature of the information which can be retrieved from spectra obtained with Fourier Transform Spectroscopy are presented. It is shown that nonlinear, least-squares analysis of the spectra is capable of retrieving types of information beyond the reach of conventional methods and with improved precision and accuracy. These studies have allowed the approval of experimental design to the analysis of spectra to be placed on a quantitative basis.

In the second phase of this work, Fourier Transform Infrared Spectroscopy has been employed to study quantitatively the kinetics and mechanisms of several chemical reactions which are of interest to atmospheric chemists and are important in the development of air pollution control strategy. The systems studied include the metastable, reactive, gaseous, species, peroxynitric acid, hypochlorous acid, and dimethylnitrosamine. Rate constants related to the formation and decay of these species and infrared extinction data necessary for the quantitative analyses of these compounds were determined.

This report was submitted in fulfillment of Grant No. R 803868 by the Ohio State University Research Foundation under the sponsorship of the U.S. Environmental Protection Agency. This report covers the period July 15, 1975 to July 14, 1979, and work was completed as of July 31, 1979.

CONTENTS

Abstract iii

Figures vii

Tables x

Acknowledgement xi

1. Introduction 1
2. Conclusions 3
3. Recommendations 5
4. First and Second Year Effort 7
   - Introduction 7
   - First Year Effort 7
   - Second Year Effort 8
5. Third and Fourth Year Effort 10
   - Introduction 10
   - Design of FTS Experiments 12
   - The Least Squares Variance-Covariance Matrix and Information Components 14
   - The Absorbing Properties of Gases 16
     - Accurate Determination of Absorber Amounts by Using Experimental Spectra for Reference 20
   - Analysis of Spectrum of Inhomogeneous Paths 24
   - Investigations of the Absorption Properties of Gases 28
6. A Kinetic Study of the Mechanism of Peroxynitric Acid Formation 36
   - Introduction 36
   - Experimental Methods 38
     - Equipment 38
     - Procedures Employed 39
   - Discussion 45
     - The Mechanism of Product Formation 45
     - Alternative Mechanisms for HO_2NO_2 48
     - The Decay Mechanism for HO_2NO_2 50
     - A Kinetic Test of HO_2NO_2 Decay Mechanisms and the Equilibrium Constant for the System, $HO_2NO_2 \rightleftarrows HO_2 + NO_2$ 61
     - The Computer Simulation of the Product Rates and a Quantitative Test of the Complete Reaction Mechanism 64
     - New Rate Constant Estimates for Some Reactions of Interest in the Troposphere 70

Preceding page blank

7. A Fourier Transform Infrared Kinetic Study of HOCl and its Absolute Integrated Infrared Band Intensities 73
  Introduction 73
  Experimental Section 74
  Results and Discussion 77
    The Generation of HOCl 77
    The Apparent First-Order Rate Constant for Cl_2 Photolysis in the Photochemical Reactor 80
    A Test of the Kinetics of Formation of HOCl and Other Products of the Irradiated Cl_2, H_2, O_3, O_2 Mixtures 86
    New Kinetic Information Related to the Cl_2, O_3, H_2, O_2 System 97
8. Rate Studies of the Reactions of the $(CH_3)_2N$ Radical with O_2, NO, and NO_2 103
  Introduction 103
  Experimental 104
  Results and Discussion 105
    Determination of Rate Constant Ratios 105
    Significance of These Results to Atmospheric Chemistry 110

References 112

Appendix A 120

Appendix B 122

Appendix C 126

TYPING GUIDE SHEET
BEGIN FIRST LINE OF TEXT HERE
CENTER OF PAGE
TOP OF IMAGE AREA
DROPPED HEAD BEGIN SECTIONS HERE

FIGURES

Number		Page
1	Ratio of the experimental spectrum with the best-fit spectrum; spectrum of a 171-m path of ground-level air	18
2	A comparison of the relative dependence of the information concerning absorber amount on the transmittance of the spectrum	21
3	Spectrum of N_2O	26
4	Solar spectrum observed in October 1975	27
5	Noise-free spectra and absorption coefficients of Voigt-shaped lines	30
6	Spectra of a Voigt line	31
7	CO spectra	33
8	The polynomial dependence of the CO line widths on m; average half-widths obtained from Benedict, Herman, and Silverman[33] and half-widths in AFGL atmospheric line listing	34
9	First-order decay plots used in the evaluation of the rate constants for Cl_2 and ClNO photolysis in the reaction chamber	41
10	Time dependence of the major products of the photolysis of Cl_2, H_2, NO_2, and NO in synthetic air	46
11	Plot of $\ln[HO_2NO_2]$ versus time for two typical HO_2NO_2 experiments during the dark decay period	51
12	First-order plots of the dark decay of HO_2NO_2 in near identical experiments	54
13	An Arrhenius plot of the first-order decay constants from the dark decay of HO_2NO_2 in gaseous mixtures with 100 ppm of NO_2	57
14	Plot of the $\ln(k_8/k_7)$ versus $1/T$	62

8-1/2"
9-1/8"
BEGIN LAST LINE OF TEXT
BOTTOM OF IMAGE AREA OUTSIDE DIMENSION FOR TABLES AND ILLUSTRATIONS
3/8"

PAGE NUMBER
EPA-287 (Cin.)
(4-76)

BEGIN FIRST LINE OF TEXT HERE
TYPING GUIDE SHEET
CENTER OF PAGE
TOP OF IMAGE AREA
DROPPED HEAD. BEGIN SECTIONS HERE

Number — Page

15 Time dependence of the major products from the photolysis of 13 nearly identical mixtures 65-69

16 Diagram of the Fourier transform infrared spectrometer and photochemical reactor 75

17 Relative intensity of the light inside the photochemical reactor versus wavelength 76

18 The time dependence of the HCl absorbance during the calibration 78

19 HCl calibration curve for absorbance at 2727 cm^{-1} versus [HCl] 79

20 Absorbance versus wavelength plot for a gaseous mixture 81

21 Absorbance growth and decay within the HOCl ν_2 infrared band 82

22 Plot of R^{o}_{HCl} and $2R^{o}_{H_2O_2}$ versus $[Cl_2]^{o}$ 85

23 Plot of $-R_{O_3}-k_{13}[O_3]$ versus $[Cl_2]$ 87

24 Absorbance of HOCl and H_2O_2 products within the 1100 to 1350 cm^{-1} region 88

25 The concentrations of products versus time in the photolysis of Cl_2, H_2, O_3, O_2, N_2 mixture 90

26 Rates of HCl formation in the photolysis of Cl_2, H_2, O_3, O_2, N_2 mixtures at varied $[H_2]/[O_3]$ ratios 92

27 Rates of H_2O_2 formation in the photolysis of Cl_2, H_2, O_3, O_2, N_2 mixtures at varied $[H_2]/[O_3]$ ratios 93

28 Rates of O_3 loss in the photolysis of Cl_2, H_2, O_3, O_2, N_2 mixtures at varied $[H_2]/[O_3]$ ratios 94

29 Rate of change of the absorbance of HOCl with time versus $[H_2]/[O_3]$ ratios from the photolysis of Cl_2, H_2, O_3, O_2, N_2 mixtures 95

30 The absolute extinction coefficients of HOCl gas as a function of wavelength in the infrared regions of the three fundamental vibrational transitions 98

31 Rates of HOCl formation in the photolysis of Cl_2, H_2, O_3, O_2, N_2 mixtures at varied $[H_2]/[O_3]$ ratios 99

BEGIN LAST LINE OF TEXT
BOTTOM OF IMAGE AREA OUTSIDE DIMENSION FOR TABLES AND ILLUSTRATIONS
3/8"

PAGE NUMBER
EPA-287 (Cin.)
(4-76)

TYPING GUIDE SHEET
BEGIN FIRST LINE OF TEXT HERE
CENTER OF PAGE
TOP OF IMAGE AREA
DROPPED HEAD: BEGIN SECTIONS HERE

Figure **Page**

32 Rates of HOCl formation in the photolysis of Cl_2, H_2, O_3, O_2, N_2 mixtures at varied $[H_2]/[O_3]$ ratios 100

33 Rates of HOCl formation in the photolysis of Cl_2, H_2, O_3, O_2, N_2 mixtures at varied $[H_2]/[O_3]$ ratios 102

34 Concentration-time profile of the products of dimethylnitrosamine photolysis in 730 torr of O_2 106

35 Plot of function A of the text and A' versus $[O_2]/[NO]$ ratio 107

36 Plot of the function B of the text and B' versus $[O_2]/[NO_2]$ ratio 109

6-1/2"
9-1/8"
BEGIN LAST LINE OF TEXT
BOTTOM OF IMAGE AREA; OUTSIDE DIMENSION FOR TABLES AND ILLUSTRATIONS
3/8"

PAGE NUMBER
EPA-287 (Cin.)
(4-76)

TYPING GUIDE SHEET
BEGIN FIRST LINE OF TEXT HERE
CENTER OF PAGE
TOP OF IMAGE AREA
DROPPED HEAD, BEGIN SECTIONS HERE

TABLES

Number		Page
1	Measurements required to detect a rate of change of 10^{-3} per year	11
2	Abundance of N_2O, CO, and H_2O in a ground-level air sample at 296 K	17
3	Abundance of N_2O, CO, and H_2O in a ground-level air sample at 290 K	17
4	Values of the physical parameters of a gas sample	19
5	Physical conditions of N_2O sample and observing conditions	22
6	Precision and accuracy with which the unknown amount of N_2O was retrieved	23
7	Precision and accuracy with which an unknown amount of N_2O was retrieved	23
8	Precision and accuracy with which the temperature, pressure, and absorber amount of a sample were retrieved	25
9	The reaction mechanism and rate constants for the photolysis of dilute Cl_2, H_2, NO_x mixtures in air	42-44
10	Rate data from the dark decay of HO_2NO_2	63
11	Summary of the reaction mechanism and rate constants applicable to the photolysis of dilute Cl_2, O_3, H_2 mixtures in synthetic air	83
12	Experimental rate data from the photolysis of Cl_2, O_3, H_2, O_2 mixtures	91

BEGIN LAST LINE OF TEXT
BOTTOM OF IMAGE AREA OUTSIDE DIMENSION FOR TABLES AND ILLUSTRATIONS
3/8"
PAGE NUMBER

EPA-287 (Cin.)
(4-76)

ACKNOWLEDGEMENT

The authors wish to acknowledge the assistance of the U.S. E.P.A. in enabling this work to be performed. In particular we have appreciated the advice and assistance of Mr. John Spence and Dr. Philip Hanst in this undertaking. It is through their efforts that the Fourier Transform Spectrometer and reaction chamber extensively used in this investigation were made available for our use.

SECTION 1

INTRODUCTION

Infrared spectroscopy is routinely used in many laboratories to aid in the identification of the composition of samples and to estimate, quantitatively, the amounts of the individual components of the sample. During the past 30 years there have been continual improvements in the design of infrared spectrometers and these have led to increased versatility in manipulating the spectra produced. Fourier Transform Spectrometers (FTS) are a new class of spectrometer and their use has been widespread in the past decade. They allow extended spectral regions to be observed in short periods of time and the collected data can be stored on magnetic tape for future use, as well as being displayed on paper or on oscilloscopes. The digital nature of the data allows mathematical operations such as addition, multiplication, or integration to be carried out on the spectra. These allow the data to be processed quickly and more accurately than the spectra obtained from earlier types of instruments where the only record consisted of the analog spectrum on a paper chart.

Despite these increases in the speed with which the data can be manipulated the typical methods used to analyze the spectra are essentially those used before the advent of sophisticated digital data displays.

During the period covered by this grant we have explored other methods of analyzing spectra. These involve the use of statistical techniques, which, while well known in some other experimental areas, have not found extensive use in spectroscopy. In particular the use of nonlinear, least-squares, regression analysis to retrieve the values of parameters of the system investigated has allowed the precision of the measurements to be increased substantially compared with previous methods. In addition, less observer interaction in the analysis is required, thus removing the possibility of observer bias. Additional types of information have been extracted from spectra beyond those customarily measured.

In these types of analysis empirical models or models based on theoretical considerations are used to describe the spectra. The values of the adjustable parameters in these models, their asymptotic standard deviations, and their asymptotic correlation matrices are estimated by curve fitting the experimental spectral data.

BEGIN FIRST LINE OF TEXT HERE
TYPING GUIDE SHEET
CENTER OF PAGE
TOP OF IMAGE AREA
DROPPED HEAD; BEGIN SECTIONS HERE

Estimates of the "nuisance" parameters, such as the position of the background in the absence of the absorber and the spectral resolution, can be obtained in addition to other information. Some examples of the type of information retrieved include:

(1) The retrieval of the individual absorbing gas amounts in a mixed sample together with its temperature and pressure. This requires a knowledge of the individual line parameters or a suitable collection of reference spectra of the absorbing gases.

(2) The determination of the mixing ratios of absorbing atmospheric gases by analyzing solar spectra collected at ground level.

(3) The retrieval of the individual line positions, intensities, and widths from spectra of groups of Voigt- or Lorentz-shaped lines.

(4) The simultaneous analysis of entire rotation-vibration bands to retrieve the upper and lower state molecular constants, the band intensity parameters, and the line-broadening parameters.

The accuracy of the results depends on the correctness of the models used. The precision of the parameter estimates depends on the quality of the spectrum analyzed. In addition to analyzing spectra the techniques can be used to predict the precision of the parameter estimates for a given experimental design. Thus quantitative criteria for choosing between different designs can be established.

These methods can be applied to other types of experimental data. However, if the data sets are large and many parameters are to be retrieved large amounts of computer time are required.

BEGIN LAST LINE OF TEXT
BOTTOM OF IMAGE AREA; OUTSIDE DIMENSION FOR TABLES AND ILLUSTRATIONS
3/8"
PAGE NUMBER
EPA-287 (Cin.)
(4-76)

SECTION 2

CONCLUSIONS

A method of analyzing infrared spectra has been developed and applied successfully to the analysis of several types of spectra and to the retrieval of different types of information from the spectra. The results obtained by analyzing a single spectrum are often superior to those previously obtained by analyzing a large number of spectra.

It has been demonstrated that the fine details of high-resolution spectra of gases are sensitive to the physical conditions of the sample, such as the temperature, pressure, and absorber amounts, and also to the spectral resolution of the instrument used to collect the spectra. Because of this sensitivity, information about these parameters can be extracted from the spectra by appropriate computer-aided analysis. These techniques remove many of the sources of error normally encountered when observer judgement is required in the data analysis.

These methods allow the determination of absorber amounts with high precision and accuracy. Since they are capable of removing the influence of slow drifts in instrument performance over long periods of time they are ideally suited to monitoring slow changes in the abundances of atmospheric gases (such as CO_2, N_2O, or O_3) which may be climatologically important.

These types of analysis can be adapted to the problem of evaluating the best design for a particular experiment. The effects of the trade-offs between different approaches to the problem can be estimated in a quantitative manner.

It has been shown that if the physical properties of a sample are to be determined by analysis of its spectrum, the accuracy of the absorbing characteristics of the absorbers is of crucial importance. This method of analysis allows these desired characteristics to be obtained rapidly to the accuracy desired.

These analytical methods can be used to analyze many other types of experimental data.

The present study has shown the great utility of Fourier Transform Infrared Spectroscopy in the quantitative study of the rates and mechanisms of chemical reactions important in the atmosphere and the design of air pollution control strategy. Three detailed kinetic studies were completed in this work. First a kinetic study has been made of the time dependence of the photolysis of dilute mixtures of Cl_2, H_2, NO_2, and NO in synthetic air.

The major products of the reaction, $ClNO_2$, HCl, $HONO_2$, HO_2NO_2, O_3, N_2O_5, H_2O_2 with smaller amounts of HONO, ClNO, and ClONO were identified and followed in situ using long-path, infrared Fourier transform spectrocsopy. The possible mechanisms for HO_2NO_2 formation and decay in this system were considered. It is concluded that HO_2NO_2 levels are controlled largely by the reactions: $HO_2 + NO_2\ (+M) \rightarrow HO_2NO_2\ (+M)$; $HO_2NO_2\ (+M)$; $2HO_2 \rightarrow H_2O_2 + O_2$; HO_2NO_2 (+ Wall) + products. From a kinetic treatment of the HO_2NO_2 data for the dark decay, estimates of the equilibrium constant for the system, $HO_2NO_2 \rightleftharpoons HO_2 + NO_2$, were derived in experiments at several temperatures (28.4 - 20.3°C). A kinetic scheme consisting of 65 elementary reactions is proposed to rationalize the rates of the many different products of the irradiated Cl_2, NO_2, NO, H_2, air mixtures. Computer simulations incorporating the present kinetic information on HO_2NO_2 show that HO_2NO_2 may rise to the ppb level in the sunlight-irradiated, NO_x-RH-polluted troposphere (25°C).

In a second study the long-path, Fourier transform infrared spectroscopy has been employed in the kinetic study of the products of the photolysis of dilute Cl_2, O_3, H_2 mixtures in excess O_2 and N_2 in experiments at 25 ± 3°C and 700 Torr total pressure. The initial rates of formation of the products of the reaction, HCl, HOCl, and H_2O_2, and O_3 loss were studied as a function of the ratio of reactants, $[H_2]/[O_3]$, over the range 0.10×10^3 to 6.8×10^3. The match of these experimental data with computer-generated rate data employing a rather complete reaction set was used to test the mechanism and refine some of the rate constant estimates. From these data, the absolute extinction coefficients for the three fundamental bands of HOCl were derived. The integrated band intensities for the ν_1, ν_2, ν_3 absorption regions were estimated to be 2.3×10^2, 3.0×10^2, and 4.3×10^1 $cm^{-2}atm^{-1}$, respectively.

In a third study the kinetics of the reactions of the $(CH_3)_2N$ radical with NO, NO_2, and O_2 were studied using FTIR spectroscopy. The nature of the products and the ratio of rate constants for these reactions were determined. The results were used to evaluate the potential for nitrosamine and nitramine formation in NO-NO_2-hydrocarbon-amine-polluted atmospheres.

SECTION 3

RECOMMENDATIONS

In the first part of this work we have developed a new approach to the retrieval of information from infrared spectra of gases and it has been applied to the analysis of many types of spectra. It has been demonstrated that more information, with higher precision can be retrieved than has previously been recognized. The applications of nonlinear, least squares techniques investigated under this grant have been exploratory in nature, and it has not been possible to explore all the possible uses which have occurred to us. Provided suitable computer programs are available large bodies of data can be analyzed rapidly and accurately and this method should prove useful to many other workers provided descriptions of the programs and their use are made available.

It is recommended that

(1) The application of these methods to the analysis of other types of experimental data be explored
(2) Descriptions of the analytical method and how it can be adapted to the facilities available in other laboratories be prepared so that it can be widely tested in other environments
(3) Extensive tests of the usefulness of the technique for routine analysis of a variety of spectral or other experimental data be undertaken
(4) The specific types of experiment for which this type of analysis is useful should be determined. It has been shown, for example, that absorber amounts can be estimated from relatively noisy FTS data with precisions of 1% with no observer bias. Few experimental techniques allow such precision on a routine basis. Thus these techniques are valuable for measuring the slow changes in the abundances of atmospheric gases with time. The wide spectral coverage obtained with FTS instruments allows the simultaneous determination of severe atmospheric constituents by analysis of a single spectrum
(5) Further investigations of the best methods of improving the knowledge of the absorbing properties of gases should be undertaken and that these methods be used to obtain improved absorption data for use in the investigations described above.

In the second part of this work we have demonstrated the quantitative nature of the results which may be obtained using long-path, Fourier transform spectroscopy in the study of complex chemical reactions of importance in atmospheric transformations. It is clear that important kinetic and mechanistic information can be obtained for many of the metastable compounds such as peroxynitric acid (HO_2NO_2), hypochlorous acid ($HOCl$), dimethylnitrosamine $[(CH_3)_2N\text{-}N = O]$, etc., which are expected to be generated in the polluted atmosphere. It is recommended that the Environmental Protection Agency utilize the Fourier transform infrared spectroscopic methods for the unambiguous detection and analysis of metastable complex species which are deemed to be of significance in the control of air pollution.

SECTION 4

FIRST AND SECOND YEAR EFFORT

INTRODUCTION

An account of the work accomplished under Grant No. R 803868, sponsored by the U.S. Environmental Protection Agency, entitled "Application of Fourier Transform Spectroscopy to Air Pollution Problems," is given in this report. The period covered by this grant extended from July 1975 to September 1979. Much of the work has been described in interim reports to EPA (see Appendix A), in papers published or accepted for publication (Appendix B), and in papers presented at meetings (Appendix C).

Since extensive accounts of the accomplishments of the first two years have been presented[1,2] only brief accounts of this work are given here. These are followed by a more complete review of the work performed during the past two years. This is broken down into two sections. The first describes progress in developing accurate methods of analyzing spectra to determine specifically the composition of the ambient air quantitatively and accurately. The second section describes progress in understanding the photochemistry of the atmosphere.

FIRST YEAR EFFORT (JULY 1975 - JULY 1976)

During this year a Digilab Fourier Transform Spectrometer (FTS) was used to obtain spectra of ground-level ambient air samples for path lengths ranging from 10 m to 1 km with high spectral resolution (0.1 cm^{-1}) between 500 and 3500 cm^{-1}. Solar spectra in the same spectral region were also obtained. These spectra were searched for the presence of absorption features of a number of gases. In addition to the well-known lines of gases such as H_2O, CO, CO_2, N_2O, CH_4, and O_3, absorption due to CCl_2F_2 near 1160 cm^{-1} was observed in solar spectra. A mean tropospheric abundance of about 0.34 ppb was estimated.[3] To aid in this search a computer program[4] was written to allow synthetic spectra to be calculated by using the compilation of the line parameters of atmospheric gases prepared by the Air Force Geophysical Laboratories.[5] This program was used to calculate spectra to match the absorption observed in experimental spectra of ground level air samples of path lengths of approximately 10, 100, and 1000 m, and solar spectra corresponding to both high and low sun elevations.[6,7] These synthetic spectra showed generally good agreement with the observed spectra although some deficiencies in the AFGL line compilation were observed.[8] An atlas of computer-generated infrared transmission spectra of the atmosphere for low and high humidity for a path length of 3 km at 296 K and 1013 mb between 700 and 3000 cm^{-1} was also prepared.[9]

In addition to these studies, the construction of a cell designed to simulate the environment of the stratosphere was initiated. This cell is designed to be cooled to -60°C and to be irradiated with ultraviolet radiation between 150 and 450 nm, and to allow path lengths of up to 100 m to be obtained. A photochemical cell capable of approximating the solar irradiance at ground level between 300 and 400 nm and of absorbing path lengths in excess of 200 m was completed. This cell has since been used continuously. One of the first studies carried out was of the photolysis of HNO_2. A value of 0.07 min^{-1} was obtained for the rate constant $HONO \rightleftharpoons HO + NO$. Additional studies of the photodecomposition of CH_2O - air mixtures, $(CH\ )_2N_2$ - NO - NO_2 - air mixtures, and HONO - H_2O_2 - NO - air mixtures were also carried out to test the feasibility of several experiments planned for future investigation.

Spectra of more than 20 gases of importance to air pollution problems, obtained under controlled concentration and pressure conditions, covering the region from 700 to 1500 cm^{-1} were also included in the first year's interim report.[1]

SECOND YEAR EFFORT (JULY 1976 - JULY 1977)

During the second year kinetic studies of several systems of interest to atmospheric chemists were completed with the photochemical system. New data were obtained concerning the rate constant for the reaction $HO + CO \rightarrow H + CO_2$ as a function of pressure. It was found[10] that this rate constant is sensitive to pressure with a value of 439 ± 24 ppm^{-1} min^{-1} at 700 Torr (air) and 203 ± 29 ppm^{-1} min^{-1} at 100 Torr (air). It was pointed out[2] that these findings made it necessary to reevaluate the influence of the HO-radical on other reactants in the lower atmosphere if previous estimates, based on the low pressure value of this constant had been used.

The experimental system was also employed to determine preliminary values for the rate constants for the reactions $HO_2 + NO_2 \rightarrow HO_2NO_2$ and $HO_2 + NO_2 \rightarrow HONO + O_2$. In 700 Torr (air) at 25 ± 2°C the experimental data indicated rate constants of 72 and 52 ppm^{-1} min^{-1}, respectively.[11] Simulations of the reactions in a typical NO_x - RH - RCHO polluted atmosphere exposed to sunlight showed that the theoretical rate of HO_2NO_2 generation is similar in magnitude to those expected (and observed in real atmospheres) for peroxyacylnitrates.

At the same time additional spectra of ground-level air samples and solar spectra were obtained and explorations of the best methods of analyzing these spectra to retrieve accurate estimates of the abundances of atmospheric gases were continued.

These methods included spectral ratioing of the air spectra to remove the features of each individual absorbing gas one at a time and by using observer judgement to estimate when the best removal had been obtained. It was found that this method allowed the abundances of gases in ground-level air samples to be estimated with precisions of a few percent. However, the method could not be used to analyze solar spectra because the atmospheric absorbing path is inhomogeneous.

The next method attempted was to remove the absorption features of the individual gases from the air spectrum by ratioing the air spectrum with spectrum calculated from the AFGL line listing. Some success was achieved in analyzing a CO spectrum,[12] although the precision with which the amount of CO in the sample could be estimated was again of the order of a few percent. This technique was used to retrieve the amounts of CO, N_2O, and CO_2 in a 171 m path of ground-level air. These amounts were obtained with estimated precisions of a few percent.[2,13] Portions of a solar spectrum analyzed in this way allowed the CCl_2F_2 feature near 1160 cm^{-1} to be revealed clearly.[2]

An attempt was made to increase the precision of the abundance estimates by converting the observer signals to absorbances and comparing these latter with the corresponding absorbances of the individual gases as calculated from the line parameters. This method of analyzing a ground-level air spectrum enabled the abundances of N_2O and CO to be estimated with precision of the order of 1%.[13] It was found, however, that the abundance estimates depended on the estimated position of the background signal in the absence of the absorber and on the spectral region analyzed. The position of the background was based on the judgement of the observer. Other differences could be due to the use of incorrect line parameter values to calculate the synthetic spectra.

The ground-level air spectrum was reanalyzed by using a nonlinear, least-squares regression method. In this method the position of the background and the spectral resolution are estimated, in addition to the abundances of the absorbing gases in the sample. It was shown[2,13] that the abundances estimated in this manner showed a precision somewhat better than that obtained by linear regression analysis of the absorbances and that there was less dependence of the absorber amounts on the spectral region analyzed. This improvement was due primarily to the removal of the observer from the process of determining the background and the spectral resolution of the observed spectrum.

The problems associated with the accurate estimation of the abundances of absorbing atmospheric gases from spectra of air samples has been explored in greater depth during the final two years of this grant and progress is described in following sections.

The estimation of the abundance of atmospheric gases by spectral analysis requires suitable reference spectrum of each absorbing gas or information about their absorbing characteristics, such as a knowledge of the position, intensity, and width of the lines. We have made extensive use of the AFGL listing of atmospheric line parameters[5] and have noted deficiencies[8] in this listing. Thus, during this second year, a series of spectrum of N_2O, HCl, CO, CH_4, and CO_2 were obtained at a nominal resolution of 0.1 cm^{-1}. The samples contained known amounts of the absorber at carefully controlled pressures and temperatures. A comparison of spectra calculated from the AFGL listing with some of these experimental spectrum was presented in the interim report for the second year of this grant.[2] Visual inspection indicated that the overall agreement is excellent but at this time we did not have a method of comparison which was quantitative in nature.

TYPING GUIDE SHEET

SECTION 5

THIRD AND FOURTH YEAR EFFORT

INTRODUCTION

The composition of the atmosphere and the changes in this composition have become topics of national and international interest. In addition to causing local concentrations of pollutants in densely populated areas it has now been realized that human activities can affect the atmosphere as a whole. Thus there has been concern about the possible effects of chlorofluorocarbon compounds and of the emissions from high-flying aircraft on stratospheric ozone. There has also recently been renewed interest in the effects of long-term changes in the abundances of gases such as CO_2 or N_2O on the atmosphere. In order to understand the changes which may occur it is necessary to know the amounts of these gases currently in the atmosphere, to measure their rates of change, and to understand the influence of these gases on the atmosphere.

We may choose N_2O as an example of such a gas; N_2O has been known as an atmospheric constituent for more than 40 years.[14,15,16] The general appearance of the bands of this gas in solar spectra obtained over this period suggest that the rate of change in the abundance, if any, has not been large, although quantitative measurements are lacking. In recent years many observations of the abundance of this gas have been reported and there is general agreement that the typical ground-level mixing ratio is about 300 ppb.

It is useful to consider the requirements of experiments designed to measure the long-term change in this abundance. It will be assumed that the amount of N_2O (u) in the atmosphere is increasing at the rate of 0.1% per year. Thus, if two measurements are made a year apart (years y and y + 1) it is expected that

$$u_{y+1}/u_y \simeq 1.001. \tag{1}$$

It is clear that y the rate of change is to be estimated with any certainty from two such measurements a year apart, they must have an accuracy of one part in 10,000 or better, or

$$\sigma/u \leq 10^{-4}, \tag{2}$$

where σ is the standard deviation associated with the measurement. The standard deviation σ_n of the mean of n measurements is related to the standard deviation of a single measurement by

$$\sigma_n = \sigma/\sqrt{n}, \tag{3}$$

EPA-287 (Cin.)
(4-76)

and, hence, from Eq. (2) and (3),

$$n \geq 10^8 (\sigma/u)^2 . \qquad (4)$$

Thus if we define the percentage accuracy associated with a single measurement as $p = 100\ (\sigma/u)$ then we obtain the values for the number of measurements required (see Table 1). Practical considerations then show that the accuracy of the measurements should be as high as possible.

The above discussion describes a model for a particular experiment. The objective of the experiment is to determine the abundance of N_2O in the atmosphere to an accuracy of one part in 10,000 or better in order to allow the annual rate of change to be estimated to an accuracy of about 10%. It has been shown that the objective can be achieved by making a small number of very precise (and accurate) measurements or a larger number of less precise (but still containing no systematic errors) measurements.

TABLE 1. NUMBER OF MEASUREMENTS REQUIRED TO DETECT A RATE OF CHANGE OF 10^{-3} PER YEAR IN THE AMOUNT OF A GAS FOR EXPERIMENTS OF VARYING ACCURACY

Percent Accuracy	n
10	10^6
1	10^4
0.1	10^2
0.01	10^0

Based on these criteria it is possible to evaluate different experimental approaches to the problem. This evaluation will include:

(1) The initial cost of the equipment and the operating expenses.

(2) The accuracy with which the N_2O abundance can be estimated. This will be dependent on the signal-to-noise ratio of the experimental data but not necessarily directly related to it. The accuracy will also depend on the possible sources of systemic error and the long-term stability of the apparatus.

Similar analysis can be carried out for other atmospheric gases and for other criteria for the accuracies with which the abundances can be estimated.

During the past two years we have been concerned with identifying the factors which influence the accuracy with which the abundances of gases can be estimated by spectral analysis and in determining the sources of systemic errors.

DESIGN OF FTS EXPERIMENTS

Many experiments are carried out with little a priori knowledge of the outcome. For example, a photochemical experiment may be undertaken to measure the rates of the reactions which occur when a mixture of gases is irradiated. This may be accomplished by observing the changes in the infrared spectrum of the system as a function of time with an FTS instrument. It can be expected that bands of some of the initial constituents will decrease in intensity as the reactions proceed and that bands of products will be observed.

The first phase of the experiment may consist of identifying the new products in order to understand the nature of the reactions. This allows models describing the reactions to be obtained. The next step is the verification of the model and the determination of the appropriate rate constants. At this point an intuitive approach to the best design is used. Estimates of the probable rate constants are made and the conditions of the initial sample are empirically chosen to allow the changes in the spectra and hence the concentrations of the sample constituents to be optimally determined. The experiment may be repeated for different initial conditions to verify the mechanisms involved and to ensure that at least one set of initial conditions is sufficiently near the optimum to allow accurate results to be obtained.

In such experiments there are many parameters which may be varied, including

(1) the initial amounts of the reactants,
(2) the pressure and temperature of the sample,
(3) the intensity and duration of the irradiation,
(4) the length of the infrared absorbing path,
(5) the extent of the spectral region surveyed and the spectral resolution of the observations, and
(6) the duration of the experiment and the frequency of the observations.

Although several weeks may be spent on the investigation of a particular set of reactions, an individual experiment may be completed in a few hours and the information obtained from it can be used to guide succeeding experiments. In such cases there is no need for a more formal representation of the experiment and the outcome of the experiment is strongly dependent on the skill of the experimenter.

In other types of experiments a considerably larger investment in time and effort may be required to obtain a desired result. One example has already been given; i.e., the estimation of the rate of change in the abundance of atmospheric N_2O. There is, in this case, available information on the typical amount of this gas in the atmosphere and at least crude estimates of the probable rate of change expected. Our prior knowledge allows us to recognize that useful results can only be obtained by measurements carried out over a period of years. Also to detect the small changes expected to occur, it is known that the measurements must be precise and not subject to systematic drifts over the years. In evaluating competing methods of observation the total cost and the accuracy of the expected results will be considered. A method of observation which does not allow the overall accuracy to be extimated in some detail should be rejected.

The discussion which follows is restricted to a specific experimental design; i.e., the use of FTS with a long-path absorption cell to obtain spectra of ground-level air samples from which the abundance of N_2O and other gases can be inferred. If one of the design criteria is that the abundance of N_2O obtained from a single spectrum is to have an accuracy of 1% or better, then a number of factors have to be considered. These may include

(1) the absorbing path length,
(2) the pressure and temperature of the sample,
(3) the spectral resolution and spectral region analyzed,
(4) the signal-to-noise ratio of the spectrum,
(5) the accuracy with which the absorption characteristics of N_2O are known together with their dependence on the pressure and temperature of the sample, and
(6) the effects of variations of other atmospheric constituents on the accuracy of the results.

These factors influence the final accuracy in different ways. It is obvious that an error of 1% in the path length will result in a 1% error in the N_2O abundance measurment. On the other hand, the effects of sample temperature variations or changes in the spectral resolution of the instrument are more subtle. To our knowledge there have been no systematic treatments of the design of spectroscopic experiments to include many of the factors described above. Until such a method exists only semiquantitative answers to the problem can be obtained.

Niple[17,18,19] has recently addressed a related problem in the design of spectroscopic measurements. This was concerned with the retrieval of information about the position, intensity, and width of a Lorentz-shaped line from a spectrum, having a resolution comparable to the line width, of a sample of known pressure and absorber amount. The results are equally applicable to the determination of the amount of absorber and the pressure of the sample if the line intensity and width are known.

Considered an experiment which measures the intensity of radiation transmitted by an absorbing gas sample at a uniform temperature and total pressure P_T sufficiently high that the line shape is Lorentzian. The signals y_i are recorded at N equally spaced frequencies ν_i from some lower frequency ν_L to an upper frequency,

$$\nu_U = \nu_L + (N-1)\Delta\nu , \qquad (5)$$

where $\Delta\nu$ is the constant frequency spacing. If the noise in the signal has a normal distribution with rms value σ, and is independent of frequency, the form of $\{y\}$ in the vicinity of an isolated absorption line is described by

$$y_i = \epsilon_i + B(\nu_i) \int_0^\infty R(\nu',\nu_i;H) \exp\left[-Su\alpha_0 P_T/\pi\{(\nu'-\nu_0)^2 + \alpha_0^2\ P_T^2\ \}\right] d\nu'$$
$$i = 1, \ldots, N. \qquad (6)$$

In this equation $B(\nu_i)$ represents the background signal with the absorber removed and is assumed to be of the form

$$B(\nu_i) = a + b(\nu_i - \langle \nu \rangle) \qquad (7)$$

with $b \simeq 0$ and $\langle \nu \rangle$ the mean frequency. This gives a background nearly independent of frequency. $R(\nu',\nu_i;H)$ is the instrumental spectral response function and is assumed to be of the form

$$\begin{aligned} R(\nu',\nu_i;H) &= (1-|\nu'-\nu_i|/H)/H, & |\nu' - \nu_i| &\leq H, \\ &= 0 & |\nu' - \nu_i| &> H. \end{aligned} \qquad (8)$$

This form is triangular with full width H at half height; ϵ_i represents the random noise.

These equations which are the model for the spectrum, assume that the combined effects of foreign- and self-broadening can be represented by the single term, $\alpha_0 P_T$. The line parameters S and α_0 are the line intensity and the pressure-broadening coefficients, respectively; ν_0 is the line center frequency; and u, the absorber amount, is the product of radiation path length and absorber partial pressure.

There are 12 parameters involved in the model; i.e., the three line parameters - ν_0, S, α_0, and nine physical parameters - ν_L, ν_U, N, a, b, H, σ^2, u, and P_T. There are two types of experiments which require the collection and analysis of spectra described by this model. In one, the line parameters α_0 and S are known and the physical parameters u and P_T are retrieved from the spectrum as well as a, b, ν_0, H, and σ^2. In the other, P_T and u are known and the line parameters are retrieved instead. In both cases ν_L, ν_U, and N are also known and the goal is to retrieve the remaining seven unknowns. One way to effect this retrieval is by nonlinear Least-Squares Regression Analysis, which is summarized in the next section.

THE LEAST SPUARES VARIANCE-COVARIANCE MATRIX AND INFORMATION COMPONENTS

When a set of observations $\{y_i\}$ is described by the model

$$y_i = \epsilon_i + f(\zeta_1^{(i)}, \ldots, \zeta_k^{(i)}; \theta_1, \ldots, \theta_p) \qquad i = 1, \ldots, N, \qquad (9)$$

where f is some function of k known variables $\zeta_1, \ldots, \zeta_k$ and p unknown parameters $\theta_1, \ldots, \theta_p$, and ϵ_i is a normally distributed random variable with variance σ^2 and mean zero, the asymptotic variance-covariance matrix of the Least-Squares estimates $\hat{\theta}_1, \ldots, \hat{\theta}_p$ for the parameters is given by

$$\hat{\underline{S}} = \hat{\sigma}^2 (\underline{J}'\ \underline{J})^{-1}. \qquad (10)$$

In this, σ^2 is the estimated noise variance and $\underline{J}$ is the Jacobian matrix of f with

$$J_{ij} = \frac{\partial f}{\partial \theta_j}\left(\zeta_1^{(i)},\ldots.,\zeta_k^{(i)};\ \theta_1,\ldots.,\ \theta_p\right)\Bigg|_{\hat{\theta}_1,\ldots\hat{\theta}_p} . \qquad (11)$$

The diagonal element $\hat{S}_{jj}$ of $\hat{\underline{S}}$ is the asymptotic variance $\hat{\sigma}_j^2$ of $\hat{\theta}_j$ and $\hat{S}_{ij}/\hat{\sigma}_j\hat{\sigma}_1$ is the asymptotic correlation coefficient between $\hat{\theta}_j$ and $\hat{\theta}_i$. The asymptotic percent uncertainty $\%\hat{\theta}_j$ is therefore given by

$$\%\hat{\theta}_j \equiv 100(\hat{\sigma}_j/\hat{\theta}_j). \qquad (12)$$

The values of $\hat{\theta}_1,\ldots,\hat{\theta}_p$ are those which minimize the sum of square deviations

$$Q(\theta) = \sum_{i=1}^{N}\left[y_i - f(\zeta_1^{(i)},\ldots,\zeta_k^{(i)};\ \theta_1,\ldots,\theta_p)\right]^2$$

Niple has recommended that the quantity

$$I_j \equiv (\hat{\theta}_j/\hat{\sigma}_j)^2 \qquad (13)$$

be used as a measure of the component or "piece" of information in a set of data about the jth unknown parameter. It is seen the I_j is large when the percent uncertainty, $\%\hat{\theta}_j$, is small and vice versa. This corresponds to the intuitive sense that if a set of data leads to a parameter estimate with a large uncertainty for the jth parameter, as reflected in a large $\%\hat{\theta}_j$, then that data set does not contain very much information about θ_j.

By exploring the dependence of these information components on the experimental conditions, the optimum designs for retrieving each parameter were established. The trade-off between signal-to noise ratio and spectral resolution was investigated for several resolution-dependent noise levels. It was shown that, for each type of dependence, there existed an optimum resolution and line center transmittance for obtaining each parameter.[19] These concepts are being extended to the analysis of the nature of the information concerning atmospheric parameters in solar spectra.

These methods can be used to obtain the best design for other spectroscopic investigations and they can be used to provide quantitative answers to many of the design problems described previously. It is necessary to know the operating characteristics of the apparatus (in this instance the primary requirement is the dependence of the signal-to-noise ratio of the measurements on the spectral resolution), the dependence of the absorption characteristics of the gas on the temperature and pressure of the sample, and the spectral resolution of the instrument.

We assume that the operating characteristics of the apparatus can be established and that the apparatus is stable and capable of giving reproducible data.

The formulation of a model which accurately describes the dependence of the absorption characteristics of a gas on the pressure and temperature of the sample is considerably more difficult. Some of our investigations into the problem are described below. We note that, in many studies, these dependencies are ignored, and systemic errors may be introduced into the final results.

At this point we leave the discussion concerning the design of FTS experiments and in particular the experiment to determine the abundance of N_2O. We note that in considering this experiment it has been possible to formulate the objectives of the experiment, to establish design criteria, to enumerate the factors which influence the design, and to describe a method capable of determining the optimum design. We have noted that one of the principal components required to evaluate the design is the knowledge of the absorbing characteristics of the gas.

THE ABSORBING PROPERTIES OF GASES

It was noted above that it is necessary to know the dependence of the absorbing properties of a gas on the pressure and temperature of the sample if accurate absorber amounts are to be determined. This is well illustrated by the data in Tables 2 and 3 taken from Chang et al.[13] In this paper attempts were made to determine the abundances of N_2O, CO, and H_2O by analyzing the portion of spectrum shown in Figure 1. These estimates were obtained by comparing the observed spectrum with a synthetic spectrum calculated from the AFGL line parameter listing.[5] Table 2 shows the results obtained by assuming a temperature of 296K and Table 3 the results for the correct temperature of 290K. It is seen that a change in temperature of 2% produces a similar change in the estimated absorber amounts, although the change depends on the particular absorber.

As a result of this experience it was recognized that the observed spectrum contained information about the temperature and pressure of the absorbing sample. In a subsequent paper, Chang et al.[20] demonstrated that this previously analyzed air spectrum could be reanalyzed to give, not only the abundances of N_2O, CO, and H_2O, and the spectral resolution and the position of the background in the absence of the absorber, but also the pressure and temperature of the sample. Some of these results are shown in Table 4. The precisions of a few percent in the pressure and temperature estimates indicates that there is a considerable amount of information[19] about these parameters in the spectrum and that the observed spectrum is surprisingly sensitive to small changes in the sample conditions.

These results demonstrate that if abundance estimates are to be made to accuracies of 1% or better, the dependence of the absorption characteristics of the gas on temperature, pressure, and spectral resolution must be accurately determined.

TABLE 2. THE ABUNDANCE OF N_2O, CO, and H_2O IN A GROUND-LEVEL AIR SAMPLE OBTAINED BY NON-LINEAR, LEAST-SQUARES ANALYSIS AND AN ASSUMED SAMPLE TEMPERATURE OF 296K.

Spectral region (cm^{-1})	2190 - 2200	2195 - 2205	2200 - 2210	2190 - 2210
Gas	Abundance (ppm)			
N_2O	0.301 ± 0.003	0.30 ± 0.003	0.318 ± 0.003	0.314 ± 0.002
CO	0.799 ± 0.011	0.810 ± 0.019	0.805 ± 0.029	0.796 ± 0.012
H_2O	---	---	0.273 ± 0.016*	0.261 ± 0.013*

* These values are to be multiplied by 10^3, they were obtained after this line position was shifted to 2205.223 cm^{-1}.

TABLE 3. THE ABUNDANCE OF N_2O, CO, and H_2O IN A GROUND-LEVEL AIR SAMPLE OBTAINED BY NON-LINEAR LEAST-SQUARES ANALYSIS FOR AN ASSUMED SAMPLE TEMPERATURE OF 290K.

Spectral region (cm^{-1})	2190 - 2200	2195 - 2205	2200 - 2210	2190 - 2210
Gas	Abundance (ppm)			
N_2O	0.307 ± 0.003	0.308 ± 0.003	0.313 ± 0.002	0.312 ± 0.002
CO	0.801 ± 0.010	0.816 ± 0.015	0.826 ± 0.021	0.802 ± 0.011
H_2O	---	---	0.309 ± 0.016*	0.300 ± 0.015*

* These values are to be multiplied by 10^3, they were obtained after the line position was shifted to 2205.223 cm^{-1}.

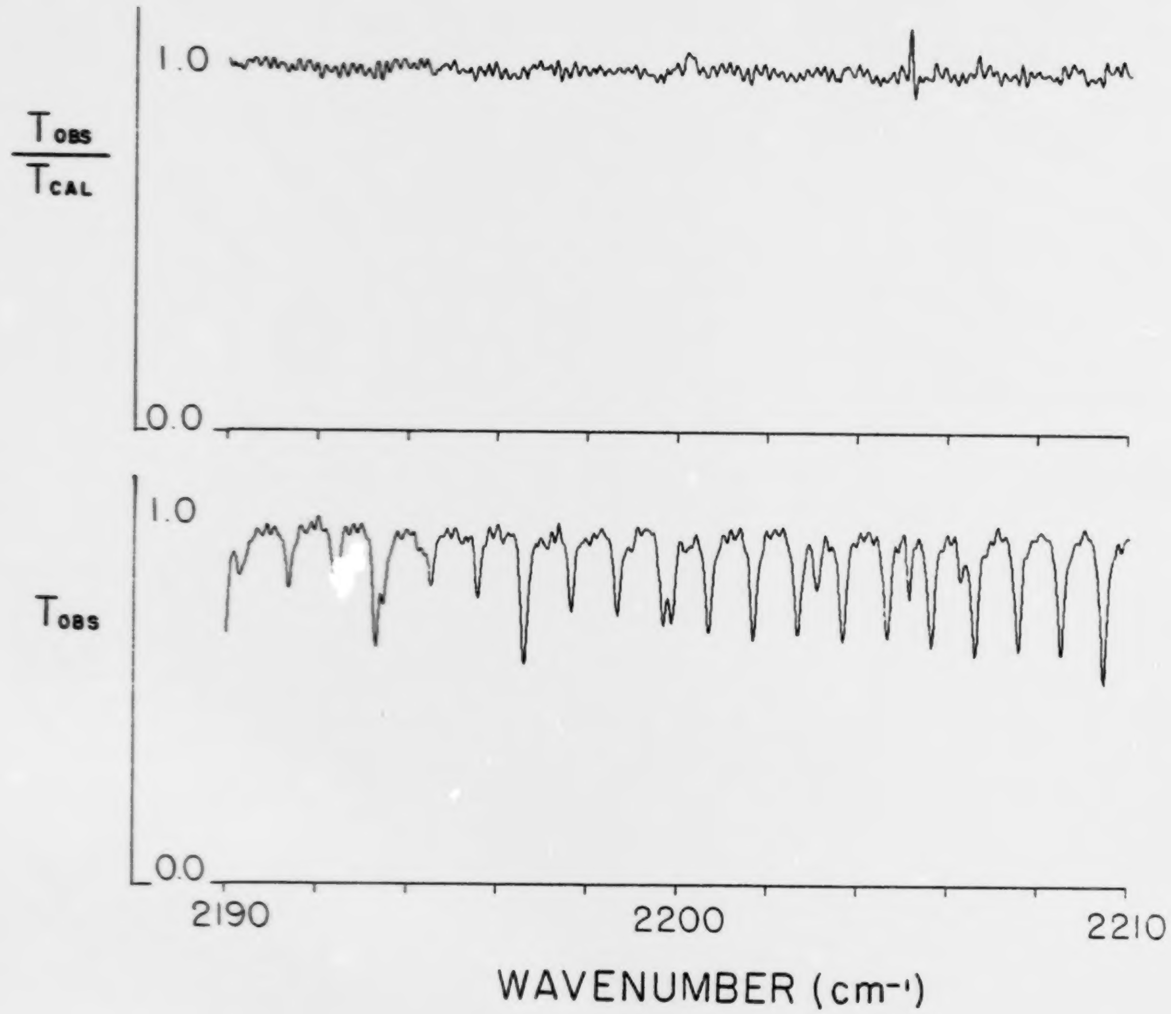

Figure 1. (a) Ratio of the experimental spectrum with the best-fit spectrum obtained by non-linear, least-squares fit analysis, (b) spectrum of a 171-m path of ground-level air at 290K and 700 torr.

TYPING GUIDE SHEET
BEGIN FIRST LINE OF TEXT HERE
CENTER OF PAGE
TOP OF IMAGE AREA
DROPPED HEAD; BEGIN SECTIONS HERE

TABLE 4. VALUES OF THE PHYSICAL PARAMETERS OF A GAS SAMPLE DERIVED BY ANALYZING ITS ABSORPTION SPECTRUM.

Spectral Region (cm^{-1})	2180-2200	2180-2210	2180-2210	2180-2210	2190-2210
Pressure (Torr)	734 ± 13	700 (fixed)	700 (fixed)	695 ± 24	785 ± 26
Temperature (K)	293.7 ± 0.2	289 ± 2	289 ± 2	289 ± 2	285 ± 3
u_{N_2O} (10^{-3} atm-cm)$_{STP}$	4.69 (fixed)	4.39 ± 0.05	4.30 ± 0.05	4.26 ± 0.08	4.49 ± 0.09
u_{CO} (10^{-2} atm-cm)$_{STP}$	1.19 (fixed)	1.14 ± 0.02	1.12 ± 0.02	1.11 ± 0.02	1.20 ± 0.03
u_{H_2O} (atm-cm)$_{STP}$	4.00 (fixed)	(removed)	(removed)	(removed)	(removed)
Triangular Response Function Width (cm^{-1})	0.095 (fixed)	0.100 (fixed)	0.082 ± 0.002	0.084 ± 0.002	0.077 ± 0.007
a*	200.9 ± 0.2	200.4 ± 0.2	200.1 ± 0.2	200.1 ± 0.2	200.1 ± 0.2
b*	0.14 ± 0.04	0.01 ± 0.01	0.00 ± 0.01	0.00 ± 0.01	0.24 ± 0.04
c*	0.004 ± 0.004	0.000 ± 0.001	0.000 ± 0.001	0.000 ± 0.001	- 0.017 ± 0.003

* Constants to give position of $I_o(v)$

BEGIN LAST LINE OF TEXT
BOTTOM OF IMAGE AREA OUTSIDE DIMENSION FOR TABLES AND ILLUSTRATIONS
3/8"
PAGE NUMBER
EPA-287 (Cin.)
(4-76)

The absorption characteristics can be obtained from reference spectra of the gas obtained for different sample conditions and spectral resolutions or they can be calculated (for a limited number of gases) from tabulations of the line parameters.[5] If the line parameters are not known (and this is true for most atmospheric gases) then the determinations of the abundances of these gases must be based on appropriate reference spectra. These two cases are discussed below.

Accurate Determination of Absorber Amounts by Using Experimental Spectra for Reference

One of the methods for estimating the unknown amount of absorber is a sample is to calculate the absorbances for an appropriate band of the absorber and to compare these with the corresponding absorbances of a known amount of the absorber. These comparisons are often made visually and by assuming that the sample conditions and spectral resolution for both spectra are the same. It is also usually assumed that Beer's Law is obeyed and that the absorbance is directly proportional to the amount of gas in the sample although it is well known[21] that deviations from Beer's Law usually occur, especially for spectra of gases. Thus a variety of systematic errors may be introduced into the measurements.

These errors may be circumvented by collecting a family of reference spectra for each gas covering a range of pressures, temperatures, absorber amounts, and spectral resolutions and choosing the appropriate one for analyses of the sample spectrum, but it is not usually practical to do this.

An alternative method has been proposed by Lin *et al.*[22,23] The first of these papers[22] contained a discussion of the accuracy with which the unknown amount of absorber in a sample could be estimated by comparing its spectrum with a reference spectrum of the same amount of gas. It was shown that this accuracy depended on the signal-to-noise ratio in the spectrum, the number of points sampled and their distribution between the band and the background, and the band transmittance. The dependence of the information[19] about the absorber amount $I(u) = (u/\Delta u)^2$ on the band transmittance is shown in Figure 2 for the cases of the background known and one observation in the band, and also of N observations distributed between the background and the band. In both cases the optimum band transmittance is close to 0.3.

The case when the sample and reference samples were the same but had different amounts of absorber wan then discussed for the particular case of an N_2O band which was expected to show marked departures from Beer's Law behavior. Beer's Law can be written as

$$I(\nu_i) = I_o(\nu_i)\exp[-K(\nu_i)u] \, , \tag{14}$$

when $I_o(\nu_i)$ are the signals in the absence of the sample, $I(\nu_i)$ are the observed signals with the sample present, and $K(\nu_i)$ are the absorption coefficients derived from some reference spectrum.

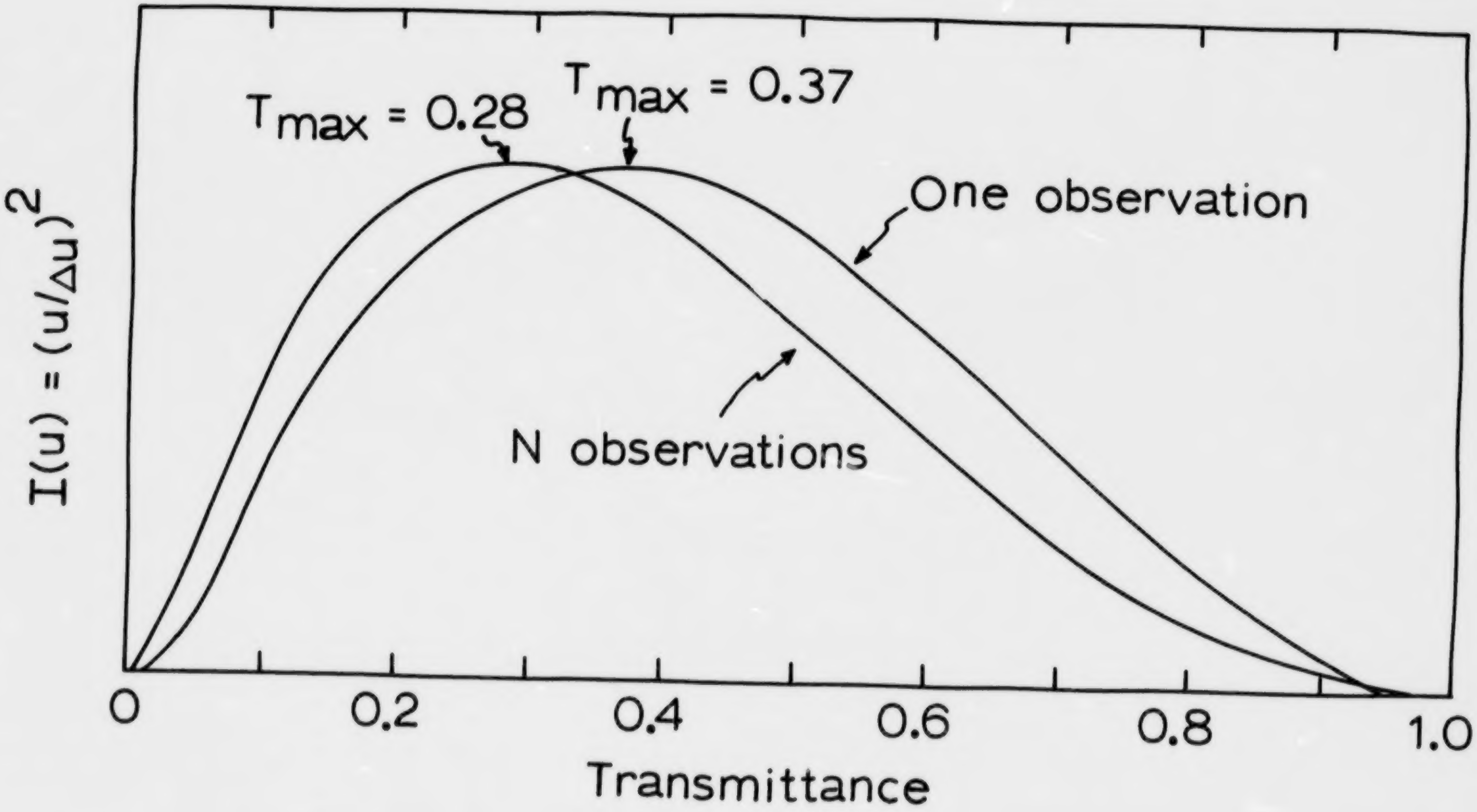

Figure 2. A comparison of the relative dependence of the information concerning absorber amount, obtained from a single measurement and many measurements in a spectrum, on the transmittance of the spectrum. The maximum values of $I(u)$ occur for transmittances of 0.37 and 0.28, respectively.

Although Eq (14) is true for spectra obtained at infinite resolution it is not universally true for spectra of finite resolution. It is found that this absorption coefficient is a function of the absorber amount.[21] If this dependence is not taken into account systematic errors in the unknown abundance will occur which will increase as the difference between the absorber amounts in the sample and reference increase.

Lin _et al_.[22] showed that these errors could be substantially reduced by obtaining the absorption coefficients k_1 and k_2 from reference spectra of amounts u_1 and u_2 of the absorber. The unknown absorber amount u_s is then determined from the modified Beer's Law relation.

$$I = I_0 \exp \left\{ -[k_1 + (\Delta k/\Delta u)\delta u]u \right\} , \tag{15}$$

when $\Delta k/\Delta u = (k_2 - k_1/u_2 - u_1)$,

$\delta u = u_s - u_1$, and

$u_1 < u_s < u_2$.

The results in Tables 5, 6, and 7 show the increase in accuracy obtained by using this approach. Table 5 gives the conditions for which the synthetic spectra of N_2O used in the analysis were calculated. Table 6 shows the accuracy and precision with which the unknown absorber amount was estimated when both reference and sample had the same N_2O amount. The results in Table 7 were obtained for different amounts of N_2O in the samples. Part A of Table 7 gives the results obtained by assuming Eq. (14) is valid and Part B was obtained by using Eq. (15). It is clear that by properly choosing u_1 and u_2 the systematic error could be still further reduced.

TABLE 5. PHYSICAL CONDITIONS OF N_2O SAMPLE AND OBSERVING CONDITIONS.

N_2O amount (atm-cm)	0.02
Temperature (K)	296
Pressure (Torr)	400
Spectral Resolution (cm^{-1})	0.2
Number of Spectral Points	840

In the second paper[23] Lin _et al_. showed that relations similar to Eq. (15) could be used to describe the dependence of the absorption coefficients on other parameters. In general, if the absorption coefficients depend on some parameter p, reference spectrum are obtained for parameter values p_1 and p_2 when $p_1 < p_s < p_2$ and p_s is the parameter value for the unknown sample. The corresponding absorption doefficient $K(p_s)$ of the sample is then obtained from

TABLE 6. PRECISION AND ACCURACY WITH WHICH THE UNKNOWN AMOUNT OF N_2O WAS RETRIEVED BY ANALYZING ITS ABSORPTION SPECTRUM WITH ABSORPTION COEFFICIENTS FROM A SPECTRUM OF FINITE RESOLUTION. BOTH SPECTRA WERE CALCULATED FOR 0.02 ATM-CM N_2O AND IDENTICAL CONDITIONS.

Noise/Signal Ratio		Retrieved N_2O Amount	
Reference %	Sample %	Precision %	Accuracy %
0	1	0.24	0.33
1	0	0.16	0.005
1	1	0.28	0.17

TABLE 7. PRECISION AND ACCURACY WITH WHICH AN UNKNOWN AMOUNT OF N_2O WAS RETRIEVED. (A) RESULTS OBTAINED BY USING ABSORPTION COEFFICIENTS FROM A SINGLE REFERENCE SPECTRUM. (B) RESULTS WITH ABSORPTION COEFFICIENTS FROM TWO REFERENCE SPECTRA.

(A)	Reference	$u = 0.02$ atm-cm N_2O	
	Sample	$u = 0.03$ atm-cm N_2O, noise 1%	
	Retrieved u:	Precision: 0.26%	Acc: 9%
(B)	Reference	$u_1 = 0.02$, $u_2 = 0.04$ atm-cm N_2O	
	Sample	$u = 0.03$, noise 1%	
	Retrieved u:	Precision: 0.22%	Acc: 1.2%

$$k(p_s) = k_1 + (\Delta k/\Delta p)S_p \, , \tag{16}$$

where $\Delta k/\Delta p = (k_2 - k_1)/(p_2 - p_1)$

and

$\delta_p = p_s - p_1$.

Table 8 from the paper by Lin et al.[23] shows the precision and accuracy with which the temperature, pressure, and absorber amount of a sample were retrieved by analyzing the spectrum shown in Figure 3 with absorption coefficients from four reference spectra of known pressure, temperature, and absorber amount but all different from that of the sample. This extreme example was primarily intended to show the versatility of the technique. In other examples shown in this paper, differences in spectral resolution and frequency shifts between the sample and reference spectra were analytically treated.

These techniques can be used to obtain the absorber amount and other information from any type of spectrum provided the samples are homogeneous. Further, since models have been used to represent the spectrum, the information measure approach described by Niple[17,19] can be used to determine the accuracy with which any of the parameters can be retrieved from a given spectrum, although we have not explored this as part of the problem. By the same token, it can also be determined which of the parameters have little influence on the spectrum.

ANALYSIS OF SPECTRUM OF INHOMOGENEOUS PATHS

At this time it does not appear feasible to model the absorption of an inhomogeneous path if the only spectral data available concerning the absorbing gases are in the form of reference spectra of finite resolution and of homogeneous paths.

Thus the above models cannot be adapted directly to analyze solar spectra. Analysis of solar spectra require a model of the variations in the physical characteristics of the system along the path and also a model of the changes in the absorption coefficients along the path. Models of the variations of atmospheric parameters with height are available and, provided the line parameters of the absorbing gas are known, the absorption along a slant path through the atmosphere can be described. Such a model has been prepared by Skinner[4] and has been used by Chang et al.[24] to determine the abundances of H_2O, CO, and N_2O by analyzing a portion of a ground-level solar spectrum shown in Figure 4. It was extimated from this spectrum that the surface humidity was 32.5 ± 0.2%, the surface densities of N_2O and CO were found to be $(6.8 \pm 0.1) \times 10^{12}$ mol/cm^3 (0.27 ppm) and $(2.8 \pm 0.1) \times 10^{12}$ mol/cm^3 (0.11 ppm), respectively. The shape and position of the background curve were also estimated. There has been no opportunity to analyze other spectral regions or other solar spectrum in a systematic manner.

24

TABLE 8. PRECISION AND ACCURACY WITH WHICH THE TEMPERATURE, PRESSURE, AND ABSORBER AMOUNT OF A SAMPLE WERE RETRIEVED BY ANALYZING ITS SPECTRUM WITH ABSORPTION COEFFICIENTS FROM FOUR REFERENCE SPECTRA OF KNOWN PRESSURE, TEMPERATURE, AND ABSORBER AMOUNT.

	u (atm-cm)		T (K)		P (Torr)	
Reference	0.02	$\frac{\Delta K}{\Delta u}$	296	$\frac{\Delta K}{\Delta T}$	400	$\frac{\Delta K}{\Delta P}$
	0.04		296		400	
	0.02		346		400	
	0.02		296		600	
Sample (1% noise)	0.03		321		500	

Retrieved u		Retrieved P		Retrieved T	
Prec %	Acc %	Prec %	Acc %	Prec %	Acc %
Fixed at 0.03 atm-cm		Fixed at 500 Torr		0.2	0.6
Fixed at 0.03 atm-cm		0.6	4		
3	2	Fixed at 500 Torr		4	22
6	11	1.5	1.9	7	7

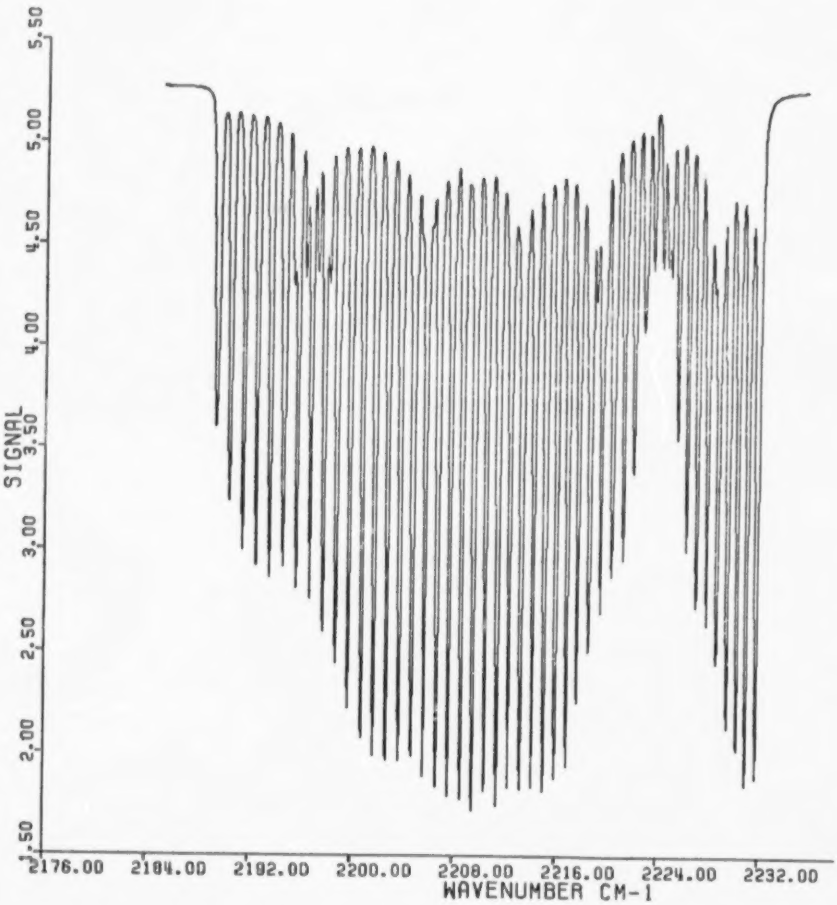

Figure 3. Spectrum of N_2O calculated from the parameters of the stronger lines between 2190 and 2230 cm^{-1} given in the AFGL line parameter listing.

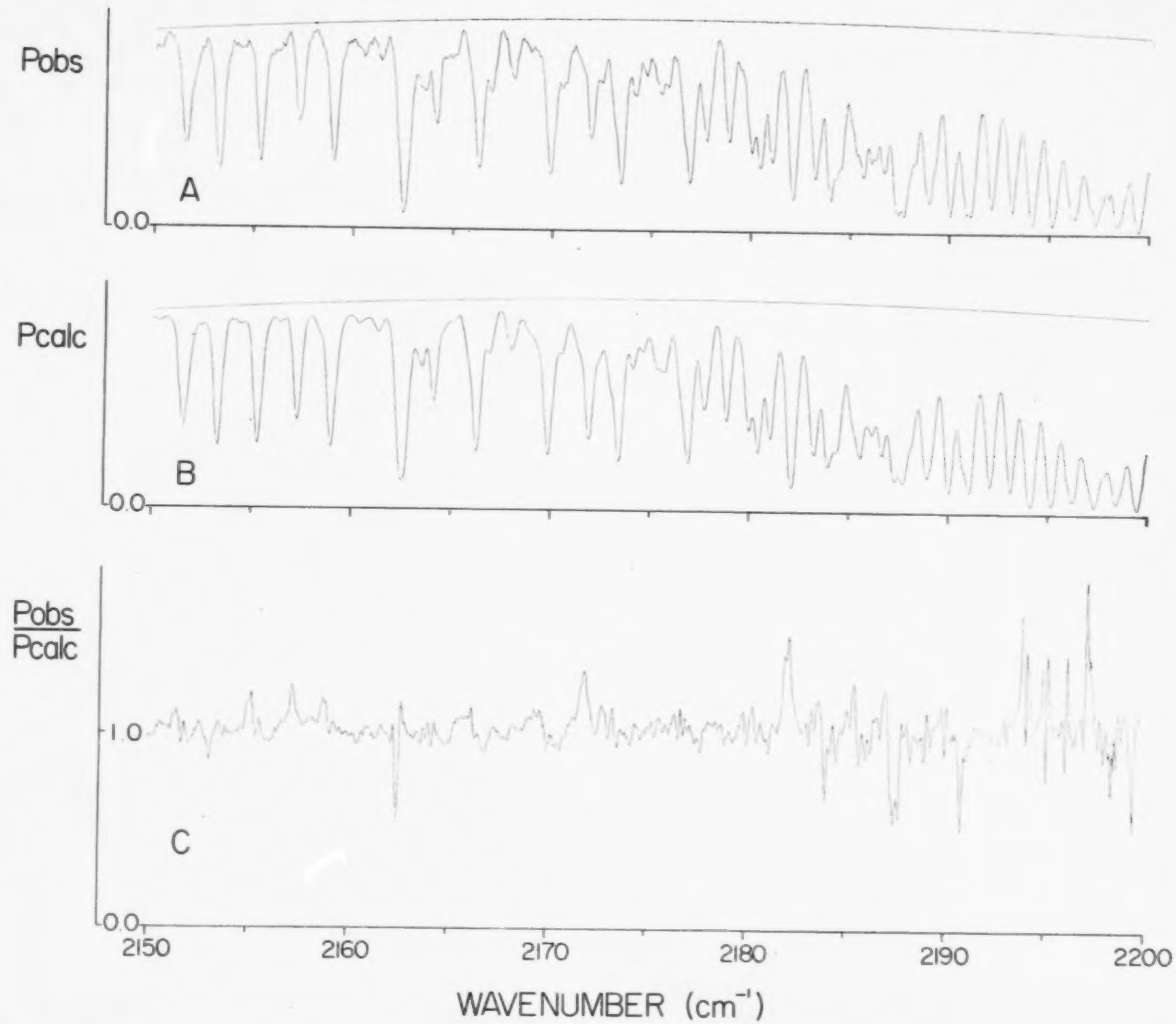

Figure 4. (a) Solar spectrum observed in October 1975 and best calculated background; (b) solar spectrum calculated from best fit values of surface densities of H_2O, CO, N_2O, and spectral resolution. The position of the background curve determined by the program is also shown; (c) ratio of the two lower curves.

These results are sensitive to the models used to describe the variations of the atmosphere parameters with height. Niple has extended his nonlinear design analysis to estimate the information contained in solar spectrum concerning these variations; however, no final results of this analysis are available at this time.

INVESTIGATIONS OF THE ABSORPTION PROPERTIES OF GASES

An accurate and detailed knowledge of the absorptive properties of gases and their dependence on the temperature and pressure of the gas is essential if absorber amounts are to be estimated accurately. Thus we have spent considerable effort in investigating techniques for measuring these quantities accurately. Considerable progress in evaluating different techniques has been made but a final solution has not been achieved. Thus, rather than generating information concerning specific gases likely to be superseded by later investigations the effort has been concentrated on improving the techniques. This effort has been directed primarily toward determining information about the individual lines in the absorption spectra of gases. Such information can be obtained relatively easily, provided the spectrum consist of individual lines or groups of lines which are reasonably well resolved. However, the bands of many gases consist of closely packed lines which are strongly overlapped. In the latter case the only absorption data which can be obtained will consist of empirical absorption coefficients, corresponding to the total contribution of all the lines, at each position in the spectrum. Lin et al.[22] have noted that in order to obtain these empirical absorption coefficients it is necessary for the observer to estimate the background curve, and that these coefficients, and thus ultimately the accuracy with which unknown absorber amounts are estimated, depend on the skill of the experimenter.

It is concluded that, whenever possible, the information concerning the absorption by gases should be that concerning the characterstics of individual lines. We have made a number of approaches to the problem during the past few years. The initial impetus was given by the earlier work of Chang and Shaw[25,26] who demonstrated that unbiased estimates of the parameters of lines of CO and H_2O could be obtained from spectra, with a grating instrument which had been digitized by hand, by application of the nonlinear, least-squares regression analysis methods described earlier.

Initial attempts to apply these methods to the FTS data (resolution ~ 0.1 cm^{-1}) available to us did not give useful results. It can now be shown, by using the information theory approach described by Niple and Shaw[19] that this was due to an insufficient number of signal values in the regions where there was significant absorption by the lines and a signal-to-noise ratio which was too low, rather than a failure of the method.

This was further demonstrated by the failure to retrieve the line parameters satisfactorily by using observer judgement to estimate the best fit between the observed spectrum and spectrum calculated for different assumed line parameters.[27]

Some success was obtained by analyzing two different experimental spectrum of the same lines simultaneously,[28] since additional data points were made available. It was shown that line parameters of the 1-0 band of HCl could be retrieved from FTS spectra even though the spacing between the frequencies at which the signal values were obtained was larger than the Lorentzian widths of the lines. The accuracy of the retrieval line parameters was demonstrated by comparison with previously reported values. Line positions were retrieved with a precision of better than 0.005 cm^{-1} and the line intensities and widths to better than 5%, even though the amount of experimental data available for analysis was minimal. It is now known that improved methods for analyzing several spectrum simultaneously can be used but we have not had the opportunity to test those on actual spectra.

The analysis of single lines described above assumed the lines had a Lorentzian shape. This is usually a good assumption provided the sample pressure is sufficiently large (greater than about 20 Torr). An interim report [29] has been prepared which describes the computer programs used in these investigations to assist others who may wish to use this technique.

At pressures less than about 20 Torr the line shape changes from the Lorentz shape to the Voigt shape; this is a combination of the Lorentz and Doppler shapes. The Voigt shape is more difficult to manipulate than the Lorentz shape since an additional parameter is required and the expressions used to describe it are more complex. However, the Voigt shape is encountered in many experiments and must be used, for example, to study the absorbing properties of the stratosphere.

Lin _et al_.[30] have demonstrated that the Lorentzian width, intensity, and position of Voigt-shaped lines, together with the spectral resolution and position of the background curve, can be obtained by application of the nonlinear, least-squares method to the analysis of synthetic data to which random noise was added. Some examples of the lines analyzed are shown in Figure 5 which shows typical Voigt-shaped lines and their absorption coefficients. The top pair of curves correspond to a line with a shape close to the pure Doppler shape, the middle pair a mixed line shape, and the bottom pair of curves are these for an essentially pure Lorentz line. The top curve in Figure 6 represents a typical data set analyzed, the next curve was calculated from the retrieved line parameter values and the ratio and difference of these spectrum are also shown. Some of the requirements of the experimental data to obtain good retrievals were identified empirically since the information measure analysis of Niple and Shaw has not been applied to this problem. The results indicate that the spectral resolution of an FTS instrument must be considerably better than 0.1 cm^{-1} if good line parameters are to be retrieved from experimental data. An interim report describing the application of the nonlinear, least-squares fit programs to retrieving the parameters of Voigt-Shaped lines has been prepared.[31]

These investigations have shown that the important line parameters required to estimate the amounts of gases in an unknown sample by analysis of its infrared spectrum can be obtained from a single spectrum or the simultaneous analysis of several spectra. It is necessary that the spectra contain sufficient information about each parameter and this requires a

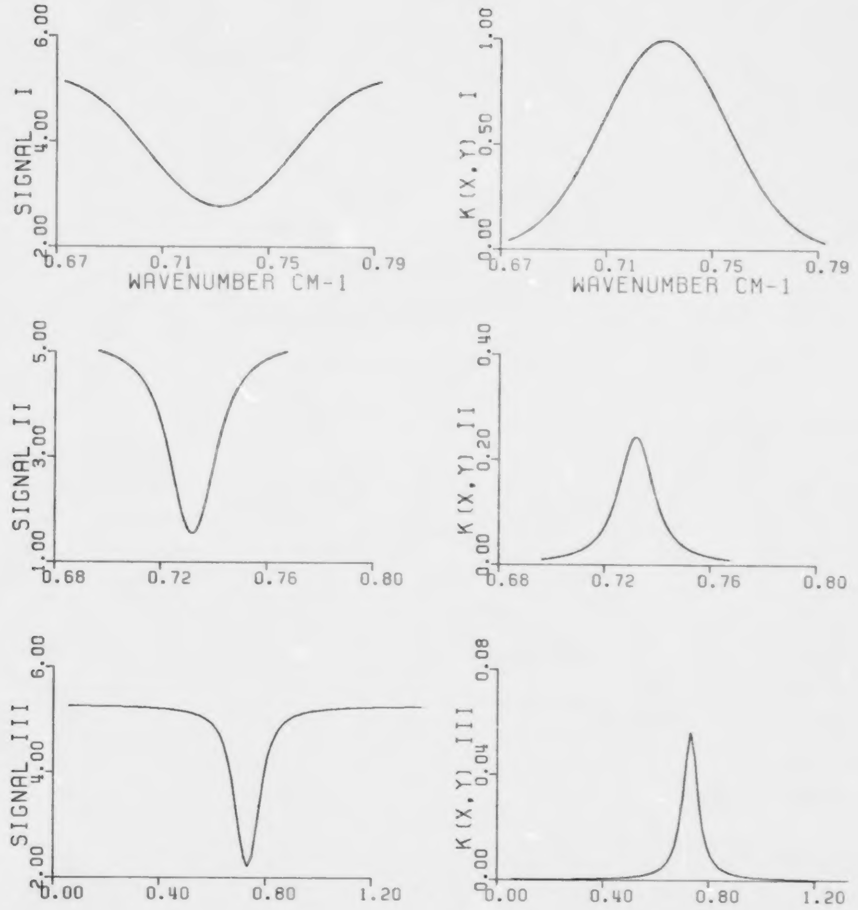

Figure 5. Noise-free spectra and absorption coefficients of Voigt-shaped lines calculated for the parameter values in Table 1. Top curve: Lorentz line; middle curve: Voigt line; bottom curve: near doppler line.

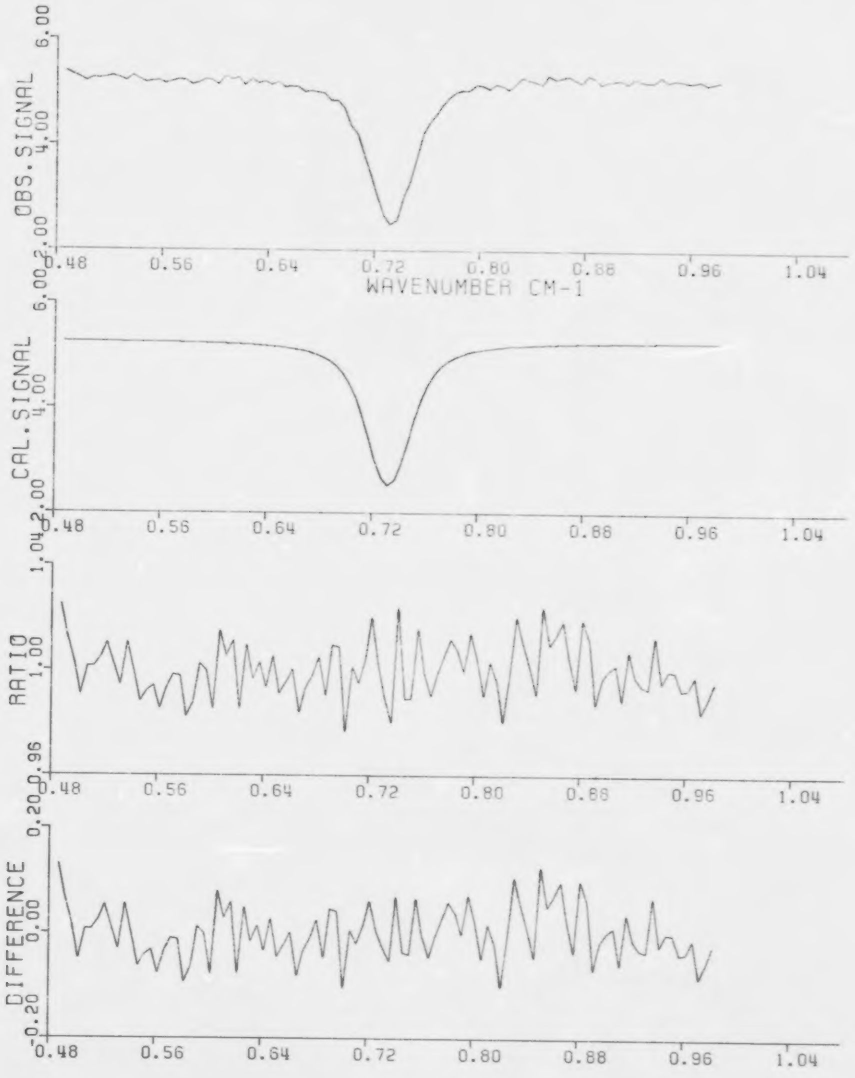

Figure 6. The top curve shows the spectrum of a Voigt line with 1% added noise, the next curve is the spectrum calculated from the retrieved values, and the bottom two curves show the ratio and differences of these spectra.

sufficient number of signal values in the region when the line absorbs a sufficient signal-to-noise ratio and the appropriate resolution. All of these can be estimated by the approach of Niple and Shaw[19] for specific situations. The results do not require observer judgment and are unbiased.

A typical absorption band consists of many lines with a wide range of intensities. Not all of the lines can be observed in a single spectrum under the appropriate conditions for accurate analysis. Thus, if the line-by-line method of analysis is used, it may be necessary to analyze small groups of lines in several spectra in order to obtain all the information required.

The theory of molecular band absorption has been highly developed and it has been shown that the individual line parameters can often be described by band models containing far fewer adjustable parameters than the number of lines which they describe. These parameters are usually obtained by first obtaining the appropriate information from single lines (such as their positions) and then reanalyzing this subset of data. This is a cumbersome and time-consuming process. A more direct approach is to retrieve the band parameters directly from the observed spectrum.

One of the final tasks undertaken was an investigation of the analysis of entire bands. Some preliminary results have been described by Lin et al.[32] In this study the line positions, widths, and intensities were described by appropriate band models and these models were used to calculate a spectrum with a resolution comparable to the observed spectra. The values of the adjustable parameters in these models were then estimated by the spectral curve fitting methods previously described.

This approach was tested by analyzing major portions of the 1-0 bands of HCl and CO. More than 3500 data points were analyzed and it was shown that up to 27 parameter values could be estimated, together with the estimated standard deviations and the correlations between the parameters. The top curve in Figure 7 shows the portion of the experimental CO spectrum analyzed, beneath it is the spectrum calculated from the parameter estimates, show and the other two curves the ratio and the difference of these spectra In Figure 8 the continuous curve represents the polynomial dependence of the CO line widths on m, calculated from the retrieved values of the half-width model parameters. The open circles represent the average values obtained by Benedict et al.[33] and the asterisks show the half widths in the latest version of the AFGL line listing for comparison.

These results are encouraging and this method promises to reduce greatly the work required to determine information about the absorbing properties of gases and it will be explored further.

The results to date of our investigations on the determination of the absorbing properties of gases have shown that methods of obtaining this information from FTS spectra are available and that they will have the accuracy required for estimating the abundances of atmospheric gases to the desired accuracy.

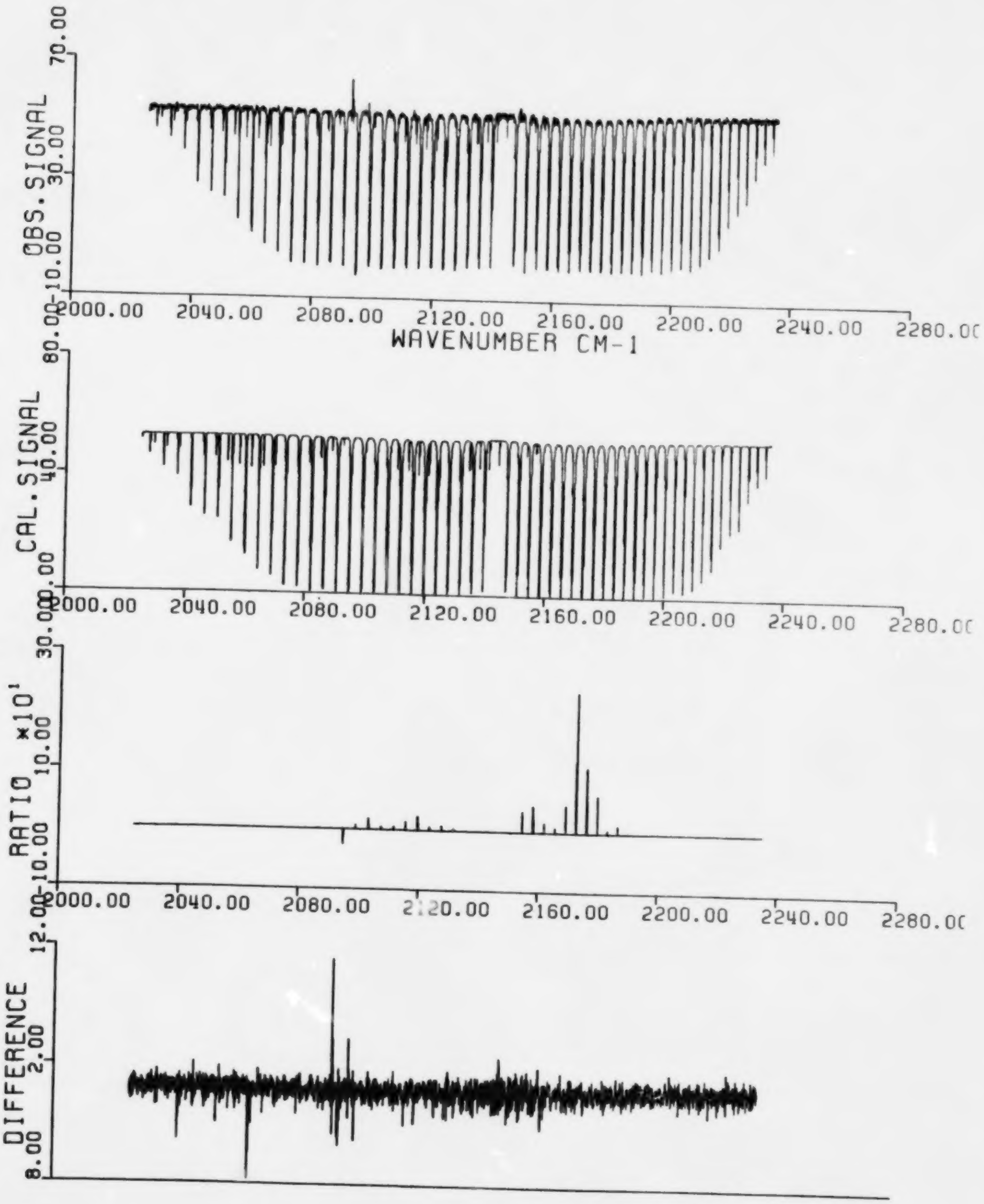

Figure 7. The experimental CO spectrum analyzed is shown in the top curve; beneath it is the spectrum calculated from the retrieved parameter values; the other two curves show the ratios and differences of these two spectra.

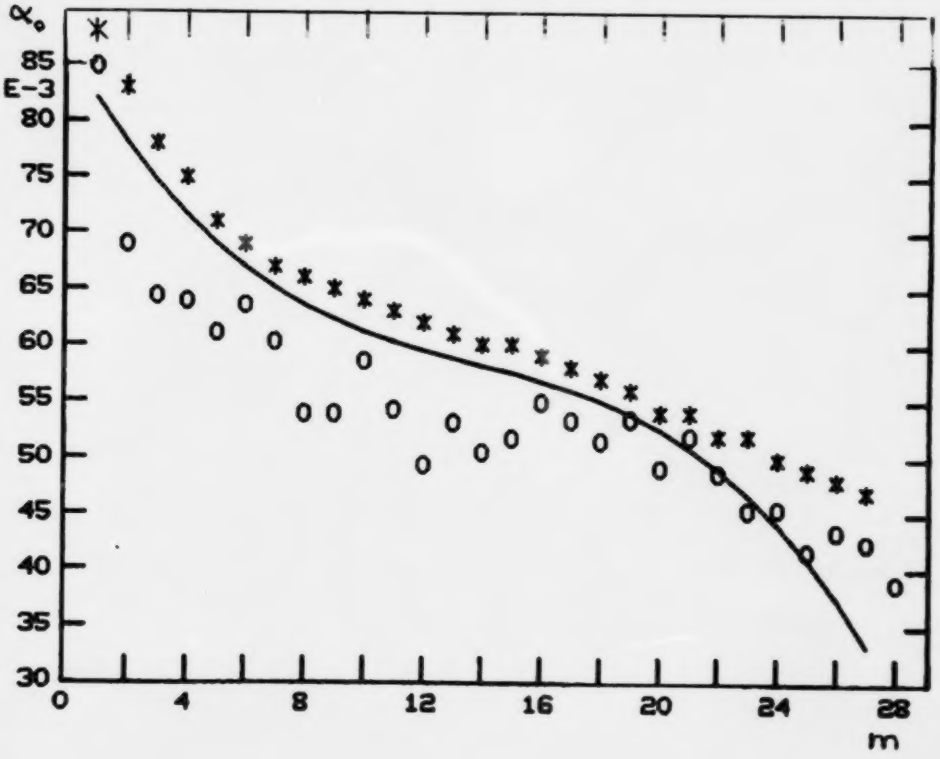

Figure 8. The continuous curve represents the polynomial dependence of the CO line widths on m calculated from the retrieved parameter values. The open circles represent the average half-widths obtained from Benedict, Herman, and Silverman[33] and the asterisks show the half-widths in the latest version of the AFGL atmospheric line listing.

In the initial stages of the work undertaken on this grant it was planned to investigate the composition of the atmosphere by using FTS techniques. This included the collection and analysis of a variety of atmospheric spectra. A series of such spectra was obtained during the first year's effort and an analysis was begun. It quickly became apparent that the methods of analysis available were inadequate to extract all the information contained in these spectra. Thus an investigation of other methods of extracting this information was undertaken. During the past two years methods have been developed which are capable of great precision and accuracy in determining the amounts of gases present in the atmosphere. These methods have demonstrated that the accuracy is no longer limited by the method of analysis but rather by inadequate knowledge of the sample characteristics including the absorption properties of the gases investigated. It has been demonstrated that the methods of analysis which have been developed will also allow these absorption properties to be determined with appropriate accuracy. In addition, the principles of experiment design have been applied to spectroscopic studies. These enable the optimum design of experiments to be determined. This work has given a solid foundation for future investigations of atmospheric properties by using FTS.

SECTION 6

A KINETIC STUDY OF THE MECHANISM OF PEROXYNITRIC ACID FORMATION

INTRODUCTION

Peroxynitric acid (HO_2NO_2) was recognized many years ago as a highly reactive, oxidizing compound of rather low thermal stability.[34] Today a strong interest exists in the kinetics and mechanisms of the formation and decay reactions of this compound in view of the high potential for its creation within the atmosphere. It is important to establish the levels to which this possible pollutant may rise in the sunlight-irradiated, NO_x-hydrocarbon-polluted troposphere, and to evaluate the significance of HO_2NO_2 as an NO_x sink within the stratosphere. Indirect evidence for HO_2NO_2 formation in gas phase reactions was reported first by Simonaitis and Heicklen.[35] They studied the 213.9 nm photolysis of N_2O in mixtures with H_2, O_2, and NO and followed [NO] as a function of time using chemiluminescence analysis methods. Their data showed an interesting and unexpected result: the oxidation of NO continued to occur after termination of the initiating radiation. This observation and the kinetics of the [NO]-time data suggested to the authors that an intermediate species of finite lifetime, presumably HO_2NO_2, was formed through the HO_2-radical association with NO_2 reaction (7)*:

$$HO_2 + NO_2\ (+M) \rightarrow HO_2NO_2\ (+M) \qquad (7)$$

It was reasoned that the thermal decay of HO_2NO_2 in (8), followed by reaction (10), led to the delayed oxidation of NO:

$$HO_2NO_2\ (+M) \rightarrow HO_2 + NO_2\ (+M) \qquad (8)$$

$$HO_2 + NO \rightarrow HO + NO_2 \qquad (10)$$

The more recent results of Simonaitis and Heicklen,[36] derived from the temperature dependence of the NO_2 formation in this same system, gave further indirect evidence in support of this hypothesis.

Recently Niki et al.,[37] identified HO_2NO_2 directly for the first time through FT IR spectroscopy of the products of the uv-irradiated, dilute mixtures of Cl_2, H_2, and NO_2 in air; they also suggested that it was formed in reaction (7) following HO_2 formation in the reaction sequence (1), (2), and (6):

---

* See Table 9 for reactions

$$\mathrm{Cl_2 + h\nu \rightarrow 2Cl} \tag{1}$$

$$\mathrm{Cl + H_2 \rightarrow HCl + H} \tag{2}$$

$$\mathrm{H + O_2\ (+M) \rightarrow HO_2\ (+M)} \tag{6}$$

$$\mathrm{HO_2 + NO_2\ (+M) \rightarrow HO_2NO_2\ (+M)} \tag{7}$$

The spectrum attributed to HO_2NO_2 was the same as that observed previously by Gay _et al._,[38] and Niki _et al._[39] in irradiated, dilute mixtures of Cl_2, CH_2O, and NO_2 in air. It was tentatively attributed to peroxyformyl nitrate by both groups. However, in view of the facts that there was no carbonyl absorption band in the unknown compound spectrum and that the formyl group need not be present in the reactants to form the same compound in the work of Gay _et al._,[38] it was reasoned that HO_2NO_2 and not $HCOO_2NO_2$ was the likely product. Hanst and Gay[40] accepted the HO_2NO_2 assignment and proposed that HO_2NO_2 formed in (7) following the generation of the reactant HO_2 through reactions (1), (66), and (67) in their system:

$$\mathrm{Cl_2 + h\nu \rightarrow 2Cl} \tag{1}$$

$$\mathrm{Cl + CH_2O \rightarrow HCl + HCO} \tag{66}$$

$$\mathrm{HCO + O_2 \rightarrow HO_2 + CO} \tag{67}$$

$$\mathrm{HO_2 + NO_2\ (+M) \rightarrow HO_2NO_2\ (+M)} \tag{7}$$

Levine _et al._[41] confirmed the IR assignment of HO_2NO_2 as they formed a product of identical infrared spectrum on irradiation of dilute mixtures of HONO, CO, and NO_2 in air. In this case the HO_2-radical reactant for reaction (7) was prepared through the sequence (15), (44), (6):

$$\mathrm{HONO + h\nu \rightarrow HO + NO} \tag{15}$$

$$\mathrm{HO + CO \rightarrow H + CO_2} \tag{44}$$

$$\mathrm{H + O_2\ (+M) \rightarrow HO_2\ (+M)} \tag{6}$$

The identification of HO_2NO_2 in gas-phase reaction systems has stimulated further kinetic studies related to this interesting compound.[41-45] The present work was initiated to help delineate the kinetics and mechanisms of HO_2NO_2 formation and decay reactions in the atmosphere and to evaluate its potential role in the sunlight-irradiated, NO_x-RH-polluted troposphere. In view of the rather common use of the Cl_2-initiated reactions leading to the HO_2-radicals[37-41,46] and the complete lack of kinetic studies related to the diverse products formed in these systems, we have chosen the photolysis of dilute Cl_2, H_2, NO_x mixtures in synthetic air (700 torr) as our source of HO_2NO_2 in this work. We believe that the present work provides at least a firm beginning to our understanding of the complex reactions in this Cl_2-containing system. We have followed the time dependence of the major IR-absorbing products of the reactions in this system using long path, FT IR spectroscopy. Although the number of products of the reactions is large and the kinetics of the system complex, these rate data, when coupled with other recent kinetic information related to the HO_2NO_2 system, provide a new insight into the mechanism of formation and decay of HO_2NO_2 and other products in this system. The present data may be used to make preliminary estimates of the theoretical levels of HO_2NO_2 anticipated for the sunlight-irradiated, NO_x-polluted lower atmosphere.

EXPERIMENTAL METHODS

Equipment

The various chemical and photochemical experiments were carried out using a Digilab FTS-20 Fourier transform spectrometer (model 496 interferometer) coupled to a photolysis cell. The large, evacuable cell was constructed of 30.5 cm diameter pyrex tubing, 6.3 m long (445 ℓ volume). It housed a modified White optical system, based upon a design of Hanst,[47] which had a base path of 5.3 m and provided a choice of pathlengths which were multiples of eight-times the base length. Most of these experiments were carried out at 170 m (32 traversals) which gave adequate absorption for the compounds studied here in the ppm concentration range. All mirror supports, cell tubing spacers, and the cell end plates were constructed of stainless steel. Thin Teflon gaskets were used to obtain the vacuum-tight seals between the four pyrex tubing sections and the end plates. The glass mirrors, covered with an aluminum reflective surface and a thin overcoat (1/8th wave) of silicon monoxide, showed no detectable deterioration even after two years of constant use of many reactive gases at low concentrations (Cl_2, NO_2, O_3, N_2O_5, HO_2NO_2, $HONO_2$, HCl, etc.). One cell endplate was equipped with KBr windows to allow the passage of the analytical IR beam. A liquid-helium-cooled Cu:Ge detector (Mullard) was employed in most experiments (450-2400 cm^{-1} range), while a liquid-nitrogen-cooled In:Sb detector (Santa Barbara Research) was used when an expanded range of spectral response was desired (to $\lambda > 4000$ cm^{-1}). Potential problems created by varying background absorption from H_2O and CO_2 in the air path between the transfer optics, Nernst glower IR source, interferometer, cell, and detector, were substantially lowered by enclosing the entire optical system in a plastic (acrylic) housing which was purged continuously with nitrogen gas. Open dishes of solid NaOH and KOH were placed in the housing to keep CO_2 levels low.

The reference gases were measured in an all-glass, grease- and mercury-free vacuum system equipped with Teflon stopcocks. Standard gases were introduced into calibrated volumes attached to the introduction manifold, and the pressures were measured using a quartz spiral gauge as a null instrument. Calibrated gauges (Wallace-Tiernan), not in contact with the gases, gave the absolute pressure readings.

The large photochemical cell was illuminated by black-light fluorescent lamps which surrounded it. An outer reflective shield of aluminum encompassed both the lamps and the cell. Room air was circulated in the space between the lamps and the cell to help stabilize the cell temperature. Thermocouples and a thermometer placed inside of the cell were used to determine the actual cell temperature during an experiment. Normally the temperature rose about 1°C during a 5 min irradiation period. The temperature of the cell could be varied from experiment to experiment within a small range (15-27°C) by regulation of the room temperature. The cell lighting was designed to mimic ground-level solar radiation, both in distribution and intensity, within the photochemically important region 300-450 nm. Direct measurements showed that this was the case. The wavelength-intensity profile of the light which was transmitted through the cell wall was determined directly using one of the lamps and a cell section together with an absolute spectrofluorimeter (Turner, Model 210). The NO_2 dissociation rate constant ($NO_2 + h\nu \rightarrow NO + O$) observed in this system, 0.60 min^{-1}, is typical of the atmospheric values for low solar zenith angles. Measurements with an ultraviolet radiant flux detector (Hewlett-Packard, 8334A) showed the radiant flux throughout the cell to be uniform to within ± 10%.

Procedures Employed

Most of the spectra were collected using 1 cm^{-1} resolution, with four scans and 8192 data points per interferogram. The extinction coefficients of all reactants and products were determined at several reactant pressures in 700 torr of synthetic air or N_2, employing 1 cm^{-1} resolution (1 cm optical retardation), and box-car apodization. The experimental values of the extinction coefficients (base e, $ppm^{-1}m^{-1}$, 25°C) for selected wavelengths employed in this work are as follows: NO, 2.74×10^{-4} (1876 cm^{-1}); NO_2, 3.40×10^{-5} (826), 4.41×10^{-4} (1575), 1.23×10^{-3} (1585); O_3, 1.29×10^{-4} (1000) 9.74×10^{-4} (1055)[49]; cis-HONO, 6.06×10^{-3} (853); trans-HONO, 3.84×10^{-3} (1264); $HONO_2$, 5.46×10^{-4} (762), 1.75×10^{-3} (878, 1.23×10^{-3} (894); N_2O_5, 4.0×10^{-3} (740); ClNO, 5.51×10^{-3} (1808); $ClNO_2$, 6.11×10^{-4} (780), 2.46×10^{-3} (793), 1.19×10^{-3} (1267); HO_2NO_2, 2.35×10^{-3} (802.7), 1.14×10^{-3} (810); HCl, in our system Beer-Lambert law was not followed well for the 23 rovibronic transitions in the fundamental band which were studied, and a calibration curve of absorbance versus P_{HCl} was made. For the stable gases, samples were taken from commercially available tank samples. HO_2NO_2 was prepared by photolyzing mixtures of either CO, HONO, NO_2, or NO in synthetic air, or Cl_2, H_2, or NO_2 in synthetic air, and a nitrogen mass balance was assumed to determine the $[HO_2NO_2]$ present at a given time. Samples of $ClNO_2$ were generated in the cell by reacting NOCl with O_3 in the dark or NO_2 and Cl_2 in the light; ClONO formation occurred significantly in the latter case; thus the estimated ϵ_{ClNO_2} was based upon the NOCl-O_3 reaction, and a mass balance was used to determine the $[ClNO_2]$ present in each case. The twin peaks for ClONO (1710, 1722 cm^{-1}) have extinction coefficients which are nearly equal to the twin peaks for $ClNO_2$[$\epsilon_{ClNO_2} = 1.08 \times 10^{-3}$ (1675); 1.23×10^{-3} (1690 cm^{-1})], respectively, as Molina and Molina have shown.[48] Thus we chose $\epsilon_{ClONO} = 1.1 \times 10^{-3}$ at 1710 cm^{-1}. N_2O_5 was generated in the dark using mixtures of NO_2 (2-15 ppm) and O_3 (2-8 ppm) in O_2 (~ 20 torr) and N_2 (680 torr); again a nitrogen mass balance was used to establish the $[N_2O_5]$. Standard samples of $HONO_2$ vapors from a 70% $HONO_2$ solution were introduced simultaneously into three calibrated volumes sealed to the introduction system. The contents of two of these were individually frozen at liquid nitrogen temperature, and the $HONO_2$ content was determined by titration with standard NaOH solution. The $HONO_2$ in the third bulb was introduced to the cell for spectral determinations. The value of ϵ reported for $HONO_2$ was derived from the average of eight different nitric acid samples (20% standard deviation).

The first-order photolysis rate constants for the photochemically active compounds studied here were determined in a series of special experiments in our cell. Data which were used in the determination of the constants for Cl_2 and NOCl photodecompositions (reactions (1) and (5), respectively, Table 9), are shown in Figure 9. In the case of the Cl_2 photolyses, 30 ppm of Cl_2 was mixed with H_2 at 8,066 ppm (closed circles) or 34,200 ppm (diamonds) and 700 torr of synthetic air. The Cl-atoms formed ($Cl_2 + h\nu \rightarrow 2Cl$) were captured effectively by the H_2 in each case, and the [HCl] was followed as a function of time. In this case the best fit of all the data shown in Figure 9 give $k_1 = 0.066\ min^{-1}$. In the case of NOCl photolysis, NOCl at 20 ppm (circles), 2.14 ppm (triangles), or 1.0 ppm (squares) was mixed with 34,200 ppm of H_2 in 700 torr of synthetic air. Either NO formation (circles) or NOCl loss (triangles, squares) was measured. The best fit of all of these data give $k_5 = 0.33\ min^{-1}$. The first-order constant for NO_2 photolysis was calculated from kinetic data based upon both photolyses of pure NO_2 at low pressures in the cell ($NO_2 + h\nu \rightarrow NO + O$; $O + NO_2 \rightarrow O_2 + NO$) and the computer simulation of NO_2, NO, and O_3 concentration-time dependence in dilute NO_2-air mixtures; these data gave $k_{16} = 0.60\ min^{-1}$. The simulation of the kinetic results from HONO and HONO-CO mixtures in air were used to derive $k_{15} = 0.11\ min^{-1}$. The $ClNO_2$ photolysis constant, $k_{59} = 0.03\ min^{-1}$, was determined experimentally, while those for H_2O_2, O_3, HO_2NO_2, and ClONO, were calculated from the known λ-intensity distribution within our cell and the measured ϵ data for the 3000-4500 Å range.

In the usual photochemical experiments designed to study HO_2NO_2 formation and decay kinetics, the desired quantities of Cl_2, H_2, NO_2, and NO were measured out in the sample introduction system and then introduced into the evacuated cell by way of five introduction ports spaced equally along the cell length. The initial concentrations could be calculated from the known dilution factor on expansion into the 445 ℓ cell. Direct IR estimates of the starting concentrations checked well with these estimates. The mixture was pressurized by adding N_2 (560 torr) and O_2 (140 torr). The only detectable impurities in the gases employed were: CH_4 (2 ppm), CO (0.14 ppm), and H_2O (always less than 100 ppm). Interferograms were collected for the initial mixture and the reacting mixture at selected times during and after the photolysis period; in each case 1 cm^{-1} resolution was employed. Usually the interferograms from four scans (8K data points, 0.08 min per scan) were coadded and recorded on magnetic tape for later processing. Following the experiment the data were resolved into wavelength-transmission spectra by computer. The concentration-time dependence of the reactants and products were derived by computer comparison of the absorbance data with those of standard compounds in the reference files. Most compounds could be determined using the characteristic regions of absorption which were free from interferences from other compounds. In the case of nitryl chloride ($ClNO_2$), absorption overlapped that of HO_2NO_2 near 800 cm^{-1}, and this was removed from the spectra through computer absorbance subtraction in order to measure the underlying HO_2NO_2 absorbance. All of the compounds (other than HCl) seem to follow the Beer-Lambert absorption law reasonably well for our range

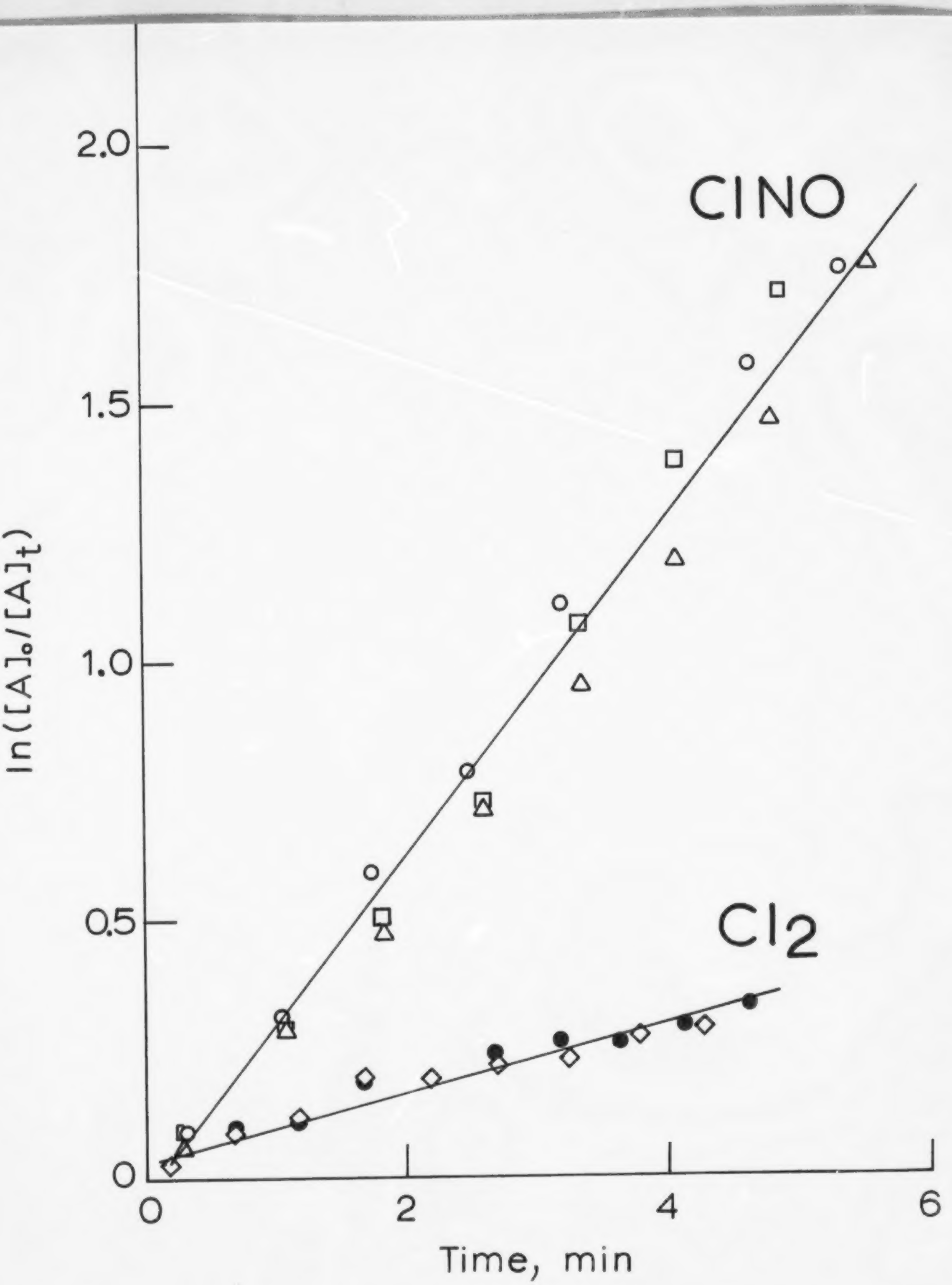

Figure 9. First-order decay plots used in the evaluation of the rate constants for Cl_2 and ClNO photolysis in the reaction chamber: data for the Cl_2 species were obtained using 30 ppm of Cl_2 with H_2 at either 8066 ppm (closed circles) or 34,200 ppm (diamonds) and in 700 torr of synthetic air; data for ClNO were obtained using mixtures of ClNO, 20 ppm (circles), 2.14 (triangles), or 1.0 (squares), with 34,200 ppm of H_2 in 700 torr of air; NO formation (circles) or NOCl loss (triangles, squares) was measured with NOCl while HCl was determined in the Cl_2 experiments.

TABLE 9. THE REACTION MECHANISM AND RATE CONSTANTS FOR THE PHOTOLYSIS OF DILUTE Cl_2, H_2, NO_x MIXTURES IN AIR[a]

	Major Reactions	Rate Constants[b]	References
(1)	$Cl_2 + h\nu \rightarrow 2Cl$	6.6×10^{-2}	This work
(2)[d]	$Cl + H_2 \rightarrow HCl + H$	2.07×10^{1}	58
(3a)	$Cl + NO_2\ (+M) \rightarrow ClNO_2\ (+M)$	1.2×10^{4}	This work
(3b)	$Cl + NO_2\ (+M) \rightarrow ClONO\ (+M)$	---	Neglected here
(4)	$Cl + NO\ (+M) \rightarrow ClNO\ (+M)$	5.5×10^{3}	This work
(5)	$ClNO + h\nu \rightarrow Cl + NO$	3.3×10^{-1}	This work
(6)	$H + O_2\ (+M) \rightarrow HO_2\ (+M)$	1.7×10^{3}	59
(7)[d]	$HO_2 + NO_2\ (+M) \rightarrow HO_2NO_2\ (+M)$	1.6×10^{3}	53
(8)[d]	$HO_2NO_2\ (+M) \rightarrow HO_2 + NO_2\ (+M)$	4.1	53
(9)[d]	$HO_2NO_2\ (+Wall) \rightarrow HONO_2 + \frac{1}{2}O_2$ (or other products)	1.2×10^{-1}	This work[c]
(10)	$HO_2 + NO \rightarrow HO + NO_2$	6.0×10^{3}	This work
(11)	$2HO_2 \rightarrow H_2O_2 + O_2$	5.3×10^{3}	59
(12)[d]	$HO + H_2 \rightarrow H_2O + H$	1.0×10^{1}	59
(13)	$HO + NO_2\ (+M) \rightarrow HONO_2\ (+M)$	1.9×10^{4}	This work
(14)	$HO + NO\ (+M) \rightarrow HONO\ (+M)$	7.6×10^{3}	This work
(15)	$HONO + h\nu \rightarrow HO + NO$	1.1×10^{-1}	This work
(16)	$NO_2 + h\nu \rightarrow NO + O$	6.0×10^{-1}	This work
(17)	$O + O_2\ (+M) \rightarrow O_3\ (+M)$	2.1×10^{1}	59
(18)[d]	$O_3 + NO \rightarrow O_2 + NO_2$	2.87×10^{1}	59
(19)[d]	$O_3 + NO_2 \rightarrow O_2 + NO_3$	4.6×10^{-2}	59
(20)	$NO_3 + NO_2\ (+M) \rightarrow N_2O_5\ (+M)$	5.6×10^{3}	59
(21)[d]	$N_2O_5\ (+M) \rightarrow NO_3 + NO_2\ (+M)$	9.5	59
(22)	$NO_3 + NO \rightarrow 2NO_2$	1.5×10^{4}	59
(23)	$2NO_3 \rightarrow 2NO_2 + O_2$	3.2×10^{-1}	59
	Additional Minor Reactions of Cl-Containing Species		
(24)	$Cl + O_2\ (+M) \rightarrow ClOO\ (+M)$	2.0×10^{1}	59
(25)	$ClOO\ (+M) \rightarrow Cl + O_2\ (+M)$	1.8×10^{8}	59
(26)	$Cl + O_3 \rightarrow ClO + O_2$	1.7×10^{4}	59
(27)	$ClO + NO \rightarrow Cl + NO_2$	2.3×10^{4}	67
(28)	$ClO + NO_2\ (+M) \rightarrow ClONO_2\ (+M)$	2.6×10^{3}	60
(29)	$ClO + ClO \rightarrow Cl_2 + O_2$	3.4×10^{3}	59

(30)	$Cl + ClNO \rightarrow Cl_2 + NO$	4.4×10^4	60
(31)	$Cl + ClNO_2 \rightarrow Cl_2 + NO_2$	5.0×10^1	59
(32)	$Cl + ClONO_2 \rightarrow Cl_2 + NO_3$ (or other products)	3.2×10^2	60
(33)	$Cl + H_2O_2 \rightarrow HCl + HO_2$	8.8×10^2	59
(34)	$Cl + HONO \rightarrow HCl + NO_2$	8.8×10^2	$k_{34} = k_{33}$ (assumed)
(35)	$Cl + HONO_2 \rightarrow HCl + NO_3$	1.0×10^1	60
(36)	$Cl + HO_2NO_2 \rightarrow HCl + O_2 + NO_2$	8.8×10^2	$k_{36} = k_{33}$ (assumed)
(37)	$Cl + HO_2 \rightarrow HCl + O_2$	3.7×10^4	46
(38)	$Cl + ClOO \rightarrow Cl_2 + O_2$	3.0×10^4	46

Additional Minor Reactions of HO-Radicals

(39)	$HO + HCl \rightarrow H_2O + Cl$	1.03×10^3	59
(40)	$HO + HONO \rightarrow H_2O + NO_2$	8.5×10^3	61
(41)	$HO + HONO_2 \rightarrow H_2O + NO_3$	1.3×10^2	59
(42)	$HO + HO_2NO_2 \rightarrow H_2O + O_2 + NO_2$	5.0×10^2	$k_{42} = k_{43}$ (assumed)
(43)	$HO + H_2O_2 \rightarrow H_2O + HO_2$	5.0×10^2	59
(44)	$HO + O_3 \rightarrow HO_2 + O_2$	7.7×10^1	59
(45)	$HO + CO \rightarrow H + CO_2$	4.4×10^2	68
(46)	$HO + ClONO_2 \rightarrow HOCl + NO_3$ (or other products)	5.8×10^2	60

Additional Minor Reactions of HO_2-Radicals

(47)	$HO_2 + O_3 \rightarrow HO + 2O_2$	1.8	59
(48)	$HO_2 + HO \rightarrow H_2O + O_2$	7.5×10^4	59
(49)	$HO_2 + NO_2 \rightarrow HONO + O_2$	< 0.8	53

Additional Minor Reactions of O-Atoms

(50)	$O + NO (+M) \rightarrow NO_2 (+M)$	3.3×10^3	59
(51)	$O + NO_2 (+M) \rightarrow NO_3 (+M)$	3.4×10^3	59
(52)	$O + NO_2 \rightarrow O_2 + NO$	1.34×10^4	59

Additional Minor Reactions of NO_x Species

(53)	$2NO + O_2 \rightarrow 2NO_2$	7.5×10^{-10}	59
(54)	$NO + NO_2 + H_2O \rightarrow 2HONO$	5.5×10^{-10}	This work
(55)	$2HONO \rightarrow NO + NO_2 + H_2O$	4.1×10^{-4}	This work
(56)	$HONO + HONO_2 \rightarrow H_2O + 2NO_2$	9.6×10^{-3}	This work
(57)	$NO_2 + NO_3 \rightarrow NO_2 + NO + O_2$	1.2×10^1	59
(58)	$N_2O_5 + H_2O \rightarrow 2HONO_2$	1.9×10^{-5}	59

Additional Minor Photochemical Reactions			
(59)	$ClNO_2 + h\nu \rightarrow Cl + NO_2$	3.0×10^{-2}	This work
(60)	$ClONO + h\nu \rightarrow Cl + NO_2$	3.5×10^{-1}	This work
(61)	$H_2O_2 + h\nu \rightarrow HO + HO$	1.5×10^{-3}	This work
(62)	$O_3 + h\nu \rightarrow O(^3P) + O_2$	4.4×10^{-4}	This work
(63)	$O_3 + h\nu \rightarrow O(^1D) + O_2$	7.1×10^{-5}	This work
(64)	$HO_2NO_2 + h\nu \rightarrow HO_2 + NO_2$	1.5×10^{-3}	$k_{64} + k_{65} = k_{61}$ (assumed)
(65)	$HO_2NO_2 + h\nu \rightarrow HO + NO_3$		

---

[a] Temperature, 25°C; pressure of air, 700 torr; relative humidity near 0%.

[b] The units on the rate constants are $ppm^{-1}min^{-1}$ for all reactions other than (1), (5), (8), (9), (15), (16), (21), (25), and (59)-(65) which are min^{-1}, and reactions (53) and (54) which are $ppm^{-2}min^{-1}$; the unit ppm used here is defined as pressure (torr)/760 x 10^6 at 25°C.

[c] This rate constant is dependent upon the NO_2 absorbed on the wall; for an increase in gaseous NO_2 pressure by a factor of 100, k_9 decreases by a factor of about 1.5; because of the heterogeneous nature of this step, the value chosen should be established experimentally for the given cell under the specific conditions employed.

[d] The temperature dependence of these rate constants was taken into account in the computer simulation of runs at temperatures other than 25°C, using the following activation energies: $E_2 = 4.3$; $E_7 = -2$; $E_8 = 19.9$; $E_9 = 19.0$; $E_{12} = 4.9$; $E_{18} = 3.0$; $E_{19} = 4.9$; $E_{21} = 21$ kcal $mole^{-1}$.

of conditions. The measured extinction coefficients and absorbances were used to calculate the concentrations of each product.

DISCUSSION

The Mechanism of Product Formation

The near uv-irradiation of a dilute mixture of Cl_2, H_2, NO_2, and NO in air leads to a variety of products, including peroxynitric acid. The time dependence of the major products of the irradiation of a typical mixture employed in this study is shown in Figure 10. It can be seen that there is a net conversion of NO to NO_2 which is accompanied by the formation of ozone and several other products, seemingly derived from NO_2; namely, $HONO_2$, HO_2NO_2, $ClNO_2$, and N_2O_5. Another major product, HCl, which can be observed, was not followed in this run because of the limited range of the wavelength response of the detector employed in this case. H_2O_2 was also identified as a major product of the system at long times, but the complete time dependence of it was not established here. In addition to these major products, small amounts of HONO (about 0.17 ppm maximum at about 1 min) and ClNO (about 0.07 ppm maximum at about 1 min) were formed as well in this experiment. In view of other work, one anticipates ClONO formation in this system; however, large absorptions due to $HONO_2$ and HO_2NO_2 in the 1700-1725 cm^{-1} region make unambiguous identification of this compound impossible here. Our best estimates suggest the maximum [ClONO] achieved is less than 0.3 ppm. Note that as the lights of the reactor were extinguished after 5.8 min irradiation, the concentrations of HO_2NO_2 and O_3 decreased as NO_2 and N_2O_5 increased somewhat; H_2O_2 also increased at this time (not shown). $HONO_2$ and $ClNO_2$ showed little change over the time scale covered here.

The chemical changes noted in Figure 10 can be rationalized qualitatively in terms of the reaction sequence 1-23 shown in the first section of Table 9. In the irradiated dilute mixtures of Cl_2, H_2, NO_2, and NO in air the reactions are initiated by the photolysis of Cl_2 in reaction (1):

$$Cl_2 + h\nu \rightarrow 2Cl \qquad (1)$$

We anticipate that the Cl-atoms will react largely in the competitive reactions (2), (3), and (4) with H_2, NO_2, or NO to form H-atoms, and the observed products $ClNO_2$ (or ClONO), and ClNO, respectively.

$$Cl + H_2 \rightarrow HCl + H \qquad (2)$$

$$Cl + NO_2\ (+M) \rightarrow ClNO_2\ (+M) \qquad (3a)$$

$$\rightarrow ClONO\ (+M) \qquad (3b)$$

$$Cl + NO\ (+M) \rightarrow ClNO\ (+M) \qquad (4)$$

In 700 torr of air, H-atoms will react almost exclusively with oxygen to develop HO_2 radicals in (6):

$$H + O_2\ (+M) \rightarrow HO_2\ (+M) \qquad (6)$$

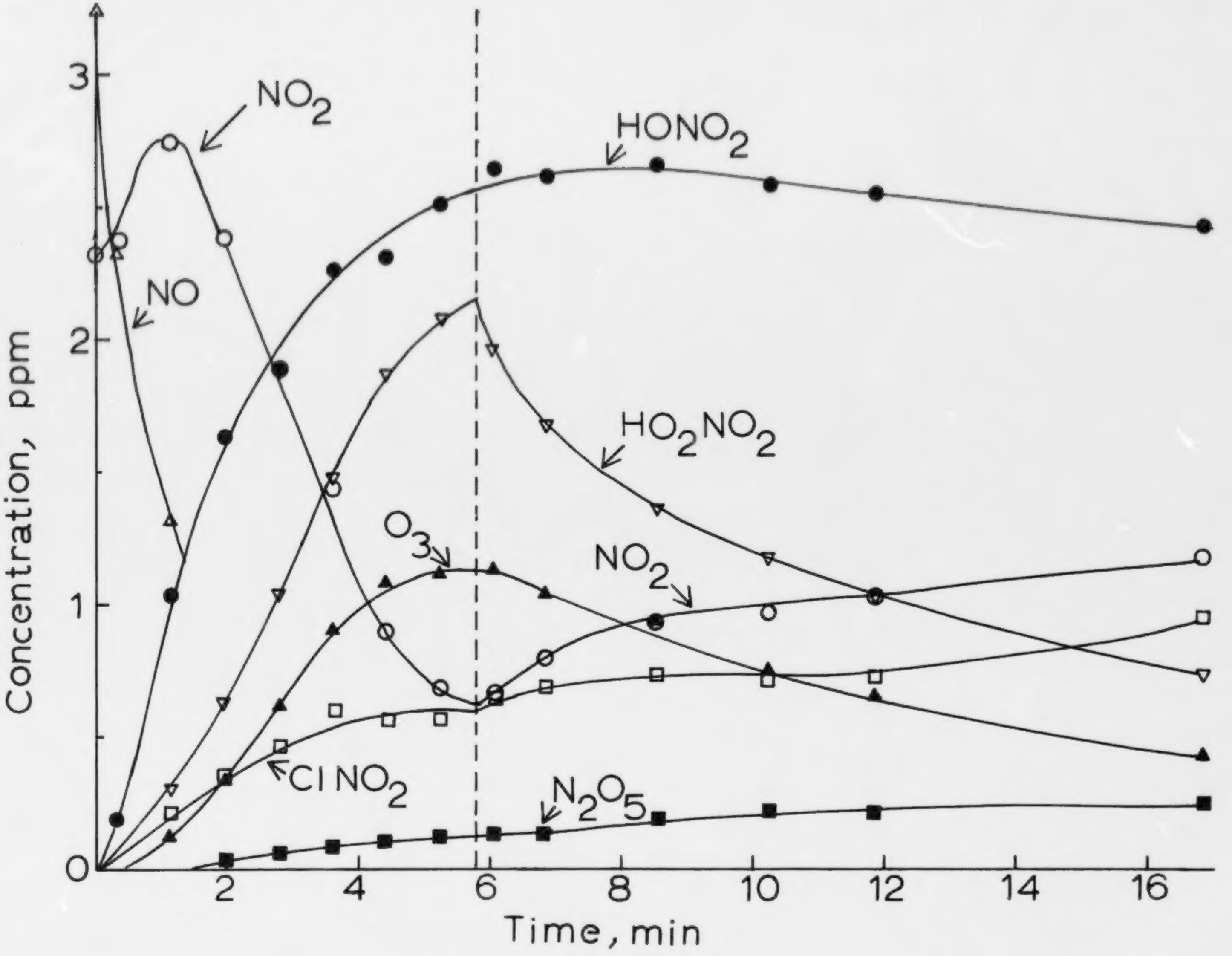

Figure 10. Time dependence of the major products of the photolysis of Cl_2(~7.5), H_2(8026), NO_2(2.32), and NO(3.25 ppm) in synthetic air (700 torr, 23°C); the irradiation was stopped at 5.8 min (vertical dashed line).

When the concentrations of NO_2 and NO are relatively large, the HO_2 radicals should react primarily with these gases; reaction with NO_2 forms HO_2NO_2 in (7), and with NO in (10) leads ultimately to HO-radicals and NO_2:

$$HO_2 + NO_2\ (+M) \rightarrow HO_2NO_2\ (+M) \tag{7}$$

$$HO_2 + NO \rightarrow HO + NO_2 \tag{10}$$

The reactive HO-radicals should generate additional H-atoms (and subseqently HO_2 radicals) in (12), $HONO_2$ in (13), and HONO in (14) through encounters with H_2, NO_2, and NO_2 respectively:

$$HO + H_2 \rightarrow H_2O + H \tag{12}$$

$$HO + NO_2\ (+M) \rightarrow HONO_2\ (+M) \tag{13}$$

$$HO + NO\ (+M) \rightarrow HONO\ (+M) \tag{14}$$

The products ClNO, ClONO, and HONO rise only to relatively low levels in this system, since they are photodissociated rapidly through reactions (5), (60), and (15):

$$ClNO + h\nu \rightarrow Cl + NO \tag{5}$$

$$ClONO + h\nu \rightarrow Cl + NO_2 \tag{60}$$

$$HONO + h\nu \rightarrow HO + NO \tag{15}$$

The ozone concentration in the mixture should be controlled largely by the rapid reactions (16), (17), and (18).

$$NO_2 + h\nu \rightarrow NO + O \tag{16}$$

$$O + O_2\ (+M) \rightarrow O_3\ (+M) \tag{17}$$

$$O_3 + NO \rightarrow O_2 + NO_2 \tag{18}$$

O-atoms formed in the photolysis of NO_2 will react mostly with O_2 in (17) to form O_3 in the O_2-rich system. O_3 destruction in reaction (18) with NO will be its dominant fate for our conditions. A photostationary state of O_3 should be established fairly rapidly for which $[O_3] \cong [NO_2]k_{16}/[NO]k_{18}$. Thus as the NO to NO_2 conversion proceeds in the system, the O_3 level is expected to rise, as we observe experimentally. As a significant ozone concentration develops, the oxidation of NO_2 to NO_3 may occur in (19), and the NO_3-radicals may combine with NO_2 in reaction (20) to form the observed product, N_2O_5:

$$O_3 + NO_2 \rightarrow O_2 + NO_3 \tag{19}$$

$$NO_3 + NO_2\ (+M) \rightarrow N_2O_5\ (+M) \tag{20}$$

As the lights were extinguished after 5.8 min irradiation in the experiment illustrated in Figure 10, the decay of HO_2NO_2 and the build-up of NO_2 and H_2O_2 (not shown) occurs, presumably through reactions (8) and (11).

$$HO_2NO_2\ (+M) \rightarrow HO_2 + NO_2\ (+M) \tag{8}$$

$$2HO_2 \rightarrow H_2O_2 + O_2 \tag{11}$$

The $[O_3]$ declines and $[N_2O_5]$ grows at early times in the dark as reactions (19) and (20) continue to occur. Thus the changes in the product concentrations with time can be rationalized qualitatively in terms of reasonable elementary reactions. Obviously quantitative considerations of these changes are necessary to test the mechanism properly. The complete mechanism which one anticipates for this system should include as well, the additional, although less important, reactions (24-65) which are listed in the later sections of Table 9. It is somewhat surprising that this seemingly simple system composed of only five reactive initial components, requires 65 elementary reactions to describe fairly completely the chemical changes which one either observes directly or anticipates in theory.

The rate constants which we have employed in this work are shown opposite each reaction in Table 9. For many of the reactions, reasonably good independent rate constant estimates have been made and can be used with confidence here. In several other cases no reliable published data are available for our conditions; for these reactions we have derived the needed constants in this work. The apparent first-order decay constants for the photochemical steps were estimated in our reactor as outlined in the experimental section. Rate constants for the thermal reactions (3), (4), (9), (10), (13), (14), (54), (55), and (56) were determined experimentally in this work (see the last section). Experimental estimates for k_{34}, k_{36}, and k_{42}, constants for steps which are relatively unimportant here, could not be had from this or other work; they were estimated by analogy with other similar reactions for which rate data were available.

There are several interesting features of the results which must be considered before the more quantitative tests of the mechanism are in order. Thus one must evaluate several possible alternative reactions leading to HO_2NO_2 formation and decay in our system; these are of special concern here in that they bear directly on our conclusions related to the predicted kinetic properties of HO_2NO_2 within the atmosphere.

Alternative Mechanisms for HO_2NO_2

There are a variety of possible reactions which in theory could lead to HO_2NO_2 formation in this system in addition to the obvious source in (7). It is important to evaluate the potential contribution of the reactions (68)-(72) in our system:

$$HO_2 + NO_2\ (+M) \rightarrow HO_2NO_2\ (+M) \tag{7}$$

$$ClNO_2 + H_2O_2 \rightleftarrows HO_2NO_2 + HCl \tag{68}$$

$$N_2O_5 + H_2O_2 \rightleftarrows HO_2NO_2 + HONO_2 \qquad (69)$$

$$HONO_2 + H_2O_2 \rightleftarrows HO_2NO_2 + H_2O \qquad (70)$$

$$HO + NO_3\ (+M) \rightarrow HO_2NO_2\ (+M) \qquad (71)$$

$$HO_2NO + O_3 \rightarrow HO_2NO_2 + O_2 \qquad (72)$$

H_2O_2 is expected as a product in this system by way of reaction (11), although its rate of generation is expected to be low at short irradiation times. Maximum values of few ppm were seen in some runs at long times. Thus this compound, together with the major products, $ClNO_2$, N_2O_5, and $HONO_2$, constitute the necessary reactants for the occurrence of (68), (69), and (70). In theory at least, reaction (69) could occur homogeneously. However if we take k_{69} to be equal to the measured rate constant for the analogous reaction (58),

$$N_2O_5 + H_2O \rightarrow 2HONO_2\ , \qquad (58)$$

then the homogeneous generation of HO_2NO_2 should be unimportant for the reactan reactant concentrations present in our system. It is not anticipated that the other complex reactions will occur significantly in the gas phase as homogeneous, elementary steps. However the estimated gas phase equilibrium constants for these reactions,* $K_{68} \cong 0.8$; $K_{69} \cong 6 \times 10^7$; $K_{70} \cong 9$ at 298 K, favor their consideration as potential wall-catalyzed reactions. These estimated equilibrium data are consistent with the HO_2NO_2 product yield results reported by Schwarz[34]; he attempted to prepare HO_2NO_2 in the liquid phase through these reactions. He was unsuccessful in making HO_2NO_2 by way of reaction (68) for which the equilibrium is not very favorable, but he employed both reactions (69) and (70) successfully. However the observed time dependence of the products suggests that these reactions do not contribute much, if any, to the HO_2NO_2 in our system at short times. Thus no induction period is observed for HO_2NO_2 formation in our experiments although this would certainly accompany the required delay in H_2O_2 formation in the initially unimportant reaction (11). Conceivably some HO_2NO_2 could arise from (69) at long times. Reaction (70) is a much less likely source. The magnitude of k_{70} and the maximum value of the product ratio, $[HONO_2][H_2O_2]/[H_2O] = 10^{-2}$ ppm, at long times, would restrict seriously the level of HO_2NO_2 ($\sim$0.09 ppm) which might be generated even if equilibrium were fully achieved by this path.

---

* In making these estimates the following approximate thermodynamic quantities were employed for $HO_2NO_2(g)$: $\Delta H f^o = -9.1$ kcal mole^{-1}(36,42,43); $S^o = 71.6$ eu (standard state, 1 atm).[50]

The coupling of HO and NO_3 species to form HO_2NO_2 in reaction (71) also seems to be unimportant here. The [HO] and $[NO_3]$ values anticipated from computer simulations of the present system, are much too low to allow appreciable HO_2NO_2 formation in (71), even in the unlikely event that the value of k_{71} is of the magnitude of the collision number. The significance of the potential reaction (72) is more difficult to evaluate, since the thermal and kinetic properties of the transient HO_2NO species [presumably formed by the collisional stabilization of the initially vibrationally-rich product of HO_2 and NO encounters, reaction (10)] can only be inferred now from those observed in solution studies.[51,52] If the concentration of HO_2NO reaches the theoretically possible maximum values (near the ppb level) and $k_{72} \geq 70$ $ppm^{-1}min^{-1}$, then (72) may be a significant cource of HO_2NO_2 in our system. However we observed that the analogous homogeneous reaction (73) of HONO with O_3,

$$HONO + O_3 \rightarrow HONO_2 + O_2 \, , \tag{73}$$

for which a very similar change in enthalpy occurs ($\Delta H_{72} \cong -50$; $\Delta H_{73} \cong -48$ kcal $mole^{-1}$), is very slow with $k_{73} \leq 4 \times 10^{-4}$ $ppm^{-1}min^{-1}$. In view of these findings, we expect reaction (72) to be unimportant here as well.

Thus we conclude that reaction (7) is probably the dominant source of HO_2NO_2 in our system, and the several other potential sources, reactions (68)-(72), may be neglected in our further considerations here. It appears that the present system does provide a good homogeneous source of HO_2NO_2 for reaction rate studies.

The Decay Mechanism for HO_2NO_2

In the previous room temperature, gas phase, infrared studies by Niki et al.[37], Levine et al.[41] and Hanst and Gay,[40] first-order decay kinetics of HO_2NO_2 was observed $\tau_{1/2}$ = 10, 8, and 10-15 min, respectively. The mechanism of the decay was either unexplained[40] or attributed to an undefined wall loss.[37,41] In this work some new and mechanistically important observations of HO_2NO_2 decay kinetics have been made. In one series of experiments we have followed $[HO_2NO_2]$ decay during the dark period following photolysis of dilute mixtures of Cl_2, H_2, and NO_2 in air (700 torr). The $\ell n[HO_2NO_2]$- versus-time plots of the data from two such experiments carried out at 24.4 and 23.3°C are shown in Figure 11. At long times the decay of HO_2NO_2 follows well a first-order decay law, as was observed and reported previously. However, note that there is a significant curvature to the first-order plots at short times for these runs in which $[HO_2NO_2]$ is relatively high and $[NO_2]$ is low; this interesting effect was apparently missed by previous workers. The complete set of data from a given experiment can be described reasonably well using an empirical rate law of the form (74):

$$-\frac{d[HO_2NO_2]}{dt} = [HO_2NO_2]^2 k_{II} + [HC_2NO_2] k_I \tag{74}$$

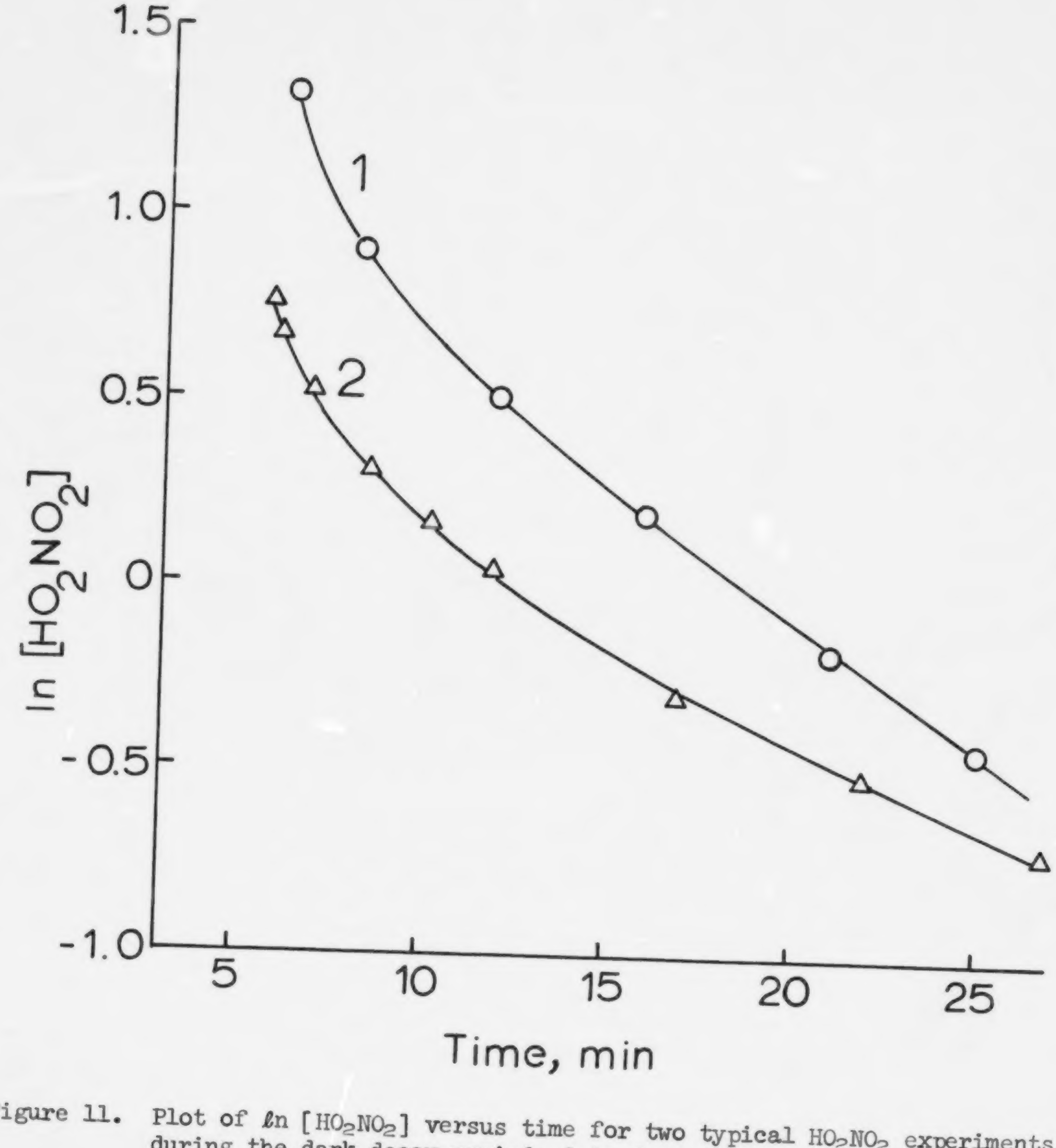

Figure 11. Plot of ℓn $[HO_2NO_2]$ versus time for two typical HO_2NO_2 experiments during the dark decay period; data from Cl_2, H_2, NO_x, air mixture photolyses; temperatures at the onset of the dark period were 24.4°C (curve 1) and 23.3° (curve 2); the initial and final slopes of the plots were used in deriving estimates of k_8/k_7 using relation (94) of the text.

TYPING GUIDE SHEET

It is instructive to consider and evaluate the mechanisms which lead to this result. In recent studies Cox and Derwent,[42] Graham et al.,[43] and Baldwin et al.,[50] have presented evidence that the homogeneous dissociation of HO_2NO_2 in reaction (8) occurs readily at room temperature, and it is now evident that this reaction must be included in our considerations.

$$HO_2NO_2\ (+M) \rightarrow HO_2 + NO_2\ (+M) \qquad (8)$$

HO_2NO_2 may be reformed from HO_2 and NO_2 molecules by the rapid association reaction (7), or the removal of HO_2, and the net loss of HO_2NO_2 may occur by reactions of HO_2 with other HO_2-radicals, O_3, NO, or conceivably other reactive molecules present in the system:

$$HO_2 + NO_2\ (+M) \rightarrow HO_2NO_2(+M) \qquad (7)$$

$$HO_2 + HO_2 \rightarrow H_2O_2 + O_2 \qquad (11)$$

$$HO_2 + NO \rightarrow HO + NO_2 \qquad (10)$$

$$HO_2 + O_3 \rightarrow HO + 2O_2 \qquad (47)$$

In HO_2NO_2 decay experiments with an added excess of NO,[42,43,53] the capture of HO_2 radicals released in (8) is ensured through the rapid reaction (10). For these conditions the decay of HO_2NO_2 is controlled by the rate of (8), and direct estimates of k_8 have been made from such data.[42,43,53] For our experimental conditions the [NO] at the beginning of the dark period is very low (<0.05 ppm), and this trace of NO is quickly oxidized by the remaining ozone (~ 1.7ppm) in reaction (18) as well as in reaction (10). Using the experimental values for k_7, k_8, k_{10}, k_{11}, and k_{47}, together with the measured concentrations of HO_2NO_2, O_3, NO, and NO_2 in our system, simulations show that reaction (11) should be the dominant homogeneous HO_2 loss reaction at early times in the dark experiments where NO_2 and NO concentrations are low. Furthermore the expected rates of (10) and (47) are much less than the observed $-R_{HO_2NO_2}$ at all times. Thus it appears reasonable to rationalize the first term of relation (74) through the reaction sequence (8), (7), and (11):

$$HO_2NO_2\ (+M) \rightleftarrows HO_2 + NO_2\ (+M) \qquad (8,7)$$

$$2HO_2 \rightarrow H_2O_2 + O_2 \qquad (11)$$

For our conditions $R_8 \cong R_7 > R_{11}$ so that the $[HO_2]$ will be given approximately by relation (75):

$$[HO_2] \cong [HO_2NO_2]k_8/[NO_2]k_7 \qquad (75)$$

If $[NO_2]$ is near constant during a given time interval and HO_2NO_2 decay occurs by this path alone, then a loss rate which is approximately second-order in HO_2NO_2 is anticipated:

EPA-287 (Cin.)
(4-76)

TYPING GUIDE SHEET
BEGIN FIRST LINE OF TEXT HERE
CENTER OF PAGE
TOP OF IMAGE AREA
DROPPED HEAD BEGIN SECTIONS HERE

$$-\frac{d[HO_2NO_2]}{dt} \cong [HO_2]^2\, 2k_{11} \cong [HO_2NO_2]^2\, (k_8/k_7[NO_2])^2 2k_{11} \qquad (76)$$

In terms of this mechanism choice, we expect that the apparent second-order rate constant k_{II} in relation (74) to be related to the function, $(k_8/k_7[NO_2])^2 2k_{11}$. We can test this postulate later after defining the origin of the first-order loss term k_I in (74).

We recognized that the addition of a large excess of NO_2 to the HO_2NO_2-containing system in the dark, should suppress HO_2NO_2 decay, provided that the mechanism (7), (8), and (11) alone describes HO_2NO_2 decay in our system and that the only product of the HO_2 interaction with NO_2 is HO_2NO_2. In order to test this hypothesis we followed HO_2NO_2 decay in otherwise identical experiments to which a large excess of NO_2 (100 ppm) was added in one mixture after the light period; while in the other matched run, the $[NO_2]$ was near the 1 ppm level of the NO_2 reactant which remained after the irradiation. In these experiments the final [NO] was very low, and reaction (10) was unimportant. These data from a set of experiments near 26.5°C are shown in Figure 12. Obviously the HO_2NO_2 decay over the time span studied here does not follow the relation (76), but it is described well by a first-ordered law. In addition, note in Figure 12 that there is very little suppression of the HO_2NO_2 first-order decay rate upon addition of 100 ppm of NO_2; only a factor of about 1.5 is seen between the decay constants of the matched runs without (~1 ppm) and with added NO_2 (100 ppm). If reactions (7) and (8) were the most important sinks and sources for HO_2 in these systems, and a steady-state level of HO_2 were established, then in the runs with excess NO_2, the $[HO_2]$ should be 1/100th of that in the experiments with low $[NO_2]$. Thus the loss of HO_2 through (11) should occur at a rate of only 1/10,000th of that in the matched experiment without NO_2 added. Reactions other than those with NO_2 which are first-order in HO_2 should occur at about 1/100th of the rate in the experiments with NO_2 added. Obviously the decay of HO_2NO_2, both in the presence of excess NO_2 and at long times in the low $[NO_2]$ experiments, is not described well by the reactions (7), (8), and (11) alone. Let us consider some alternative mechanisms which may rationalize these results.

There are three possible mechanistic alternatives which we should evaluate in our attempts to explain the experimentally observed HO_2NO_2 first-order dark decay. Presumably HO_2NO_2 is in near equilibrium with NO_2 and HO_2 in the rapid reactions (7) and (8):

$$HO_2NO_2\ (+M) \rightleftarrows HO_2 + NO_2\ (+M) \qquad (8,7)$$

Then in theory a first-order loss of HO_2NO_2 may result from any of the following: (1) the slow bleed-off of HO_2 radicals in the homogeneous reaction (49); (2) the slow, homogeneous, first-order rearrangement of HO_2NO_2 to HONO and O_2 in (77); or (3) the slow removal of HO_2NO_2 at the wall of the cell in (9):

$$HO_2 + NO_2 \rightarrow HONO + O_2 \qquad (49)$$

BEGIN LAST LINE OF TEXT
BOTTOM OF IMAGE AREA; OUTSIDE DIMENSION FOR TABLES AND ILLUSTRATIONS

PAGE NUMBER
EPA-287 (Cin.) (4-76)

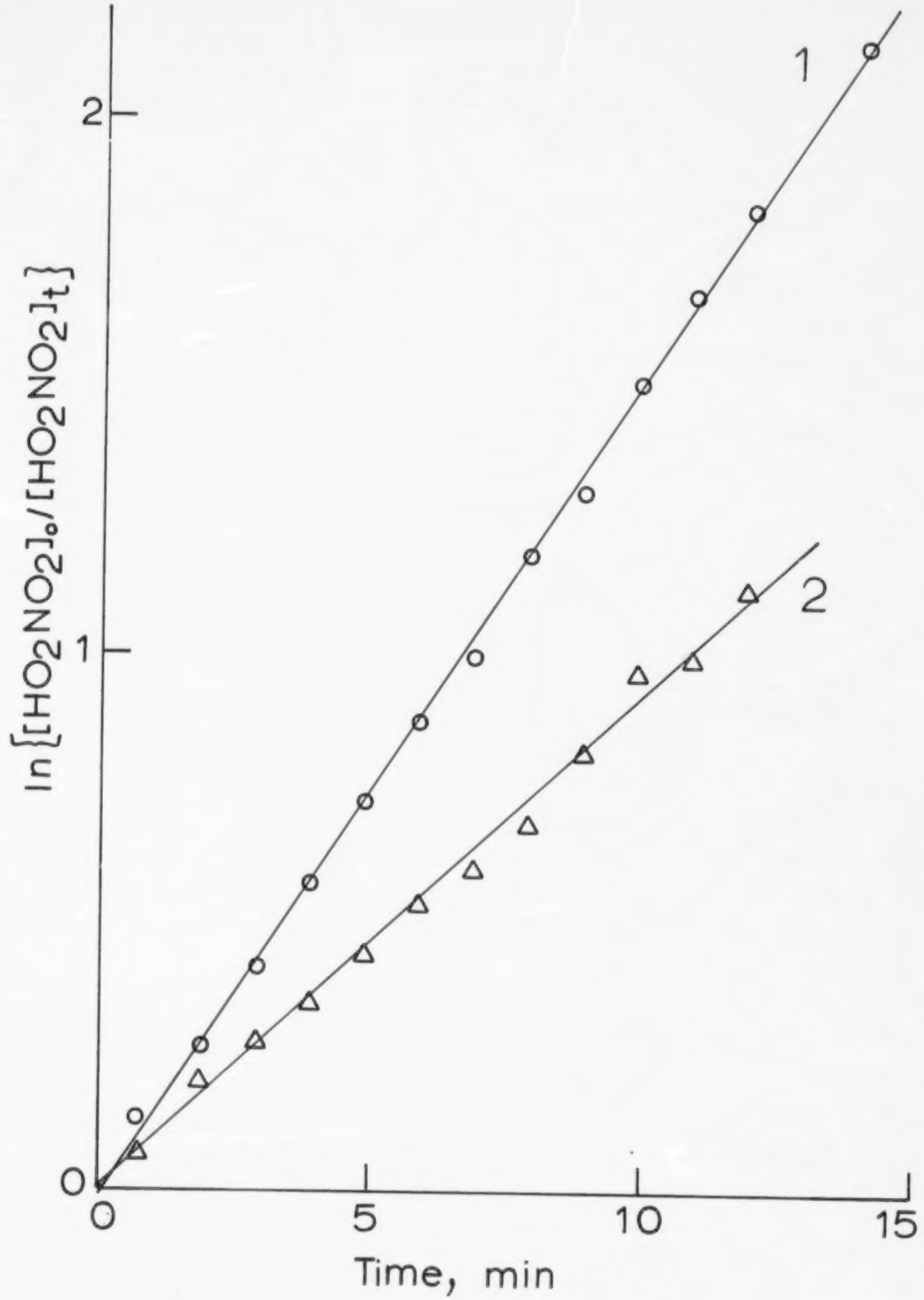

Figure 12. First-order plots of the dark decay of HO_2NO_2 in near identical experiments to which 100 ppm of NO_2 were added in one (curve 2) and in the other only about 1 ppm of NO_2 was present (curve 1); initial concentrations (ppm): Cl_2, 20; H_2, 26,300; NO_2, 10.8; in air (700 torr; temp., 27.2 (curve 1), 26.0° (curve 2); data for curve 1 excluded the earliest time regime where the second-order contribution to HO_2NO_2 decay was observed.

$$HO_2NO_2\ (+M) \rightarrow HONO + O_2\ (+M) \qquad (77)$$

$$HO_2NO_2 + Wall \rightarrow HONO_2 + {}^1\!/\!_2 O_2 \text{ (or other products)} \qquad (9)$$

All three mechanisms are consistent with both the observed first-order decay of HO_2NO_2 at long times, and the relative insensitivity of the rate to added NO_2 gas.

First consider the occurrence of (49) with (7) and (8). In experiments with added NO_2, the HO_2 radical concentration would be greatly suppressed such that $R_{49} \gg R_{11}$. For these conditions one expects the observed first-order decay region to be described by (78):

$$\frac{d[HO_2NO_2]}{dt} \cong [HO_2NO_2]\ \{1 - k_7\ (k_7 + k_{49})\}\ k_8 \qquad (78)$$

In terms of this mechanism the apparent first-order rate constant is a function of k_7, k_8, and k_{49}. Using estimates of k_7 and k_8 from the pressure- and temperature-dependent functions reported by Graham *et al.*[53] together with the apparent first-order decay constants observed in our experiments with the 100 ppm of NO_2 added, 0.0936 ± 0.0026 at 26.0°C and 0.0495 ± 0.0042 at 20.6°C, one estimates $k_{49} \cong 32$ (26°) and 35 $ppm^{-1}min^{-1}$ (20.6°C). It is interesting to apply this acheme to the data of Graham *et al.*,[53] for 4.5°C; this gives $k_{49} \cong 12.8 \pm 1.2\ ppm^{-1}min^{-1}$, independent of added N_2 pressure (10-700 torr). However using the same treatment on the Graham *et al.*,[53] data for -12°C, we get values of k_{49} which vary widely with pressure, and obviously they do not follow the expectations based upon relation (78). If we use only our data for 26 and 20.6°C and that of Graham *et al.*,[53] for 4.5°C, which are in accord with relation (78), we extimate $k_{49} \cong 1.6 \times 10^7\ e^{-(7.7\ kcal\ mole^{-1})/RT} ppm^{-1}min^{-1}$. If this mechanism were operative then the temperature dependence of the hypothetical reaction (49) would require that the fraction of HO_2 radicals reacting through it decrease markedly at low temperatures and high pressures as reaction (7) becomes favored. However for the experimental conditions used by Howard[44] in the measurement of the rate constant for reaction (7) (i.e., room temperature, low pressures), this mechanism choice including (49) requires that this reaction dominate over the thermolecular reaction (7). This expectation is contrary to the experimental observations of Howard; he estimated that $k_{49} \leq 4.4\ ppm^{-1}min^{-1}$ at 27°C. Graham *et al.*,[53] did not observe HONO in the products of HO_2NO_2 decay and concluded that $k_{49} \leq 0.0005\ k_7$ at 1 atm pressure and temperatures in the range from -19 to 10°C, or $k_7 \leq 0.8\ ppm^{-1}min^{-1}$. Thus this alternative mechanism including (49) is incompatible with the findings of Howard[44] and Graham *et al.*[53] If k_7 at room temperature and 1 atm pressure is a factor of 10 or 20 lower than that estimated by Graham *et al.*,[53] then the HO_2NO_2 decay scheme of reactions (8), (7), (49) and (11) becomes a viable alternative. This seems to be unlikely. The apparent need for the relatively rapid rate of the possible reaction (49) forming HONO and O_2 products in our previous study[41] is removed when the then unknown reaction (8) is included in our reaction mechanism. Although the present data and those of other workers can not exclude the occurrence of (49) to a small extent in these systems, we now concur with the conclusions from other recent investigations[37,41,42,44,53] that the dominant mode of HO_2-NO_2 interaction leads to HO_2NO_2 formation in reaction (7).

Consider the second alternative of HO_2NO_2 decay by internal rearrangement in reaction (77). Presumably this would occur through the transfer of an H-atom and the subsequent or simultaneous loss of an O_2 molecule as HONO is formed:

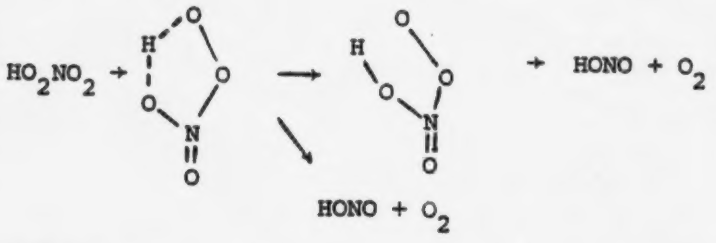

(77a)

(77b)

A spin inversion must occur at some point in the reaction if the O_2 product molecule is to be formed in its ground state. The overall enthalpy change for reaction (77) forming $O_2(^3\Sigma_g^-)$ is $\Delta H_{77} \cong -9.5$ kcal mole^{-1}. If spin were conserved throughout the reaction and O_2 were formed originally in the $^1\Delta_g$ state, then $\Delta H_{77} \cong +13$ kcal mole^{-1}. Hendry and Kenley[54] estimated theoretically that $E_{77} \geqq 21$ kcal mole^{-1}, with $O_2(^1\Delta_g)$ as the product. In view of this and the low preexponential factor required in theory for the cyclic transition state of (77), they concluded that HO_2NO_2 decay forming $O_2(^1\Delta_g)$ and HONO would not compete with the HO_2NO_2 decay reaction (8). It is interesting to consider the present data in terms of reaction (77) and to estimate the apparent rate constant k_{77}. An Arrhenius plot of the available, first-order HO_2NO_2 decay constants from our NO_2-added experiments and those of Graham et al.[53] is shown in Figure 13. Our data fit a reasonably good linear form consistent with the occurrence of (77) and with $k_{77} \cong 2.2 \times 10^{10}$ $e^{-(15.6 \pm 3.4 \text{ kcal/mole})/RT}$ min^{-1}. It is interesting and perhaps significant that the extrapolation of our Arrhenius line intercepts one of the low-temperature data points derived from the work of Graham et al.[53] This suggests only that whatever the nature of the first-order loss reaction for HO_2NO_2, the same mechanism may apply to both our system and that of Graham et al.[53] The relatively low activation energy and the small preexponential factor observed experimentally for the first-order HO_2NO_2 dark decay here, appear to be consistent with the occurrence of reaction (77) with the O_2 product in the ground state. In contrast to the case for reaction (49), this mechanism and our kinetic results are not in conflict with the kinetic observations of Howard[44] and Graham et al.[53] However there is another serious problem which argues strongly against the significant occurrence of this mechanism. We and others have not observed the expected HONO product of the dark decay of HO_2NO_2 by reaction (77). In view of the findings of Kaiser and Wu that HONO and $HONO_2$ react at a significant rate,[55] it is possible that if HONO were formed in (77), its removal by reaction with the major product $HONO_2$ in (56) might keep the resulting [HONO] at the very low values we observed:

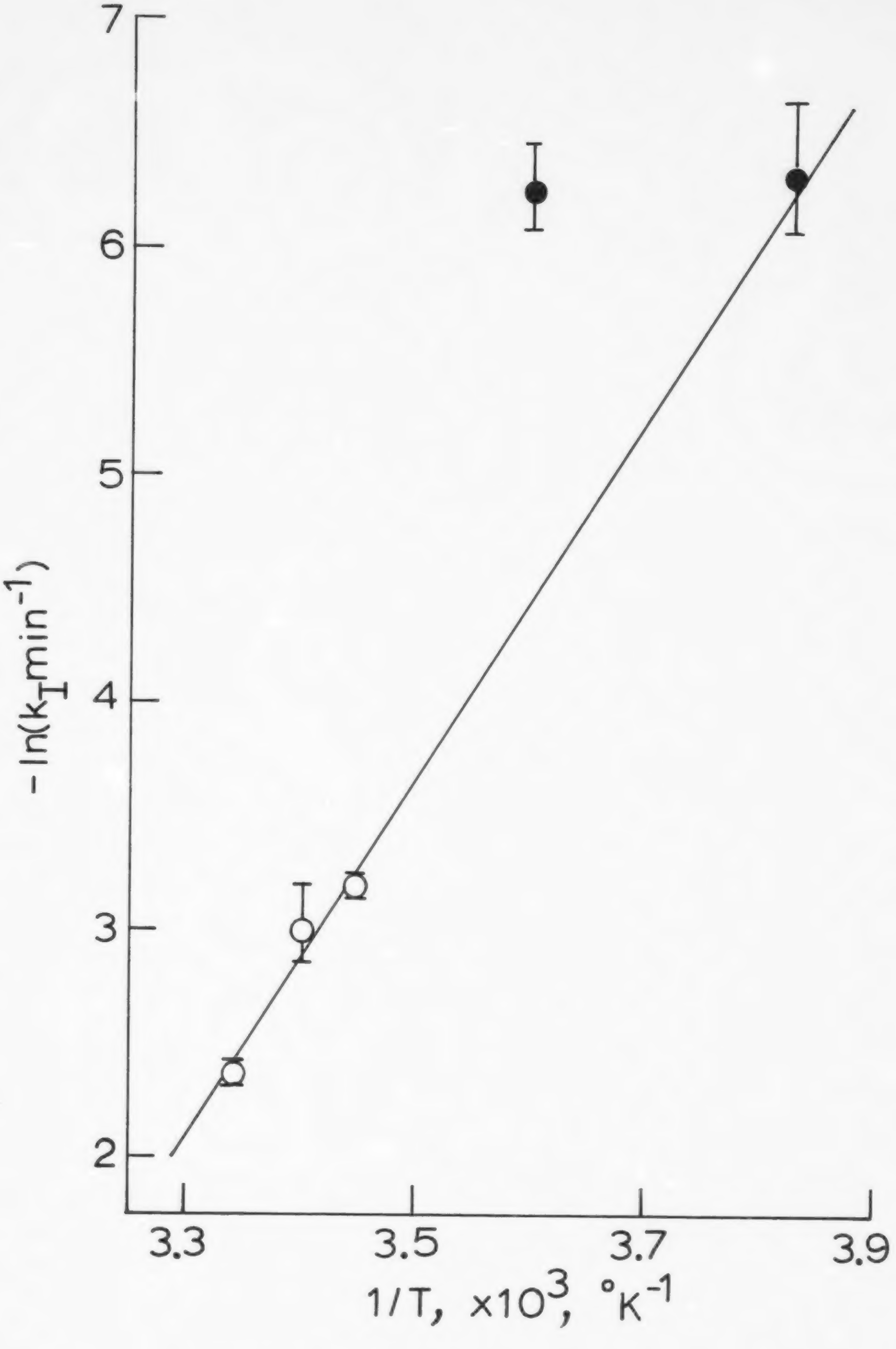

Figure 13. An Arrhenius plot of the first-order decay constants from the dark decay of HO_2NO_2 in gaseous mixtures with 100 ppm of NO_2 added; open circles are from this work and closed circles from the studies of Graham et al.[53]; the line drawn represents the least-squares fit of our data.

$$HONO + HONO_2 \rightarrow 2NO_2 + H_2O \qquad (56)$$

However we find that the apparent second-order rate constant for reaction (56) in our system, $k_{56} \cong (9.6 \pm 0.3) \times 10^{-3}$ ppm^{-1} min^{-1} (24.6°C), together with the occurrence of reaction (77), would lead to a readily observable increase in HONO, which in fact is not the case. Thus we must conclude that although the occurrence of reaction (77) is consistent with the observed kinetics, it also is probably an unimportant pathway for HO_2NO_2 decay for our conditions. If presently unidentified HONO removal paths are subsequently found in this system, obviously reactions (49) and (77) must be reconsidered.

We favor the third alternative, reaction (9), in explanation of the observed HO_2NO_2 first-order decay in our system. This suggests that the decay of HO_2NO_2 in the presence of a large excess of NO_2 is a consequence of a first-order removal of HO_2NO_2 at the wall of the reaction vessel. Note that for our experimental conditions the theoretical rate of diffusional transport of HO_2NO_2 to the wall is consistent with this hypothesis. Thus at 294 K the observed first-order rate constant for HO_2NO_2 loss was about 0.05 min^{-1}, while the apparent first-order rate constant for the reaction of HO_2NO_2 diffusion a distance equal to the radius of our reaction vessel ($r = 15$ cm) in air at 700 torr and 25°C should be about 0.03 min^{-1}; $k = D/r^2$, where $D = 0.1$ cm^{2}s^{-1}. Graham et al.[53] proposed that their observed loss reaction for HO_2NO_2 was a result of an unspecified reaction of either HO_2 or NO_2NO_2 at the wall. The very large radius of their reaction cell demands a much greater time for molecular diffusion to the wall than in our case. We would expect an apparent first-order constant of about 10^{-5}s^{-1} for $P_{N_2} = 700$ torr. This is in accord with the values they found, 1.7-5.2 x 10^{-5}s^{-1}. However the apparent agreement between the diffusional transport rates and observed loss rates is somewhat fortuitous, since in Graham's experiments the first-order rate constant for wall loss was seemingly independent of added gas pressure over a wide range (1-760 torr).

In order to test the nature of the HO_2NO_2 loss reaction in our system we have followed HO_2NO_2 decay in separate experiments at 100 torr total pressure. The observed first-order rate constant for the loss of HO_2NO_2 with 100 ppm of NO_2 added, 0.0411 ± 0.0007 at 16.7°C, shows no significant change from those measured at 700 torr pressure when proper account is taken of the temperature differences. Thus if we invoke the reaction (9) to rationalize HO_2NO_2 loss in experiments with added NO_2, then transport of HO_2NO_2 to the wall cannot be rate limiting, but the chemical reaction at the wall must control this rate. This requirement is supported by the strong temperature dependence of the first-order decay constant observed in both experiments, with or without added NO_2. If this mechanism choice is operative then the compatibility of our data with that of Graham et al.[53] (Figure 13) suggests that there is little difference between the nature of wall reaction (9) on the Teflon wall of Graham et al.[53] and the borosilicate glass wall used in our studies. The very large effect of temperature on the first-order decay constant is inconsistent with a rate process controlled by diffusion but supports the hypothesis of a chemical, rate-limiting step. If reaction (9) is important here, the rapid transport of HO_2NO_2 to the walls by processes other than molecular diffusion, presumably turbulent diffusion resulting from temperature gradients, etc., must occur, and the equilibration of gaseous absorbed species with the wall must also be fast. For these conditions the mechanism may involve (79) and (80):

$$HO_2NO_2(g) \rightleftarrows HO_2NO_2(\text{Wall}) \qquad (79)$$

$$HO_2NO_2(\text{Wall}) \rightarrow \text{Products} \qquad (80)$$

In this case the rate law should be given by (81):

$$-\frac{d[HO_2NO_2]}{dt} = [HO_2NO_2]k_{79}k_{80} \qquad (80)$$

Here $k_9 = K_{79}k_{80}$ and $E_9 = \Delta H_{79} + E_{80}$. If one couples the observed value of $E_9 \cong 15.6 \pm 3.4$ with a reasonable estimate for $\Delta H_{79} \cong -7$, he estimates $E_{80} \cong 23 \pm 3$ kcal mole^{-1}, a value in the range of those observed for the homogeneous decay of HO_2NO_2 in reaction (8): $E \cong 25$[37], 23 ± 2[43], 20.7 ± 0.5[44], and 19.9 ± 0.5 kcal mole^{-1}.[50] This similarity supports the hypothesis that the loss of HO_2NO_2 at the wall may involve the same elementary step (i.e., the rupture of the HO_2-NO_2 bond) as in the homogeneous gas phase reaction (8):

$$HO_2NO_2(\text{Wall}) \rightarrow HO_2(\text{Wall}) + NO_2(\text{Wall}) \qquad (80a)$$

The choice of the wall loss mechanism for the HO_2NO_2 first-order decay is also favored by the finite, but not negligible, difference between the apparent rate constants with and without added NO_2. The factor of about 1.5 lowering of the first-order dark decay constant with a 100-fold increase in the NO_2 present can not be rationalized in terms of the possible mechanisms involving reactions (49) or (77) considered previously. In terms of the occurrence of reaction (9), the observed decrease in k_9 with increased NO_2 may reflect the changed nature of the wall surface and its efficiency for HO_2NO_2 decay. The surface loading of absorbed NO_2 molecules must be increased with 100 ppm of NO_2 added. This may increase the rate of recapture of HO_2 radicals formed at the wall in (80a) and lead to a lowered rate of HO_2NO_2 decay. Although successive experiments gave reproducible values for k_9 at a given temperature and NO_2 pressure, experiments made over a long period of time showed variations in k_9 which one would associate with a heterogeneous reaction such as (9). Thus although we had anticipated that homogeneous decay mechanisms for HO_2NO_2 would be favored in our system with its relatively low surfact-to-volume ratio, all of our observations of the first-order HO_2NO_2 loss reaction point to the occurrence of the heterogeneous process (9).

In principle the nature of the products formed as HO_2NO_2 decays in the dark could help to establish the details of the HO_2NO_2 first-order decomposition mechanism. Reaction (11) is unimportant in the dark decay of HO_2NO_2 in runs with added NO_2, and the nature of the products formed in these experiments should provide the best insight into the nature of reaction (9). In an experiment at 26°C with 100 ppm of NO_2 added (an experiment from which the HO_2NO_2 decay data of curve 2 of Figure 12 were derived), the following overall chemical changes can be inferred from the observed IR-spectral changes which occurred in a 12 min dark period and the required mass balance for Cl, N, O, and H: $6.2\ NO_2 + 0.64\ N_2O_5 + 0.73\ O_3 + 2.0\ HO_2NO_2 + 2.4\ Cl_2 + 2.4\ HCl \rightarrow 2.2\ O_2 + 2.3\ HONO_2 + 6.1\ ClNO_2 + 1.0\ NOCl + 1.0\ H_2O$; here the coefficients represent the ppm of the reactant or product used or formed during the dark period. One set of reactions which are consistent with these net changes are the following:

	Reaction extent, (ppm)	Approximate equilibrium constant (gases 25°C)
(82) HO_2NO_2 (Wall) $\rightarrow$ HONO (Wall) + O_2	1.0, HO_2NO_2	1.0×10^{21} ppm
(83) HO_2NO_2 (Wall) $\rightarrow$ $HONO_2$ (Wall) + $\frac{1}{2}O_2$	1.0, HO_2NO_2	4.2×10^{3} ppm$^{1/2}$
(84) HONO + HCl (Wall) $\rightarrow$ H_2O + NOCl (Wall)	1.0, HONO	2.0×10^{4}
(19) $O_3 + NO_2 \rightarrow O_2 + NO_3$	0.73, O_3	
(20) $NO_3 + NO_2 \rightarrow N_2O_5$	0.73, NO_3	
(85) N_2O_5 + HCl(Wall) $\rightarrow$ $ClNO_2$ + $HONO_2$ (Wall)	1.37, N_2O_5	4.7×10^{7}
(86) $NO_2 + \frac{1}{2}Cl_2$ (Wall) $\rightarrow$ $ClNO_2$ (Wall)	4.7, NO_2	1.5×10^{1} ppm$^{-1/2}$

The equilibrium constants are favorable for the significant occurrence of each of the heterogeneous steps. According to this scheme HO_2NO_2 decay at the reactor surface may lead initially to HONO and $HONO_2$ products in the experiments at high $[NO_2]$. In view of the temperature dependence of the wall reaction, the primary step in the decay sequence (82)-(86) may be reaction (80a):

$$HO_2NO_2\ (Wall) \rightarrow HO_2\ (Wall) + NO_2\ (Wall) \tag{80a}$$

The net chemical changes observed may be rationalized through the sequential, heterogeneous reactions (80a) and (87)-(93), together with (19) and (20):

$$HO_2 + NO_2\ (Wall) \rightarrow HONO\ (Wall) + O_2 \tag{87}$$

$$2HONO\ (Wall) \rightarrow NO + NO_2 + H_2O\ (Wall) \tag{88}$$

$$HO_2 + NO\ (Wall) \rightarrow HO + NO_2\ (Wall) \tag{89}$$

$$HO + NO_2\ (Wall) \rightarrow HONO_2\ (Wall) \tag{90}$$

$$HONO + H^+\ (Wall) \rightarrow H_2ONO^+\ (Wall) \tag{91}$$

$$H_2ONO^+\ (Wall) = NO^+ + H_2O\ (Wall) \tag{92}$$

$$NO^+ + Cl^-\ (Wall) \rightarrow ClNO\ (Wall) \tag{93}$$

In summary we conclude that the dark decay of HO_2NO_2 which we and others have observed is consistent with the simultaneous occurrence of the homogeneous decomposition reaction (8) and a first-order, heterogeneous wall loss of HO_2NO_2 which leads to a variety of final products including $HONO_2$, $ClNO$, etc., in our system. The present data show the dominant loss reaction for HO_2NO_2 in the Cl_2, H_2, NO_x, air systems for $[HO_2NO_2]/[NO_2]^2 < 0.2$ ppm^{-1}, is the heterogeneous decay at the wall of the reactor. Obviously the clean atmosphere analogue to this process would be the interaction of HO_2NO_2 with aerosol particles, the ground, or other surfaces. Thus HO_2NO_2 decay by such processes is expected to be relatively minor in the atmosphere where the surface area available to the HO_2NO_2 is very small.

A Kinetic Test of HO_2NO_2 Decay Mechanisms and the Equilibrium Constant for the System, $HO_2NO_2 \rightleftarrows HO_2 + NO_2$

Having arrived at a reasonable mechanism for the HO_2NO_2 empirical decay law observed in this work [relation (74)] we may test in a more quantitative fashion the suggested HO_2NO_2 decay mechanism (7), (8), (9), and (11), using the data of Figure 11 and other similar data from experiments at several temperatures. From relations (74) and (76) we expect (94) to hold:

$$(k_8/k_7)^2 2k_{11} = \left\{ \left[-\frac{d\ \ln[HO_2NO_2]}{dt} \right]_t - k_9 \right\} \frac{[NO_2]_t^{\,2}}{[HO_2NO_2]_t} \qquad (94)$$

From the $\ln[HO_2NO_2]$-versus-time plots (Figure 11 and other similar data), we have measured the slopes at the beginning of the dark period ($d\ \ln[HO_2NO_2]_o/dt$), the $[NO_2]_o$ and $[HO_2NO_2]_o$ values for the same time, and the slope of the linear portion of the plot at long times (k_9). These data for experiments at several temperatures are summarized in Table 10. Coupling these estimates with the literature value for $k_{11} = 5.3 \times 10^3$ ppm^{-1}min^{-1},[50] values of $K_8 = k_8/k_7$ were calculated using relation (94). In the last two columns of Table 10 these estimates are compared with those calculated using the temperature-dependent functions for k_8 and k_7 from the work of Graham et al.,[53] and Howard.[44] The agreement is excellent. The present results certainly provide an independent confirmation of the reliability of the direct rate constant estimates, and supports indirectly the assumption made by Graham et al.[53] that $E_7 \cong -2.0$ kcal mole^{-1}. Figure 14 shows a plot of $\ln k_8/k_7$ versus $1/T$ using the present data. A reasonably good linear relationship between the variables is seen, and, within the error of the data, they follow well the dashed line which is the locus of points derived from the functions of Graham et al.[53] From the present data we estimate $\Delta E_8^o \cong 23.8 \pm 2.7\ (2\sigma)$ kcal mole^{-1}, $\Delta S_8^o \cong 40.5 \pm 8.8\ (2\sigma)$ eu (standard state, 1 atm). The functions of Graham et al.[53] give $\Delta E_8^o \cong 21.9$; $\Delta H_8^o \cong 22.5$ kcal mole^{-1}, $\Delta S_8^o \cong 36$ eu (standard state, 1 atm). The temperature range of our data is much too small to provide accurate thermodynamic data related to K_8, but the results appear reasonable. If one accepts the theoretical estimate of S^o for $HO_2NO_2 \cong 71.6$ eu of Baldwin et al.[50], then $\Delta S_8^o \cong 40.2$ eu (1 atm, standard state). If we accept the magnitude of our k_8/k_7 estimates together with this value of ΔS_8^o as correct, we derive our present best estimate of $\Delta H_8^o \cong 23.7$ kcal mole^{-1} from which we estimate $\Delta H_f^o(HO_2NO_2) \cong -10.8$ kcal mole^{-1} (25°C).

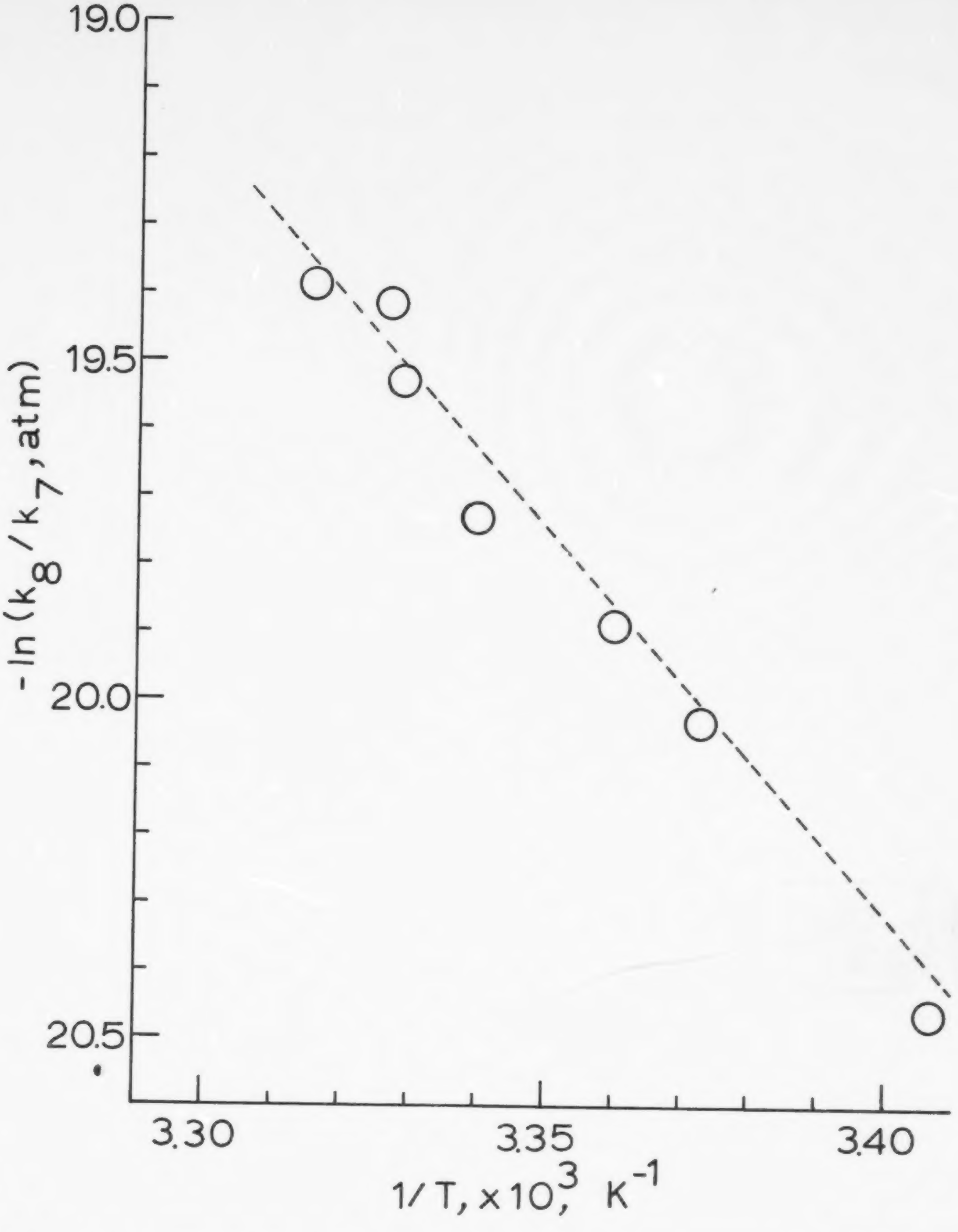

Figure 14. Plot of the ln (k_8/k_7) versus 1/T; open circles are from our estimates employing relation (94) and initial rate data for HO_2NO_2 dark decay; the dashed line is the locus of points predicted from the individual rate constant functions for k_7 and k_8 estimated from the results of Graham et al.[53] and Howard[44].

TABLE 10. RATE DATA FROM THE DARK DECAY OF HO_2NO_2 AND ESTIMATES OF THE EQUILIBRIUM CONSTANT k_8/k_7 FOR THE SYSTEM: $HO_2NO_2 \rightleftarrows HO_2 + NO_2$ (8,7)

Temp. (°C)	$\frac{-d\ \ln[HO_2NO_2]_o}{dt}$	k_9 (min^{-1})	$[NO_2]_o$ (ppm)	$[HO_2NO_2]_o$ (ppm)	k_8/k_7, atm x 10^9 This work[a]	Refs. 44, 53[b]
28.4	0.29	0.166	1.9	2.87	3.8	3.9
27.4	0.21	0.147	2.4	2.54	3.7	3.5
27.2	0.30	0.154	2.0	5.12	3.3	3.3
26.2	0.46	0.0826	0.85	3.59	2.7	3.0
24.4	0.29	0.0724	1.0	3.76	2.3	2.4
23.3	0.40	0.044	0.51	2.15	2.0	2.1
20.3	0.20	0.0684	0.92	5.80	1.3	1.4

[a] Calculated from relation (94) of the text using our kinetic data given here for the initial decay of HO_2NO_2 in the dark, taking $k_{11} = 5.3 \times 10^3\ ppm^{-1}min^{-1}$, independent of the temperature in the range from 28.4 to 20.3°C.

[b] Calculated using the temperature dependent rate constant functions for k_8 and k_7 presented by Graham et al.[53] in their relations (6) and (7) which were derived from their kinetic data on reaction (8) and that of Howard[44] for reaction (7).

The method and data analysis employed here appear to offer a convenient, new method of estimation of the equilibrium constants for the system, $HO_2NO_2 \rightleftarrows HO_2 + NO_2$. This approach may be useful also for the study of the alkyl peroxynitrates such as $CH_3O_2NO_2$, where the rate constant for the alkylperoxy radical second-order decay reaction ($2CH_3O_2 \rightarrow$ Products) is well established.

The Computer Simulation of the Product Rates and a Quantitative Test of the Complete Reaction Mechanism

We have combined reactions (1)-(65) in computer simulations to attempt a match of the product data of many different experiments involving a range of initial $[Cl_2]$, $[H_2]$, $[NO_2]$, and [NO] values.

A reasonable fit of all of the experimental product trends was achieved using the rate constant choices shown in Table 9. The temperature dependences of the constants for reactions (2), (7), (8), (9), (12), (18), (19), and (21), which are those of major significance, were taken into account. Small mismatches observed for some of the products were random in direction from experiment to experiment, and our rate constant choices for reactions (3), (4), (10), (13), and (14) were based upon the best fits of many such experiments for a variety of initial conditions.

The reproducibility of our experiments was very good for a given set of starting conditions. Note the product concentration-time data given in Figure 15 for a series of 13 very similar runs in which the initial product concentrations (ppm) were NO_2, 11.2 ± 1.6; Cl_2, 15; and H_2, 8026 in air at 700 torr. The major variables between experiments which account for the scatter seen were the temperature (21.8-26.1°C) and the initial $[NO_2]$ (12.7 to 9.6 ppm). Computer-generated concentrations for some of the major products at selected times are shown for this series in Figure 15. The effect of variation of k_{10} on the fit to the data can be seen. Simulations were also made for the range of temperatures and initial NO_2 concentrations employed; the resulting range of product concentrations predicted by computer simulations is shown as a vertical bar for each product in Figure 15 at the 6 min irradiation time point. It is seen that this range brackets well the large share of the experimental data. We conclude from such comparisons that the chemical changes observed are in accord with the mechanism outlined, and a reasonable knowledge of the origin and fates of HO_2NO_2 within the atmosphere may be surmised from this study.

If one utilizes the homogeneous reactions involving HO_2NO_2 formation and decay together with the rather complete chemical model for a sunlight-irradiated, NO_x-hydrocarbon-polluted atmosphere, including realistic variation of the solar zenith angle with time, typical levels of the pollutant molecules, continued NO, NO_2, and RH emissions, and varied mixing height th throughout the day, then one predicts that HO_2NO_2 may build up to about the 1 ppb level during the day (atmospheric temperature, 25°C).[56] Other calculations of Hendry and Kenley[54] show similar results. This predicted HO_2NO_2 level is consistent with the direct observations of Pitts _et al._[57] from the FT IR spectroscopic analysis of air samples in Riverside, California; they conclude that an upper limit to the peroxynitric acid

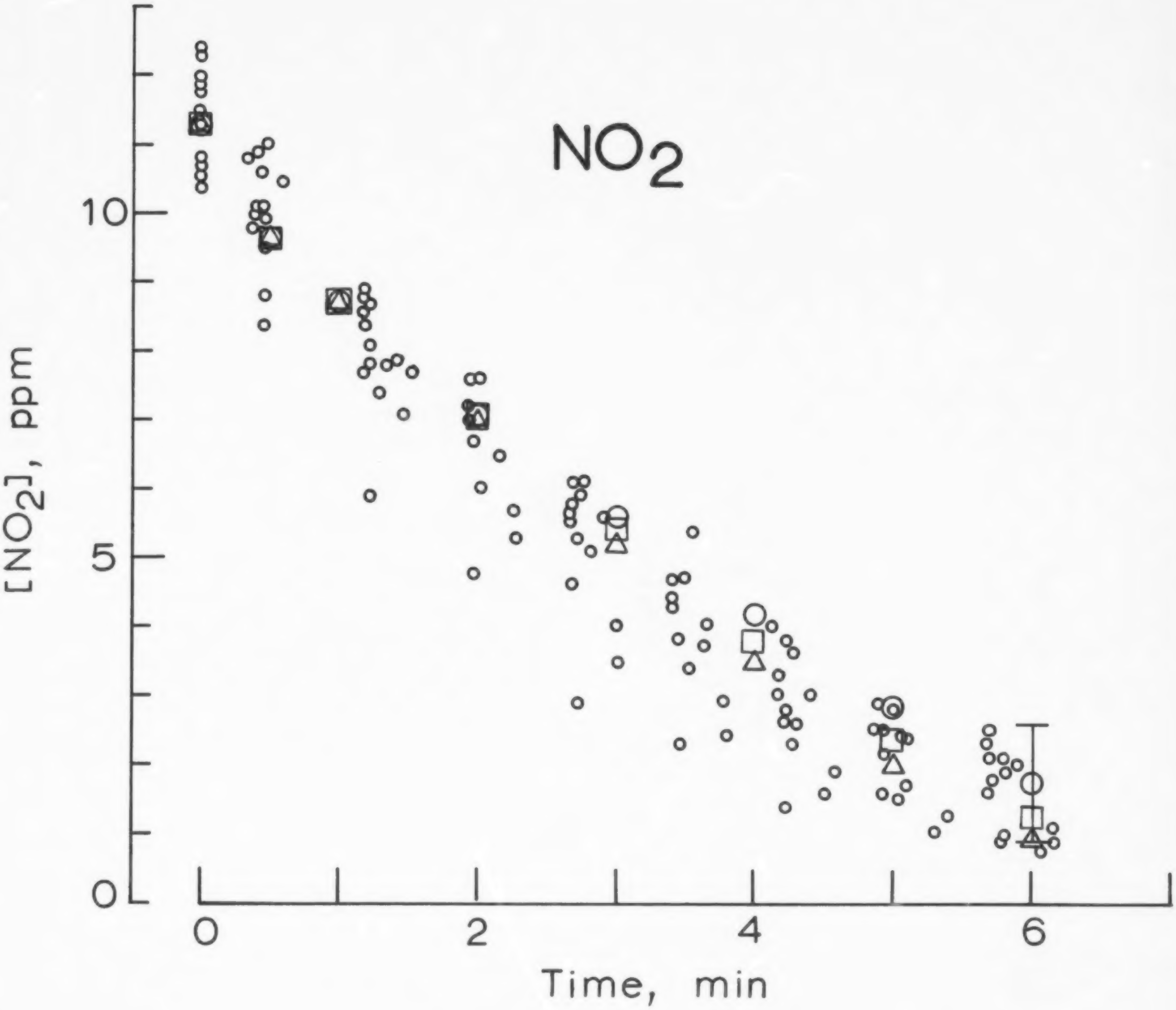

Figure 15a.

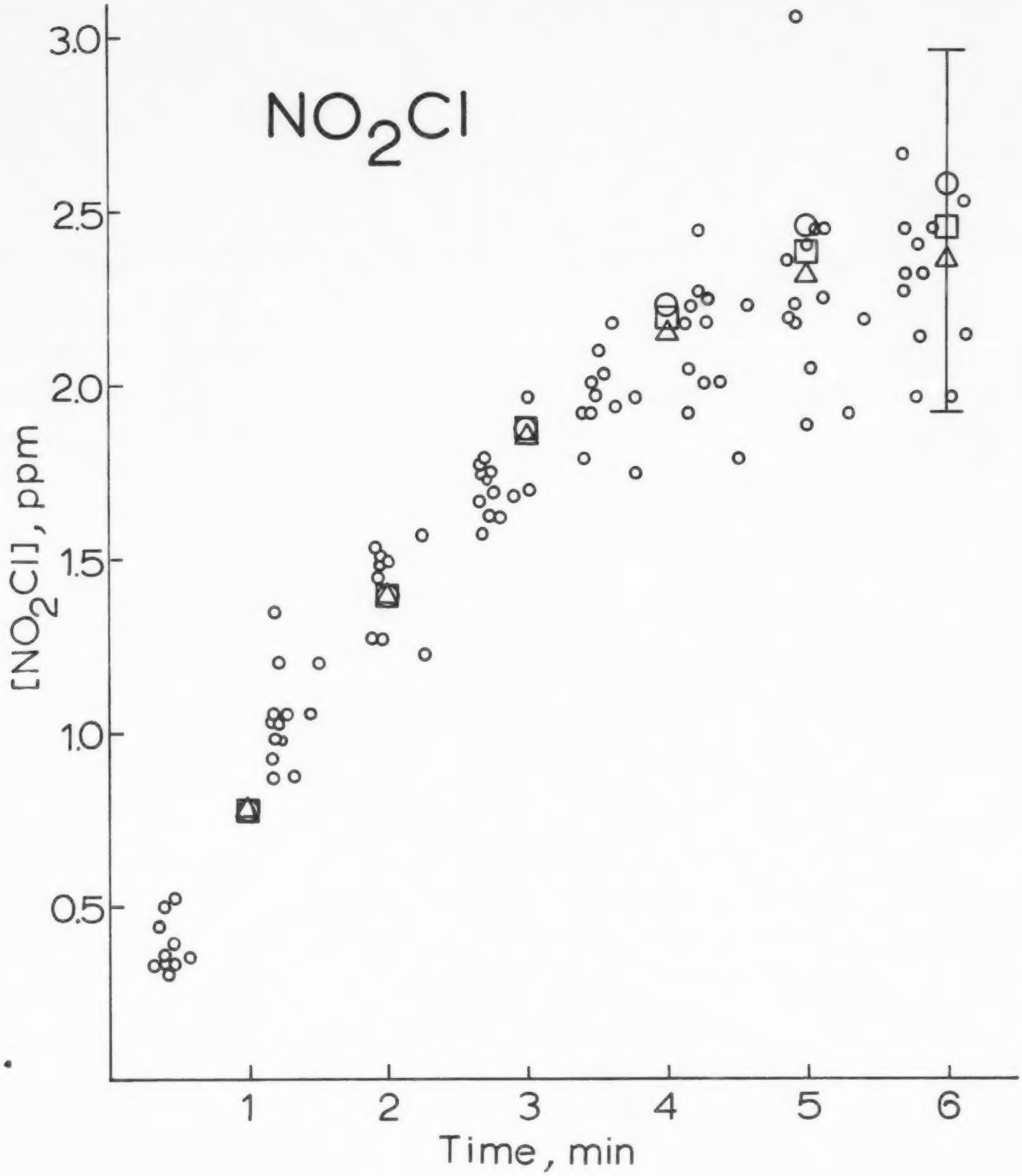

Figure 15b

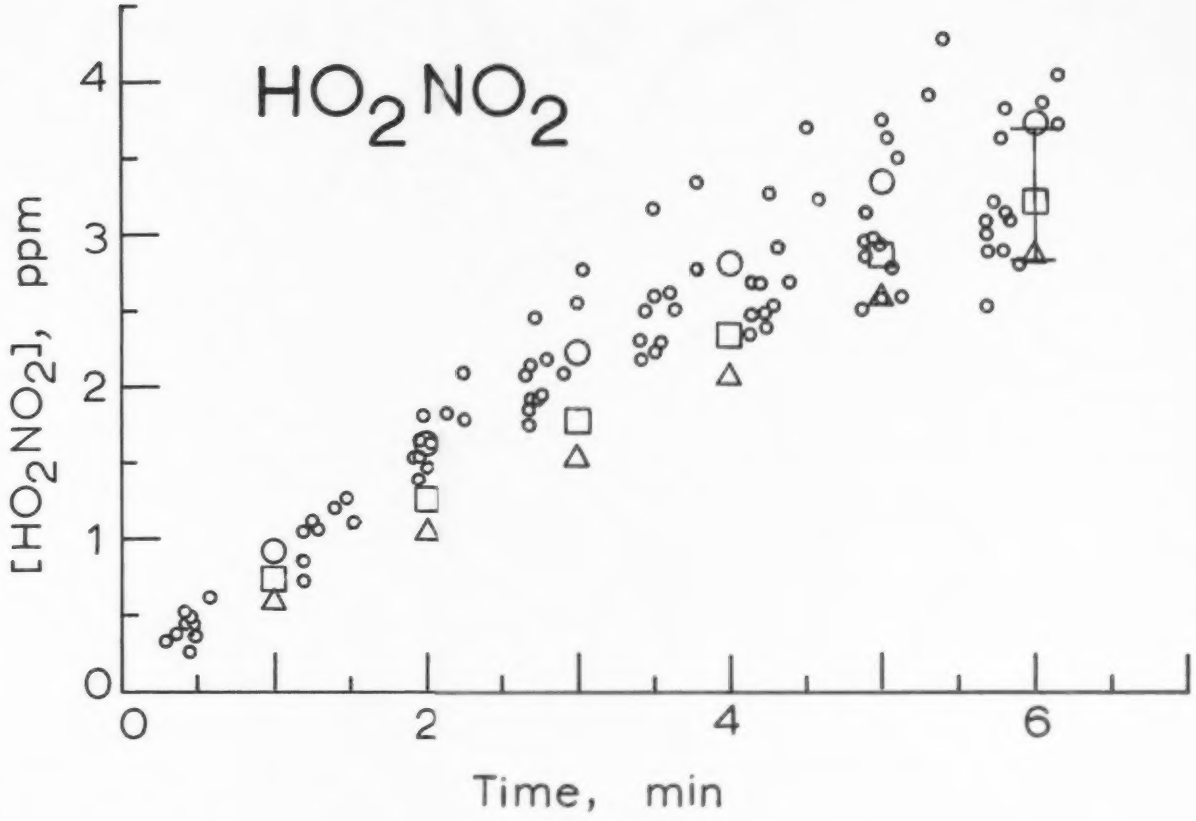

Figure 15c

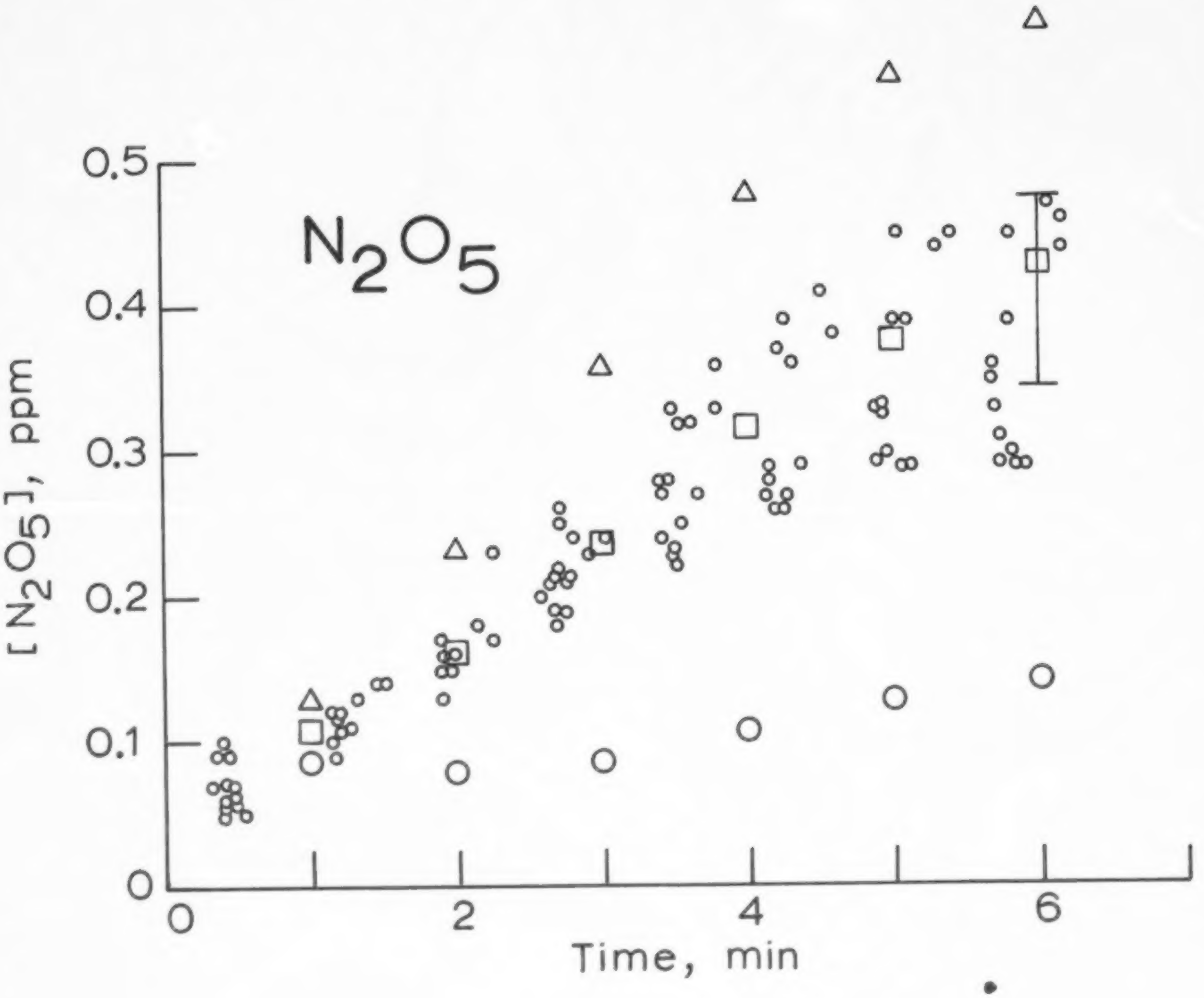

Figure 15d

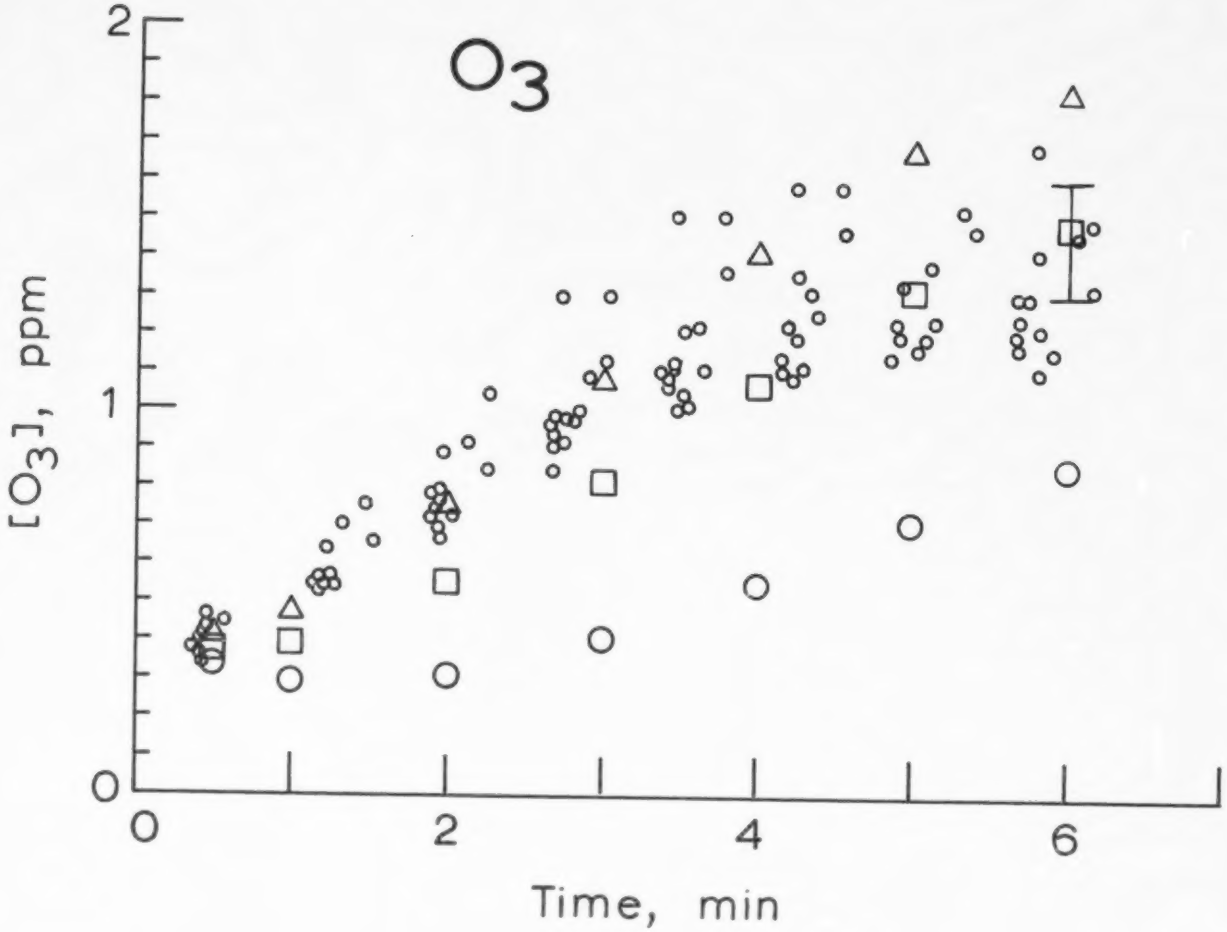

Figure 15e

The time dependence of the major products from the photolysis of 13 nearly identical mixtures: initial concentrations (ppm) -- NO_2, 11.1 ± 1.6; Cl_2, 15; H_2, 8026; in air (700 torr; temperature, 21.8 - 27.2°C); small points are the measured data points; circles, squares, and diamonds are the computer-generated product concentration points using the mechanism outlined in Table 9, $[NO_2]$ = 11.3 ppm, temp., 25°C, but with values of k_{10} = 1.6×10^3, 6.0×10^3, and 1.2×10^4 $ppm^{-1}min^{-1}$, respectively; the bar drawn at the 6 min point shows the range of product concentrations predicted for simulations using starting NO_2 concentrations and temperatures over the range employed.

concentration is $[HO_2NO_2] \leq 4$ ppb (0.5 cm^{-1} resolution and 1 km path length). Higher levels of HO_2NO_2 are expected theoretically at lower atmospheric temperatures. Whether this quantity of the highly reactive HO_2NO_2 has a significant influence on the health of man, animals, and plants is unevaluated today, but it seems premature to conclude that HO_2NO_2 will be unimportant in the lower troposphere.[42,53] Although the rate of HO_2NO_2 dissociation in reaction (8) is very fast ($1/k_8 = \tau_8 \cong 15$ s at 25°C), the reassociation of HO_2 and NO_2 in (7) becomes more favorable as the $NO \rightarrow NO_2$ conversion proceeds throughout the day; hence not insignificant levels (ppb) of HO_2NO_2 may build up, as we found in simulations.

New Rate Constant Estimates for Some Reactions of Interest in the Troposphere.

Much quantitative kinetic data for atmospheric free radicals are available from the accurate and highly specific resonance fluorescence methods. However such kinetic data for radical associations apply to only that small range of low pressures which could be employed successfully in the studies. Extrapolation of these data to 1 atm of air, which is of particular concern to the tropospheric chemist, is often subject to a great uncertainty because of the unknown form of the pressure dependence of the rate constant in the transition region between third- and second-order kinetics. The present work does provide some useful estimates of a few of the radical association reactions for tropospheric conditions (700 torr air, 25°C). These were derived by computer fit of the observed product data, and in each case the estimates depend upon the choice of a rate constant for a well-studied, bimolecular reference reaction which is not pressure sensitive.

Through this technique we derived estimates for the apparent second-order rate constants for Cl and HO-radical association reactions with NO_2 and NO. The rate constant for reaction (2), $k_2 = 2.07 \times 10^1$ $ppm^{-1}min^{-1}$,[58] was used as the reference for reactions (3) and (4):

$$Cl + H_2 \rightarrow HCl + H \qquad (2)$$

$$Cl + NO_2\ (+M) \rightarrow ClNO_2\ (+M) \qquad (3a)$$

$$Cl + NO_2\ (+M) \rightarrow ClONO\ (+M) \qquad (3b)$$

$$Cl + NO\ (+M) \rightarrow ClNO\ (+M) \qquad (4)$$

Our value for $k_{3a} \cong 1.2 \times 10^4$ $ppm^{-1}min^{-1}$ may be compared with those derived from low pressure, third-order rate-constant measurements made, assuming no fall off in the constant up to 700 torr: $k_{3a} \cong 2.4 \times 10^4$;[59] 3.4×10^3 $ppm^{-1}min^{-1}$.[60] Although the dominant product which we observe from the Cl-atom-NO_2 interactions is $ClNO_2$, the occurrence of the alternative reaction (3b) which results in Cl-O bond coupling, does occur in our system to a measurable extent. The maximum in [ClONO], ~ 0.1 ppm, occurs at early times. However, the ClONO photolysis rate constant in our system, $k_{60} \cong 0.35$ min^{-1}, estimated from the ϵ data of Molina and Molina[48] and the energy-wavelength distribution of the light within our cell, is expected to keep the [ClONO] at the low levels observed even if k_{3b} is of the magnitude of k_{3a}. No reliable estimate of k_{3b} can be had from our data, and we have neglected its participation in the present system. This should not cause any major perturbations on the kinetic treatment of the other products observed. Our value for $k_4 \cong 5.5 \times 10^3$ ppm^{-1}min^{-1} depends on the choice of k_2 and also the experimental value for the photolysis rate constant, $k_5 \cong 0.33$ min^{-1}:

$$ClNO + h\nu \rightarrow Cl + NO \qquad (5)$$

The levels of ClNO achieved are very low, and hence the accuracy of our k_4 estimate is low. Our k_4 value is somewhat higher than that derived from the low-pressure, third-order rate constant, assuming no fall off with increase in pressure to 700 torr: $k_4 \cong 3.7 \times 10^3$ ppm^{-1}min^{-1}.[60]

The rate constants for the HO association reactions (13) and (14) with NO_2 and NO were estimated by computer match of the $HONO_2$ and HONO product rates, employing for reference reaction, $k_{12} = 1.0 \times 10^1$ ppm^{-1}min^{-1} [59] and our experimental HONO photolysis rate constant determined in this work, $k_{15} \cong 0.11$ min^{-1}.

$$HO + NO_2\ (+M) \rightarrow HONO_2\ (+M) \qquad (13)$$

$$HO + NO\ (+M) \rightarrow HONO\ (+M) \qquad (14)$$

$$HO + H_2 \rightarrow H_2O + H \qquad (12)$$

$$HONO + h\nu \rightarrow HO + NO \qquad (15)$$

The present estimate of $k_{13} \cong 1.9 \times 10^4$ ppm^{-1}min^{-1} is in reasonable agreement with that derived for 700 torr and 25°C from the analytical expression for k_{13} given in Ref. 60, $k_{13} \cong 1.6 \times 10^4$ ppm^{-1}min^{-1}. Our value of $k_{14} \cong 7.6 \times 10^3$ is somewhat lower than that estimated by Cox _et al_.[61] for 760 torr of air: $k_{13} = k_{14} \cong 1.7 \times 10^4$ ppm^{-1}min^{-1}.

The fit of the O_3, N_2O_5, and NO_2 profiles was somewhat sensitive to the rate-constant choice for reaction (10). We picked $k_1 \cong 6 \times 10^3$ at 25° and 700 torr of air; this depended upon the recent estimate of $k_7 \cong 1.6 \times 10^3$ ppm^{-1}min^{-1} for these conditions.[53] Our k_{10} estimate is somewhat larger than the previous indirect measurements of this constant at 1 atm pressure, $k_{10} \cong 1.6 \times 10^3$,[62] and 1.8×10^3 ppm^{-1}min^{-1},[63] and is a factor of 2 less than the newer, more direct value obtained at low pressures, $k_{10} \cong 1.2 \times 10^4$ ppm^{-1}min^{-1}.[64] The use of the direct, low-pressure value of k_{10} in our simulations, causes O_3 and N_2O_5 growth rates to be somewhat over-estimated and HO_2NO_2 to be underestimated (see Figure 15). The theoretical significance of a possible pressure dependence of k_{10} has been discussed recently in terms of the participation of the transient HO_2NO molecule at high pressures.[52] The accuracy of the present estimate of k_{10} is not great, and one cannot rule out the possibility that the apparent disagreement is the result of unforeseen kinetic complications in this complex system.

The reaction (55) involving HONO decay was restudied in our glass reaction vessel by injecting relatively pure HONO vapors at concentrations far above the values in equilibrium with NO, NO_2, and H_2O vapors.

$$2HONO \rightarrow NO + NO_2 + H_2O \quad (55)$$

$$NO + NO_2 + H_2O \rightarrow 2HONO \quad (54)$$

The rate follows second-order kinetics well over a 100 hour period; data for experiments near 25°C gave $k_{55} \cong (4.1 \pm 0.1) \times 10^{-4}$; at 16°C, $k_{55} \cong (1.2 \pm 0.1) \times 10^{-4}$. The value at 25° is a factor of 3 lower than that observed by us in previous studies of this reaction in a stainless steel reactor[65]; it is a factor of 27 faster than that reported recently by Kaiser and Wu at 27°C: $k_{55} \cong 1.5 \times 10^{-5}$ ppm^{-1}min^{-1}.[66] It now seems evident to us, as well as others, that this reaction is sensitive to the nature of the wall of the reactor, even in the large vessel employed here. Hence it may be partly or wholely a heterogeneous reaction in our system. We have obtained the rate constant for the reverse reaction, $k_{54} \cong 5.5 \times 10^{-10}$ at 25°C, by employing our estimate of k_{55} and the equilibrium constant K_{55}.[65] In view of the studies of Kaiser and Wu[66] and our present findings, we must conclude that our previous estimates of HONO formation rates in H_2O, NO-rich plumes by the homogeneous reactions (54) and (55) must be lowered by at least a factor of 3.[65] The extent to which the heterogeneous and homogeneous generation of HONO occurs in actual aerosol- and water droplet-laden plumes remains unevaluated. The reaction (56) between HONO and $HONO_2$ has been restudied in this work as well.

$$HONO + HONO_2 \rightarrow 2NO_2 + H_2O \quad (56)$$

For experiments at 24.6°C, we found $k_{56} \cong (9.6 \pm 0.3) \times 10^{-3}$ ppm^{-1}min^{-1}. This result is only four-tenths of the minimum value of k_{56} (27°C) estimated by Kaiser and Wu[55]; in confirmation of their conclusion, the observed reaction (56) may be hetergeneous in whole or in part.

SECTION 7

A FOUIER TRANSFORM INFRARED KINETIC STUDY OF HOCl AND ITS ABSOLUTE INTEGRATED INFRARED BAND INTENSITIES

INTRODUCTION

Molina and Rowland[69] first suggested in 1974 the potential role of the chlorofluoromethanes and other chlorine-containing compounds in perturbing significantly the natural stratospheric ozone levels. Interest has grown since that time in the quantitative evaluation of the extent of this perturbation. In theory one anticipates that the measurable depletion of ozone should occur slowly, some years after Cl-compound injection, so only indirect observations related to the proposed reaction mechanism can be made to test the O_3-depletion hypothesis today. In this regard there has been active research related to both the kinetics of the intermediates and the elementary processes involved, as well as the experimental measurements of the atmospheric abundance of the chlorine-containing species presumed to be involved in the O_3 depletion mechanism (Cl, ClO, HCl, $ClNO_2$, etc.).[70] The comparison of the measured and the predicted levels of each species provides a significant, although indirect, test of the hypothesis.

It has been suggested that HOCl might form in the stratosphere through the occurrence of the homogeneous reaction (1)[70-74] and conceivably on aerosol surfaces through the heterogeneous reaction (2)[74]:

$$HO_2 + OCl \rightarrow O_2 + HOCl \qquad (1)$$

$$ClONO_2 + H_2O\ (+aerosol) \rightarrow HOCl + HONO_2\ (+\ aerosol) \qquad (2)$$

Recent kinetic studies favor HOCl involvement in that they show k_1 to be large, about 3.8×10^{-12} cc $molec^{-1}s^{-1}$.[75-77] However, recent measurements of the ultraviolet spectrum of HOCl suggest a rapid photolysis of HOCl will occur in the stratosphere; this leads to the conclusion that the HOCl will not provide a significant sink for inert chlorine in the stratosphere.[78] The direct spectroscopic measurement of stratospheric HOCl at its characteristic infrared absorption regions could provide a valuable test of the current hypotheses concerning this molecule. However, absolute IR extinction coefficients for gaseous HOCl are not now available. With this in mind we have carried out the present work to provide experimental estimates of the needed integrated infrared band intensities of the gaseous HOCl molecule. This highly reactive species is not stable in our system as a result of heterogeneous reactions which lead to destruction at the wall of our reaction chamber, so a kinetic study involving long-path, Fourier transform, infrared spectroscopy was chosen to obtain these data.

In addition to the HOCl IR-band intensity data, our study provides a direct test of the reliability of several of the rate constants of the reactions of the intermediate OCl radical. Furthermore, the results presented here provide an interesting example of the utility of the FT-IRS system and the complications which are encountered in the kinetic study of a reactive species by this method.

EXPERIMENTAL SECTION

All of the studies described in this work were carried out using a Digilab FTS-20 Fourier transform spectrometer (model 496 interferometer) coupled to a photolysis cell (see Figure 16). The large, evacuable cell was constructed of 30.5-cm-diameter pyrex tubing, 6.3 m long (445 liter volume). It housed a modified White optical system, based upon the design of Hanst[79]; it had a base path of 5.3 m and provided a choice of pathlengths which were multiples of 8-times the base length. All of our experiments reported here were carried out at 170 m (32 traversals) which gave adequate absorption in the ppm range for the compounds studied. The details of the cell construction have been given elsewhere[80] and need not be reported here. A liquid-helium-cooled Cu:Ge detector (Mullard) was employed for signal detection. Potential problems created by variable background absorption from H_2O and CO_2 in the air path between the transfer optics, Nernst glower IR source, interferometer, cell, and detector were substantially lowered by enclosing the entire optical system in a plastic housing which was purged continuously with N_2 and contained dishes of solid NaOH reagent.

The large photochemical cell was illuminated by black-light fluorescent lamps which surrounded it. An outer reflective shield of aluminum encompassed both the lamps and the cell. Room air could be circulated in the space between the lamps and cell to help stabilize the cell temperature. A thermometer placed inside the cell was used to determine the actual cell temperature during an experiment. The cell lighting was designed to mimic ground-level solar radiation both in distribution and intensity within the photochemically important region, 300-450 nm. Direct measurements showed this to be the case (see Figure 17).

All of the gases (Cl_2, HCl, H_2, N_2, and O_2) employed in this work were purchased from the Matheson Gas Co., and they were used without further purification; O_3 was generated by the discharge of O_2 with two Tesla coils. Reference gases were measured in an all-glass, grease- and mercury-free vacuum system equipped with Teflon stopcocks, calibrated volumes, and a quartz spiral gauge employed as a null instrument together with calibrated gauges (Wallace-Tiernan) which were not in direct contact with the gases.

All of the spectra obtained in kinetic runs and calibrations were collected using 1 cm^{-1} resolution, with 8192 data points per interferogram. Extinction coefficients of all reactants and products were determined at several pressures in 700 torr of synthetic air or N_2, employing 1 cm^{-1}

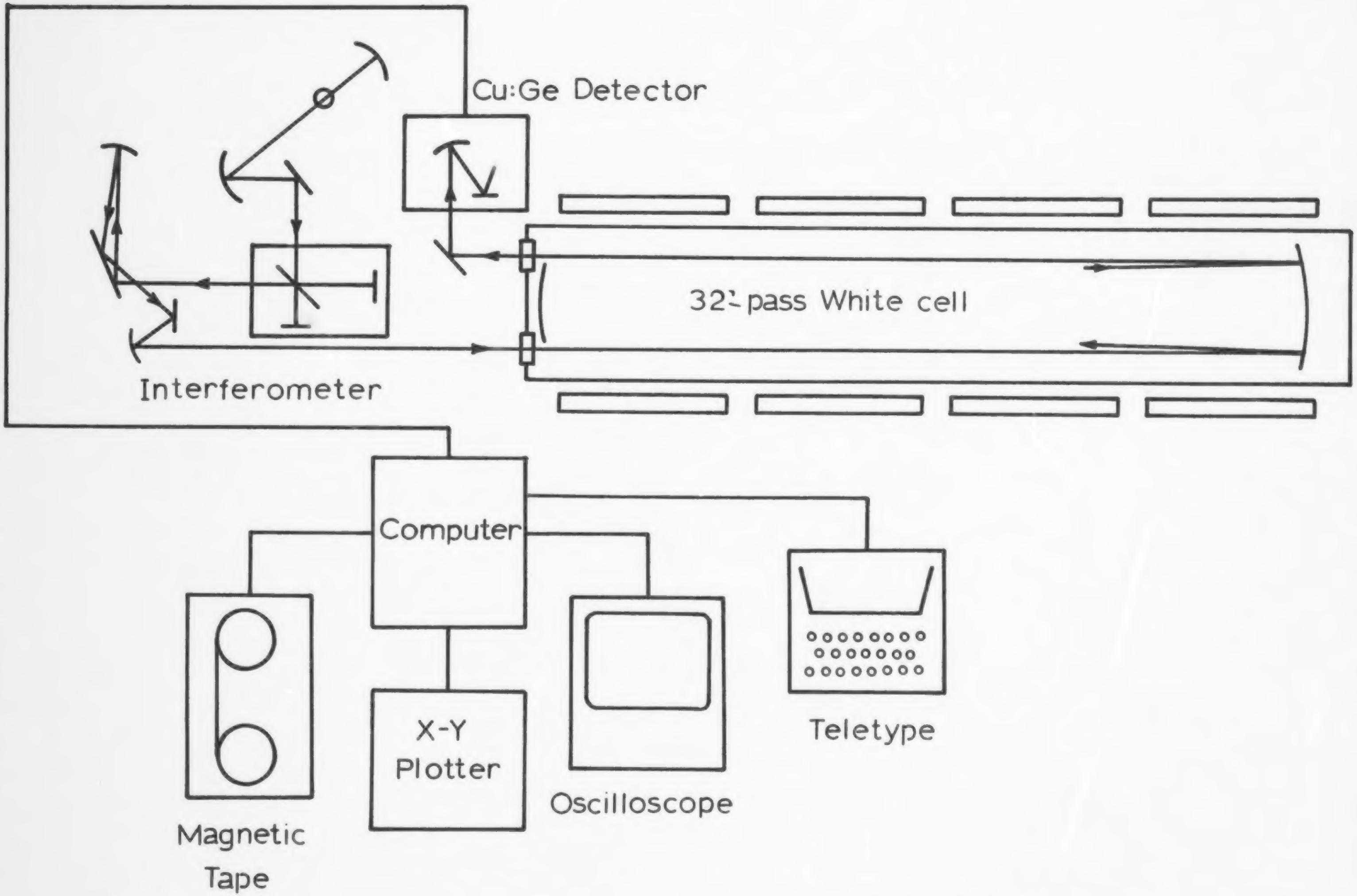
Cu:Ge Detector
32'-pass White cell
Interferometer
Computer
Magnetic Tape
X-Y Plotter
Oscilloscope
Teletype

Figure 16. Diagram of the Fourier transform infrared spectrometer and photochemical reactor used in the studies reported here.

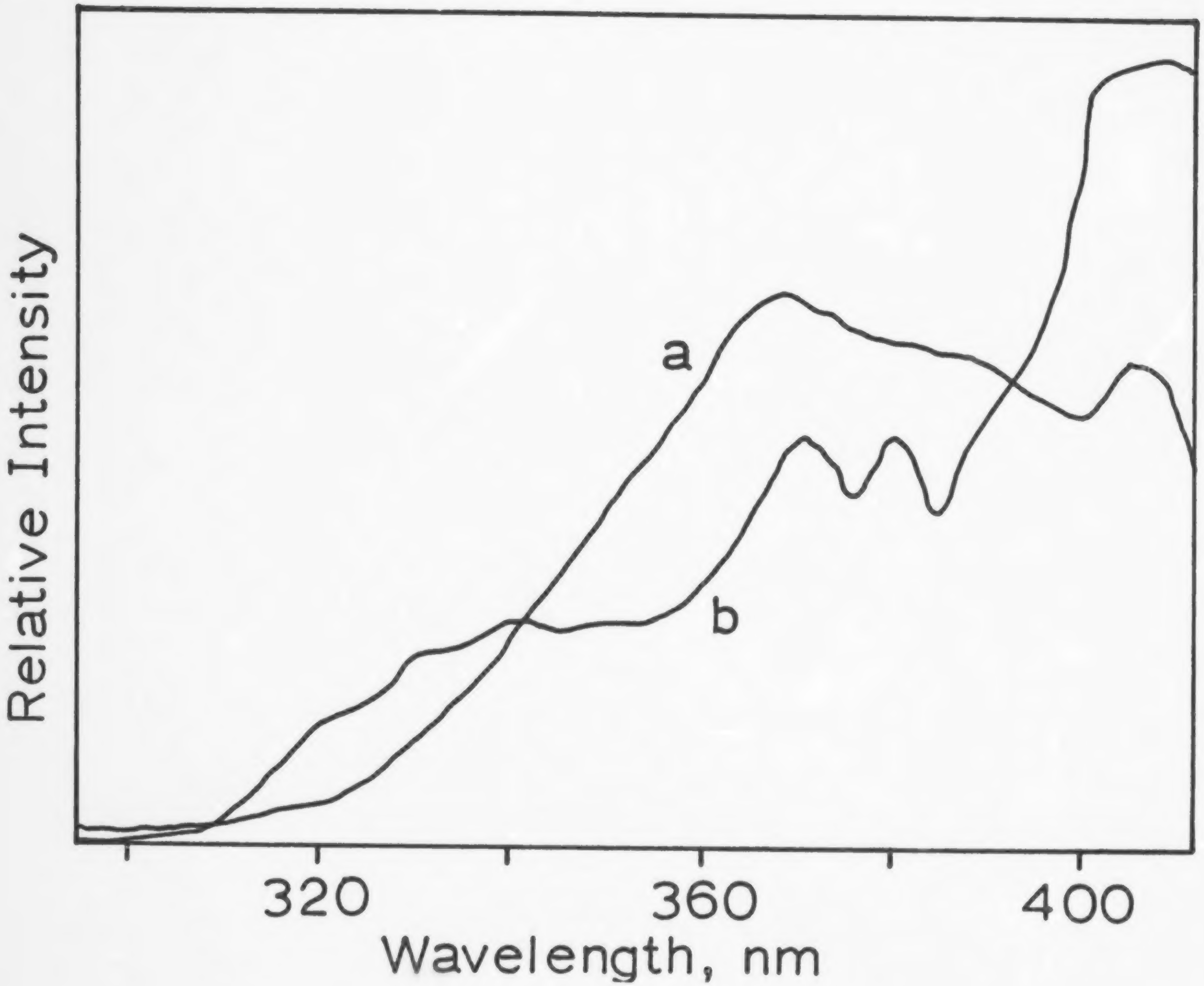

Figure 17. Relative intensity (quanta) of the light inside the photochemical reactor versus wavelength (curve a) and a typical distribution of sunlight incident within the atmosphere near ground level (curve b).

resolution (1 cm optical retardation) and box-car apodization. The simple Beer-Lambert law dependence of absorbance on concentration held well for most reference gases.[80] The experimental values of the extinction coefficients (base e, $ppm^{-1}m^{-1}$ at 25°C) for selected wavelengths employed in this work are as follows: H_2O_2, 1.00×10^{-3} (1266 cm^{-1}); O_3, 9.74×10^{-4} (1055 cm^{-1}); HOCl, 5.36×10^{-4} (1226 cm^{-1}); the last value was estimated from a kinetic analysis of the products of O_3, Cl_2, H_2, O_2 mixture photolyses which is described in the following section. Another important product of the irradiated Cl_2, H_2, O_3, O_2 mixtures (namely, HCl) also required some special experimentation for calibration. The very sharp lines characteristic of the HCl absorption in the infrared do not follow the simple absorption law at the relatively low spectral resolution (1.0 cm^{-1}) which we employed here. Thus a calibration curve of absorbance versus P_{HCl} was required. These measurements were further complicated by the slow, heterogeneous loss of HCl at the cell wall following injection of a sample. Thus after sample introduction the absorbance of HCl was followed as a function of time, and the absorbance data were then extrapolated back to zero time (see Figure 18). Eight peaks of the P-branch of the spectrum were measured in order to improve the signal-to-noise ratio. From more than 50 different HCl measurements, the relative absorbances of these eight peaks were estimated to be ($\pm 2\sigma$): 0.54 ± 0.06 (2702 cm^{-1}); 1.00 (2727); 1.83 ± 0.20 (2751); 2.47 ± 0.32 (2775); 3.00 ± 0.60 (2797); 3.47 ± 0.60 (2820); 3.63 ± 0.40 (2842); 1.72 ± 0.18 (2864). The experimental calibration curve of the absorbance (2727 cm^{-1}) versus P_{HCl} which was derived from these data is shown in Figure 19.

RESULTS AND DISCUSSION

The Generation of HOCl

In theory one anticipates that HOCl should be produced readily in the photolysis of dilute mixtures of Cl_2, H_2, and O_3 in a large excess of O_2. Following Cl-atom formation from Cl_2 photolysis in reaction (3), the OCl and HO_2 radicals should be formed in Cl-atom reactions with O_3 and H_2, reactions (4) and (5) followed by (6), respectively:

$$Cl_2 + h\nu \rightarrow 2Cl \qquad (3)$$

$$Cl + O_3 \rightarrow OCl + O_2 \qquad (4)$$

$$Cl + H_2 \rightarrow HCl + H \qquad (5)$$

$$H + O_2\ (+M) \rightarrow HO_2\ (+M) \qquad (6)$$

Provided that we adjust the initial reactant concentrations so that $[O_3]k_4 \simeq [H_2]k_5$, then the near equality of rates of generation of OCl and HO_2, and the rapid rate of reaction 1 between HO_2 and OCl[75-77] should allow HOCl formation to compete successfully with the major alternative sinks for these radicals; namely, reactions (7-10):

$$HO_2 + OCl \rightarrow HOCl + O_2 \qquad (1)$$

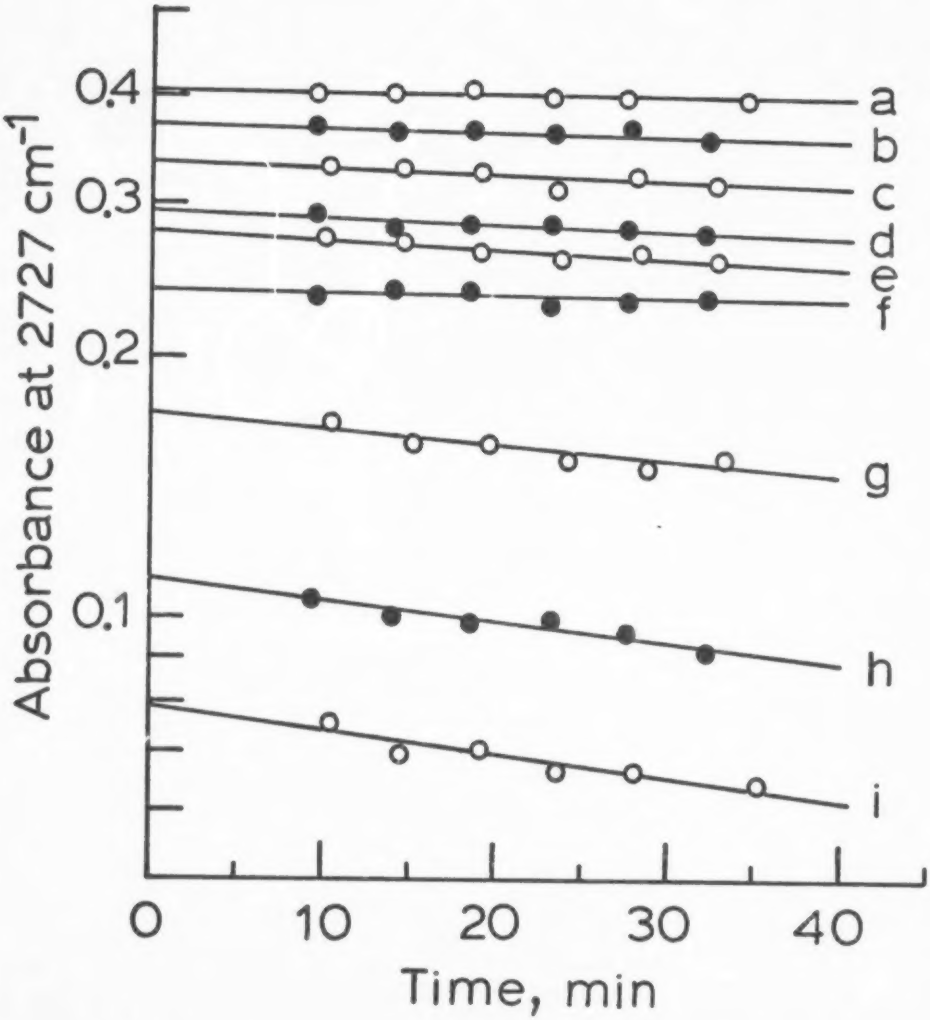

Figure 18. The time dependence of the HCl absorbance during the calibration; points are averaged results at 2727 cm^{-1}; initial concentrations of HCl for lines labeled a through i, respectively, are (ppm): 9.55, 8.18, 6.82, 5.22, 4.10, 3.30, 2.64, 1.09, 0.56; the system was pressurized with synthetic air: N_2(600 torr) and O_2 (100 torr) in each case.

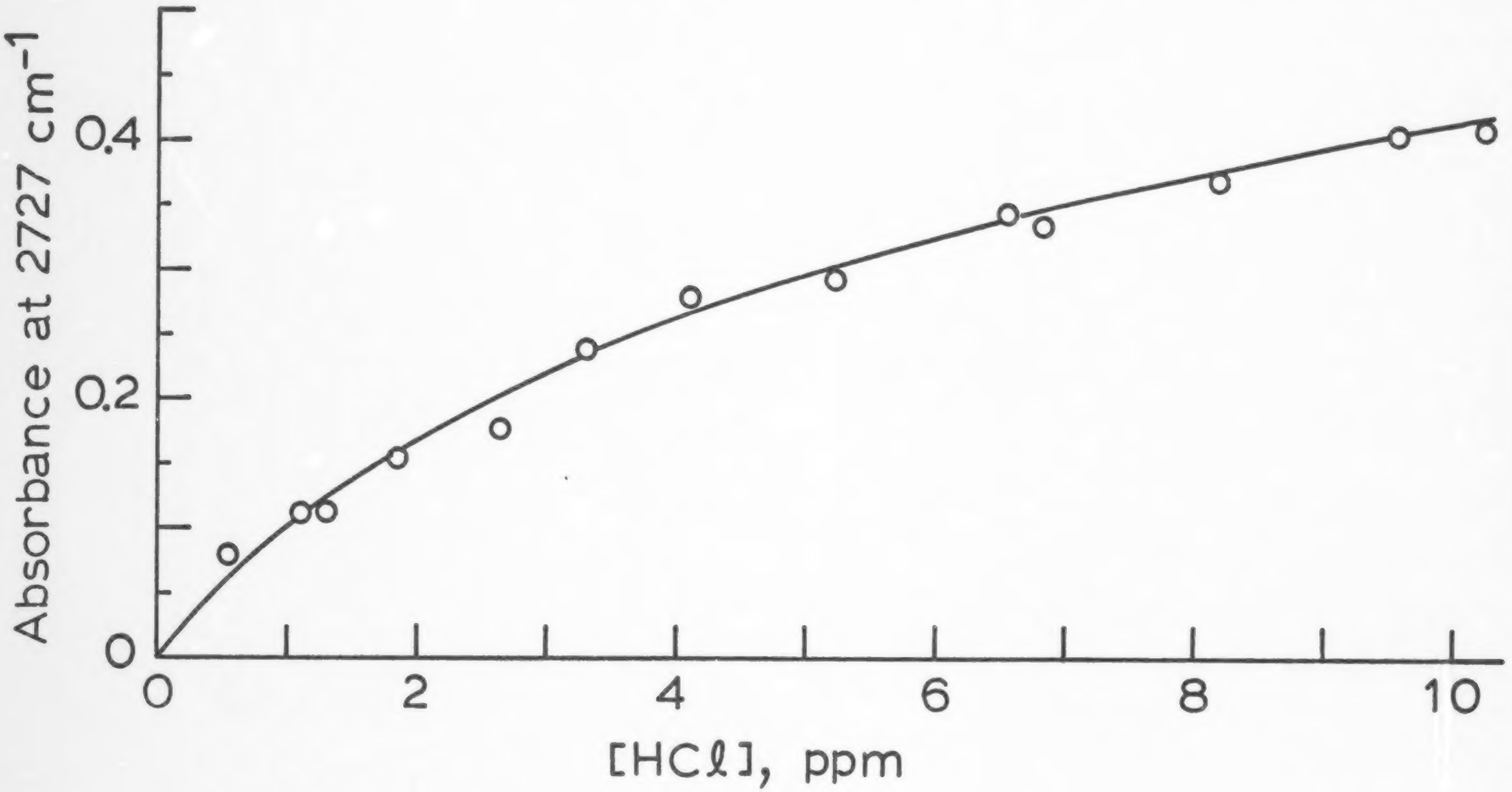

Figure 19. HCl calibration curve for absorbance at 2727 cm^{-1} versus [HCl]; conditions as outlined in Figure 18 caption.

$$2HO_2 \rightarrow H_2O_2 + O_2 \tag{7}$$

$$2OCl \rightarrow Cl + ClOO \tag{8}$$

$$2OCl \rightarrow Cl_2 + O_2 \tag{9}$$

$$2OCl \rightarrow OClO + Cl \tag{10}$$

Indeed this can be seen to be the case in the results of Figure 20. The infrared spectrum of an initial mixture of Cl_2 (60 ppm), O_3 (23.5 ppm), H_2 (20 ,400 ppm), O_2 (44 torr), and N_2 (641 torr) is shown in spectrum A. The second spectrum (B) was taken after 5.12 min of irradiation; there is clear evidence of HOCl absorption in the 1200-1300 cm^{-1} region. The absorptions due to the additional expected products HCl and H_2O_2 are also observed to increase, as those due to the reactant O_3 decrease. Spectrum C, the absorbance difference spectrum (B - A), shows more clearly the HOCl, H_2O_2, and HCl product absorptions together with the negative peaks for O_3 loss. The CH_4 and CO absorptions in A and B result from small impurities in the O_2 and N_2 gases employed. They are essentially unchanged in the irradiated mixtures since Cl-atoms react largely with H_2 and O_3 for these conditions; thus they are absent in the difference spectrum C. Spectra such as these taken at regular times during the photolysis can be treated easily to establish the time dependence of the products of the reaction. Note in Figure 21 the growth of the HOCl ν_2 band near 1226 cm^{-1} as the irradiation time of a Cl_2, H_2, O_3, O_2 mixture is increased. The absorption due to H_2O_2 can be observed to grow in also at the later times. Observe in the time sequence of the spectra shown in Figure 21, obtained after the irradiation was stopped, that HOCl is not stable in our system, and the decay of its characteristic absorbance occurs with increasing dark time. In view of this we had to adopt a special series of experiments to derive the needed extinction coefficient data for HOCl. It was clear that initial rate studies in this system would provide the simplest approach to obtaining meaningful information on this reactive compound.

The Apparent First-Order Rate Constant for Cl_2 Photolysis in the Photochemical Reactor

The reaction sequence which one would anticipate to be operative in the photolysis of dilute mixtures of Cl_2, H_2, and O_3 in O_2 is summarized in Table 11. Most of the rate constants for these reactions have been derived in recent years, and they are known within reasonable error limits. The apparent first-order photolysis rate of Cl_2 in our system, the key to the rate of initiation of the entire reaction sequence, had to determined experimentally for our conditions. At the very low Cl_2 concentrations which we employed, the photolysis of Cl_2, reaction (3), should follow well first-order kinetics, since the limiting form of Beer's law should apply for these conditions:

$$Cl_2 + h\nu \rightarrow 2Cl \tag{3}$$

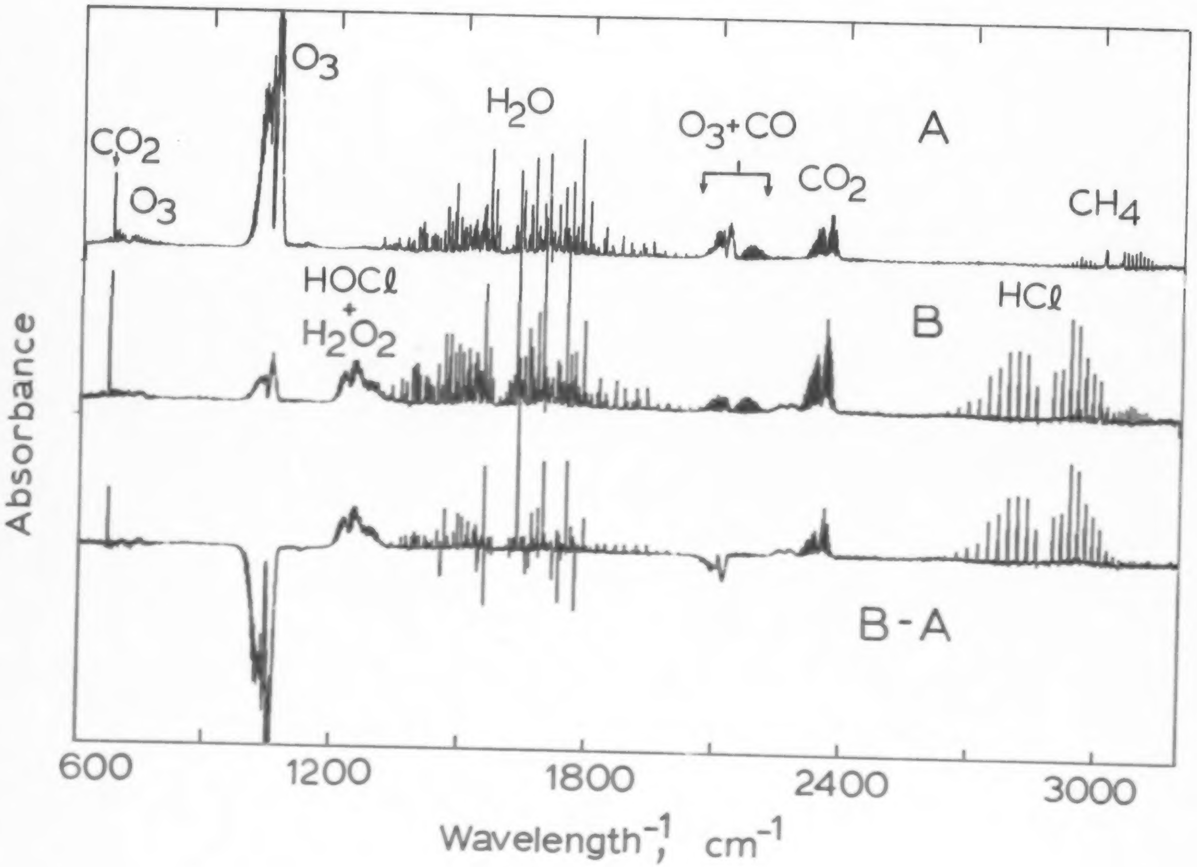

Figure 20. Absorbance versus wavelength plot for a gaseous mixture of initial composition, Cl_2(60 ppm), O_3 (23.5 ppm), H_2 (20,400 ppm), O_2 (44 torr), N_2 (641 torr); the CH_4, CO, CO_2, and H_2O are trace impurities present in the initial reactants; curve A prior to photolysis; curve B after 5.12 min of photolysis; curve C is a difference spectrum (B - A) which was used to estimate product concentrations.

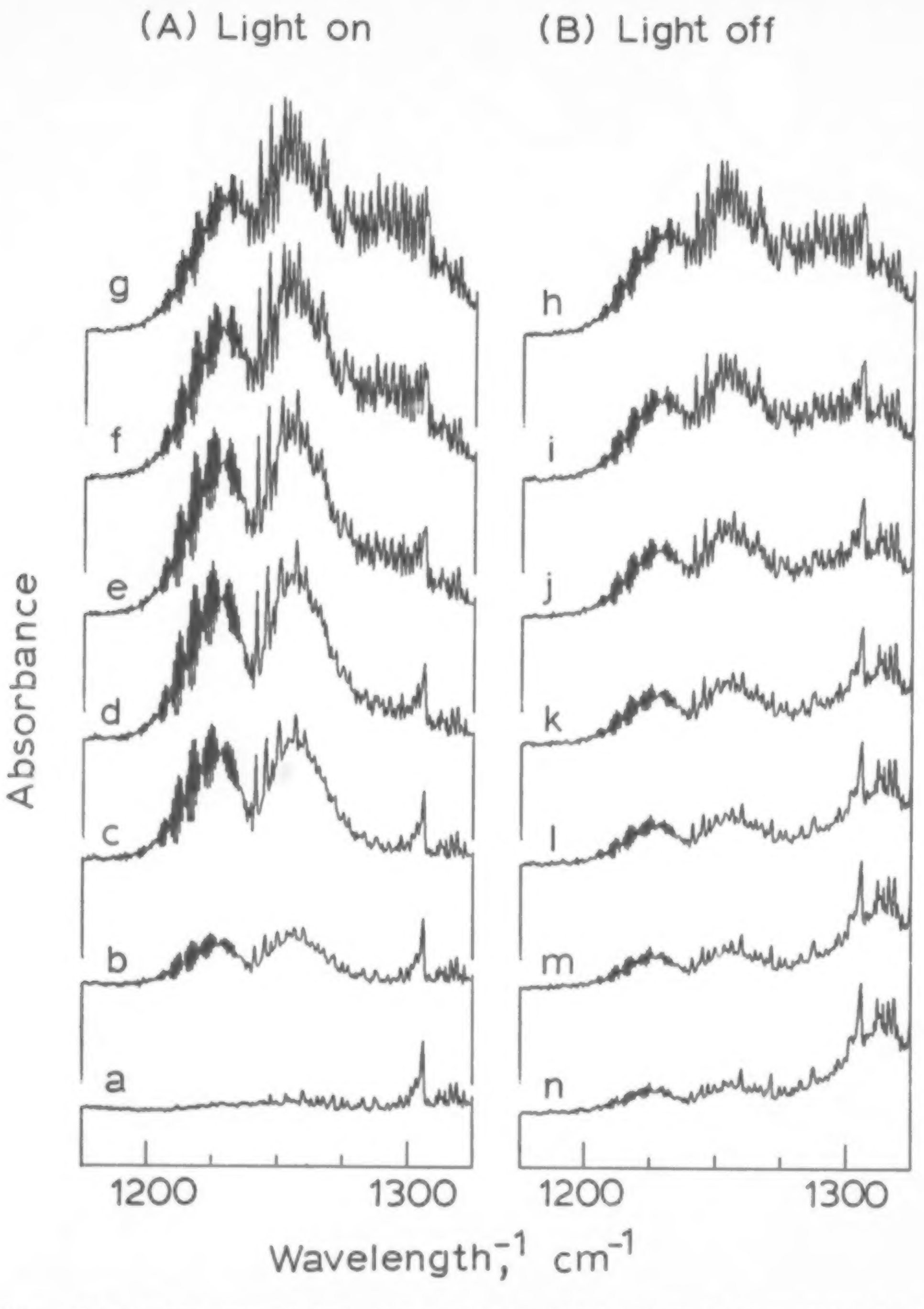

Figure 21. Absorbance growth and decay within the HOCl ν_2 infrared band with increasing time of irradiation of a Cl_2, H_2, O_3, O_2, N_2 mixture of the composition listed in Figure 20 caption (A, light on), and increasing time in the dark (B, light off); the time of each spectrum labeled a through n, respectively, is (min): 0, 0.61, 1.74, 2.87, 3.99, 5.12, 6.25, 7.43, 8.55, 9.68, 11.93, 14.18, 16.43, 20.48.

TABLE 11. SUMMARY OF THE REACTION MECHANISM AND RATE CONSTANTS APPLICABLE TO THE PHOTOLYSIS OF DILUTE Cl_2, O_3, H_2 MIXTURES IN SYNTHETIC AIR

Reaction	Rate constant[a]	Reference
(3) $Cl_2 + h\nu \rightarrow 2\ Cl$	3.5×10^{-2}	This work
(4) $Cl + O_3 \rightarrow OCl + O_2$	1.7×10^{4}	81
(5) $Cl + H_2 \rightarrow HCl + H$	1.8×10^{1}	This work[b]
(6) $H + O_2\ (+M) \rightarrow HO_2\ (+M)$	1.7×10^{3}(700 torr)	82
(1) $HO_2 + OCl \rightarrow HOCl + O_2$	5.6×10^{3}	75-77
(7) $2HO_2 \rightarrow H_2O_2 + O_2$	4.6×10^{3}	83
(8) $2OCl \rightarrow Cl + ClOO$	2.3×10^{1}	82
(9) $2OCl \rightarrow Cl_2 + O_2$	1.2×10^{1}	82
(10) $2OCl \rightarrow OClO + Cl$	1.8	82
(11) $ClOO\ (+M) \rightarrow Cl + O_2\ (+M)$	4.8×10^{7}(700 torr)	82
(12) $Cl + O_2\ (+M) \rightarrow ClOO\ (+M)$	3.7×10^{1}(700 torr)	82
(13) O_3 (+Wall?) + $h\nu \rightarrow 3/2\ O_2$ (+Wall?)	0.03	This work
(14) $HO_2 + O_3 \rightarrow HO + 2O_2$	$< 3.0 \pm 1.5$	This work
(15) $H + O_3 \rightarrow HO + O_2$	4.3×10^{4}	82
(16) $HO + O_3 \rightarrow HO_2 + O_2$	7.8×10^{1}	82
(17) $HO + H_2 \rightarrow H_2O + H$	1.0×10^{1}	82
(18) $OClO + h\nu \rightarrow OCl + O$	2.4×10^{-1}	This work; 81
(19) $HOCl + h\nu \rightarrow HO + Cl$	4.2×10^{-3}	This work; 78
(20) $Cl + HOCl \rightarrow HCl + OCl$	$\sim 1.0 \times 10^{2}$	Our estimate
(21) $Cl + H_2O_2 \rightarrow HCl + HO_2$	6.9×10^{2}	81
(22) $ClOO + Cl \rightarrow OCl + OCl$	1.6×10^{4}	82
(23) $ClOO + Cl \rightarrow Cl_2 + O_2$	2.4×10^{5}	82
(24) $OCl + H_2 \rightarrow HOCl + H$	$< 1.5 \times 10^{-5}$	This work
(25) $OCl + H_2O_2 \rightarrow HOCl + HO_2$	$< 6.9 \times 10^{2}$	This work

---

[a] Rate constants are in units of $ppm^{-1}min^{-1}$ (25°C) except for those of reactions (3), (11), (13), (18), and (19), which are min^{-1}; data for 25°C and 700 torr total pressure.

[b] Obtained from our best estimate of the ratio $k_4/k_5 = (9.5 \pm 1.5) \times 10^{2}$ and the literature value for k_4.[81]

We used two different types of experiments to establish the present value of k_3 in our large photochemical reactor. In the first series of experiments we irradiated small amounts of Cl_2 (5-30 ppm) in a large excess of H_2 (about 20 torr) and O_2 (about 100 torr), pressurized to 700 torr with N_2. Of course Cl_2 itself cannot be observed in the infrared, but the important products, HCl and H_2O_2, can be followed readily. One anticipates from the known reactions and the rate constants of the Cl, H, and HO_2 species that the only important reactions involving these products during a short irradiation of the reactants (about 1 min) will be the following:

$$Cl_2 + h\nu \rightarrow 2Cl \tag{3}$$

$$Cl + H_2 \rightarrow HCl + H \tag{5}$$

$$H + O_2\ (+M) \rightarrow HO_2\ (+M) \tag{6}$$

$$2HO_2 \rightarrow H_2O_2 + O_2 \tag{7}$$

Thus one expects k_3 to be related to the initial rates of HCl and H_2O_2 formation by relations I and II, independent of the concentration of H_2 and O_2 which are present in large excess:

$$R^{o}_{HCl} = 2k_3[Cl_2] \tag{I}$$

$$R^{o}_{H_2O_2} = k_3[Cl_2] \tag{II}$$

The experimental data bear out these expectations. In Figure 22 we have plotted R^{o}_{HCl} (circles) and $2R^{o}_{H_2O_2}$ (squares) versus the $[Cl_2]^{o}$. Within the experimental error of the data, both rate functions determine the same linear function; the least squares slope ($0.068 \pm 0.008\ min^{-1}$) gives $k_3 = 0.034 \pm 0.004\ (2\sigma)\ min^{-1}$.

A second simple system, dilute mixtures of Cl_2 and O_3 in synthetic air mixtures (700 torr), was studied to provide an independent estimate of the constant. In these experiments the initial rate of O_3 decay was determined. The following reactions of Cl, O_3, and ClO should describe well this system at short irradiation times:

$$Cl_2 + h\nu \rightarrow 2Cl \tag{3}$$

$$Cl + O_3 \rightarrow OCl + O_2 \tag{4}$$

$$2OCl \rightarrow Cl + ClOO \tag{8}$$

$$2OCl \rightarrow Cl_2 + O_2 \tag{9}$$

$$2OCl \rightarrow OClO + Cl \tag{10}$$

$$ClOO\ (+M) \rightarrow Cl + O_2\ (+M) \tag{11}$$

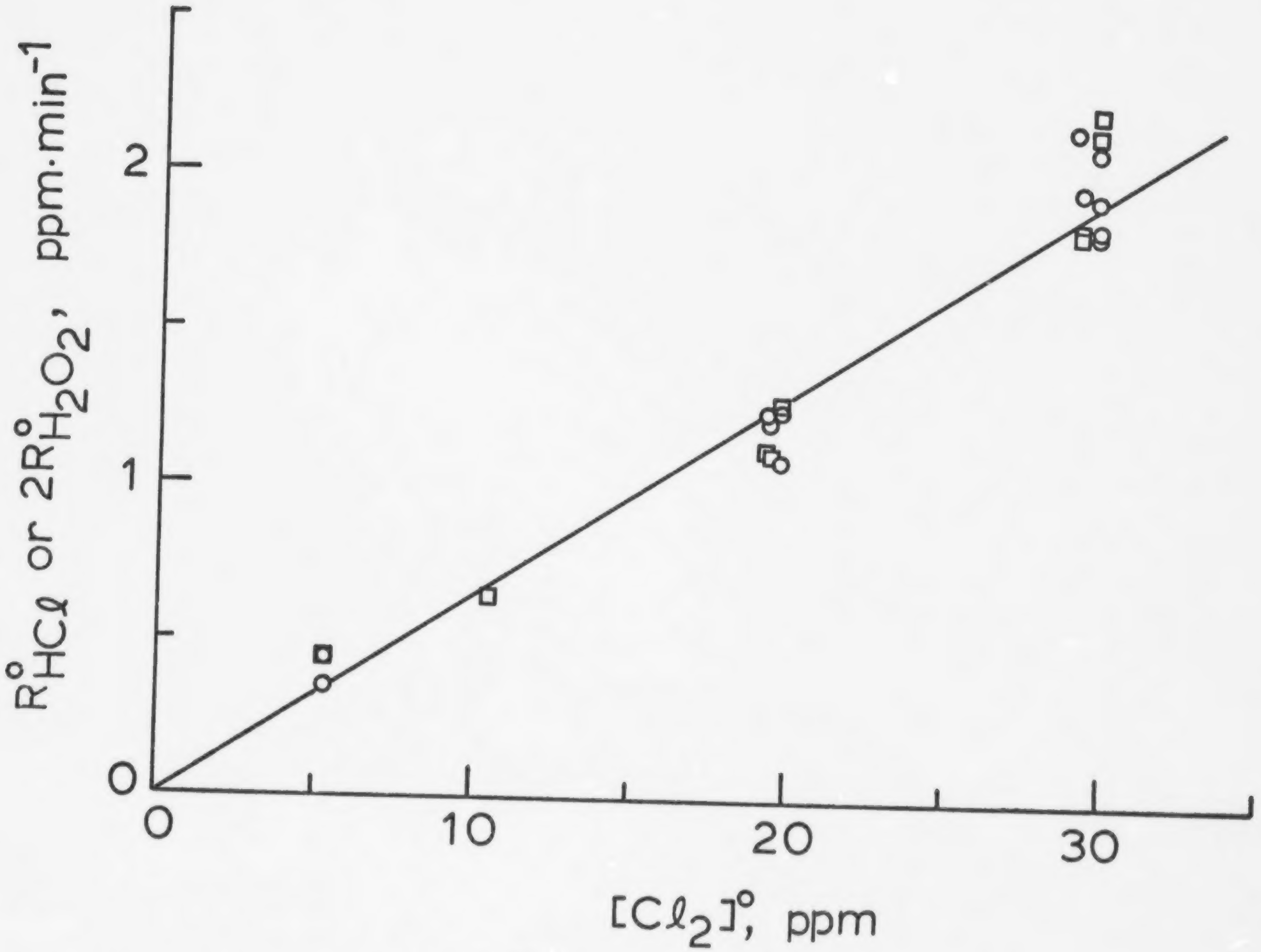

Figure 22. Plot of R°_{HCl} (circles) and $2R^{\circ}_{H_2O_2}$ (squares) versus $[Cl_2]^{\circ}$; experimental conditions: P_{O_2} = 100 torr, P_{H_2} = 20 torr, P_{N_2} = 580 torr; temperature, 25 ± 3°C.

$$Cl + O_2\ (+M) \rightarrow ClOO\ (+M) \tag{12}$$

$$O_3 + h\nu\ (+Wall?) \rightarrow 3/2\ O_2\ (+Wall?) \tag{13}$$

For our conditions the Cl-atoms formed in (3) will react largely with O_3. The equilibrium, $Cl + O_2 \rightleftarrows ClOO$ involving (11) and (12), lies well to the left in our experiments. However note that a fraction of the OCl radicals formed, $(k_8 + k_{10}/2)/(k_8 + k_9 + k_{10})$, regenerate Cl-atoms in reaction (8) followed by (11) and in (10). A kinetic analysis of this system suggests that the rate of O_3 loss will be given by relation III:

$$-R_{O_3} = 2k_3[Cl_2](1 + R + R^2 + R^3\ .\ .\ .) + [O_3]k_{13} \tag{III}$$

Here $R = (k_8 + k_{10}/2)/(k_8 + k_9 + k_{10})$. The present published estimates for the rate constants k_8, k_9, and k_{10} give $R \simeq 0.658$. The value of $\sum_{n=0}^{\infty} R^n = (1 - R)^{-1}$, and hence relation IV should describe the rate of O_3 loss in our system:

$$-R_{O_3} - [O_3]k_{13} = 2k_3[Cl_2](1 - 0.658)^{-1} = (5.84)k_3[Cl_2] \tag{IV}$$

Our experimental results show that O_3 decay in the irradiated Cl_2, O_3, O_2 system is zero order in $[O_3]$ over a large part of the reaction. This is the expected result from relation IV for the condition $-R_{O_3} \gg [O_3]k_{13}$. The experimental rate data from the photolysis of these mixtures has been plotted in the form of relation IV in Figure 23. From the slope of this plot (0.230 ± 0.031) we estimate $k_3 = 0.230/5.84 = 0.039 \pm 0.005\ min^{-1}$. This compares reasonably well with our more direct estimate derived from the Cl_2, H_2, O_2 mixtures ($0.034 \pm 0.004\ min^{-1}$). Our data thus support the recent literature rate constant values k_8, k_9, and k_{10} which determine the partitioning of the OCl-OCl reaction between its alternative pathways. We feel that our best estimate of k_3 from all of the data is $0.035 \pm 0.003\ min^{-1}$, and this value was used in the subsequent product rate simulations.

A Test of the Kinetics of Formation of HOCl and Other Products of the Irradiated Cl_2, H_2, O_3, O_2 Mixtures

In order to test the mechanism of formation of HOCl and other products formed in the irradiated Cl_2, H_2, O_3, O_2 mixtures, a series of kinetic experiments was carried out over a wide range of reactant ratios, $[H_2]/[O_3] = 0.10 \times 10^3$ to 6.79×10^3. An initial concentration of Cl_2 of 60 ppm was employed in these experiments. Time-dependent absorbance data for reactants and products before and during the irradiation were determined in the fashion illustrated in Figure 21. The resolution of the absorbances with overlapping spectral features, such as HOCl and H_2O_2 in the 1200-1275 cm^{-1} region, was accomplished by subtracting some measured fraction of the standard absorbance for a known quantity of the pure compounds. This procedure is illustrated in Figure 24. Here the absorbances due to CH_3 (small impurity in the O_2 supply) and H_2O_2 have been subtracted from the absorption spectrum to reveal the 1200-1275 cm^{-1} ν_2 band of HOCl alone. From the amount of H_2O_2 which was subtracted to resolve this spectrum, the amount of H_2O_2 present at that time was estimated. In this way the time dependence of the concentrations of the

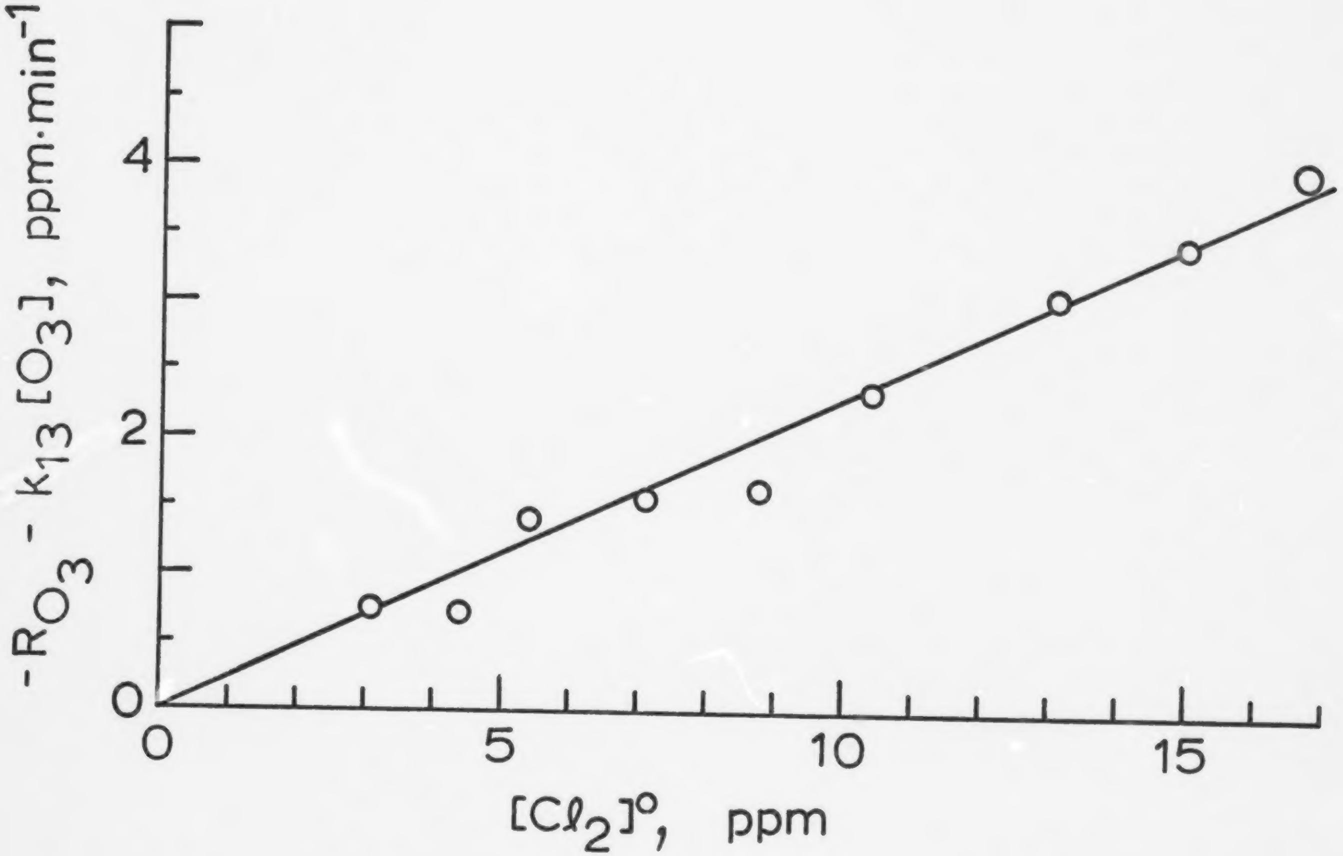

Figure 23. Plot of $-R_{O_3}$ $-k_{13}[O_3]$ versus $[Cl_2]$ from the photolysis of Cl_2, O_3 (about 20 ppm initially), $P_{O_2} = 10$, $P_{N_2} = 690$ torr; temperature, 25 ± 3°C.

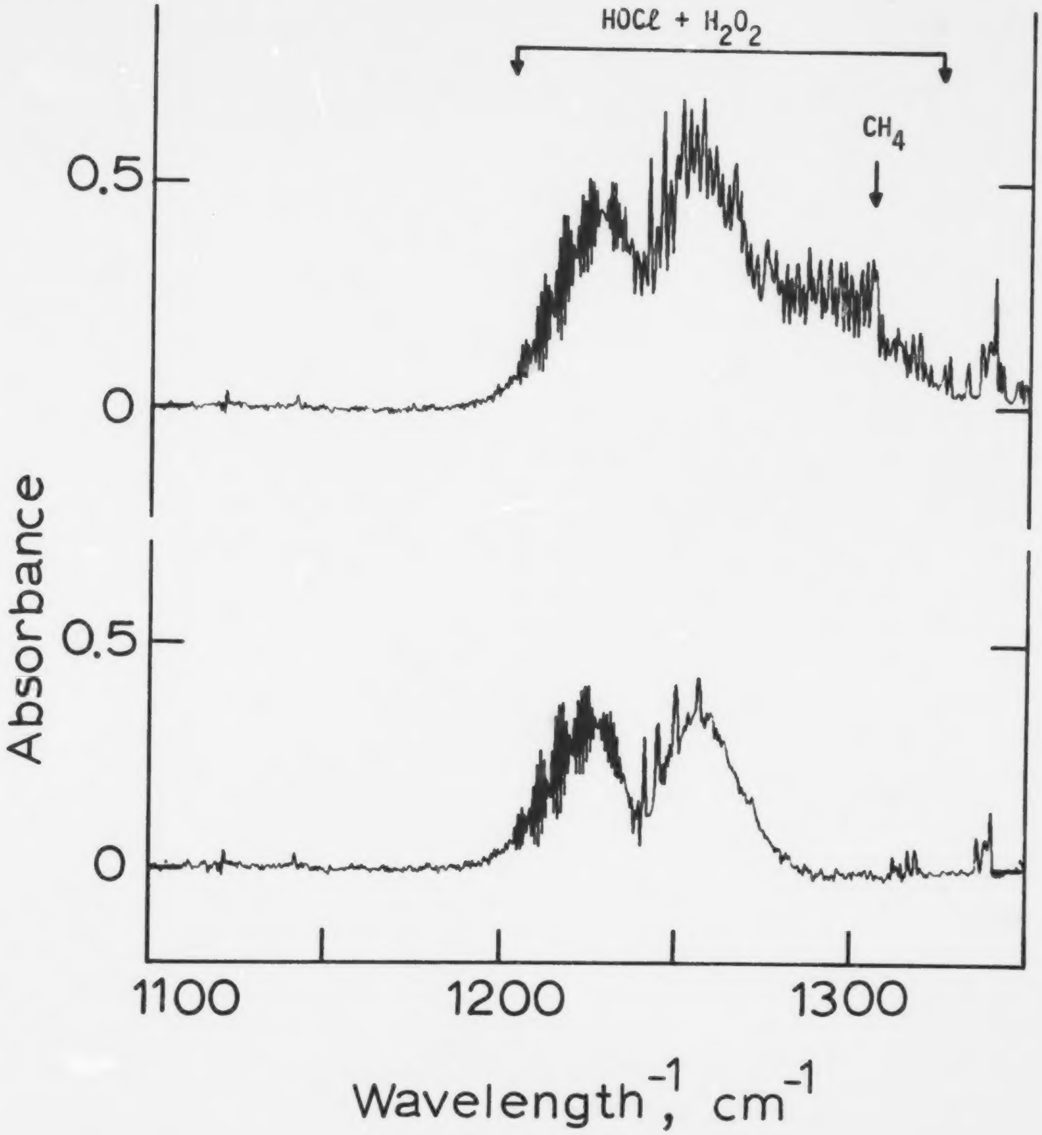

Figure 24. Absorbance of HOCl and H_2O_2 products within the 1100 to 1350 cm^{-1} region; upper spectrum is from the products after 5.12 min irradiation of the mixture of the composition listed in Figure 20 caption; lower curve, absorbance spectrum of HOCl remaining after absorbance of standard samples of H_2O_2 and CH_4 were used to balance out contributions from these species; remaining absorbances beyond 1300 cm^{-1} result from H_2O impurity.

products H_2O_2 and HCl and the reactant O_3 were determined. Since the absolute extinction coefficients for HOCl were not available at the outset of our experiments, only the time dependence of the absorbance of the product HOCl could be determined initially. A typical profile of the time dependences of the various species formed in one of the kinetic runs is shown in Figure 25. These data were used in turn to determine the rates of product formation at short irradiation times (see Table 12 and Figures 26-29).

The reactions (1), (3-10) should describe well most of the chemistry in the irradiated dilute mixtures of Cl_2, H_2, O_3, in O_2. However there are several other reactions which contribute somewhat to the observed chemistry. Thus O_3 decay in the H_2-rich mixtures can occur through reactions (14), (15), and (16):

$$HO_2 + O_3 \rightarrow HO + 2O_2 \tag{14}$$

$$H + O_3 \rightarrow HO + O_2 \tag{15}$$

$$HO + O_3 \rightarrow HO_2 + O_2 \tag{16}$$

Simulations show that only reaction (14) contributes measurably to O_3 decay for our conditions; even it is unimportant at low $[H_2]/[O_3]$ ratios. The HO radical formed in (14) will react primarily in (17) with the large excess of H_2 which is present, and ultimately another HO_2 radical will be regenerated in (6):

$$HO + H_2 \rightarrow H + H_2O \tag{17}$$

$$H + O_2\ (+M) \rightarrow HO_2\ (+M) \tag{6}$$

We observe OClO, presumably formed in (10), as a product at low concentrations in Cl_2, O_3, O_2 mixture photolyses (absence of H_2) through its characteristic absorption near 1109 cm^{-1}. In this case the ClO-ClO interactions (8-10) are the dominant loss steps for ClO. Reactions (8-10) are much less important in the Cl_2, H_2, O_3, O_2 mixture photolyses at high H_2 since the fast reaction (1) is the highly favored reaction when the $[HO_2]$ is relatively high:

$$HO_2 + OCl \rightarrow O_2 + HOCl \tag{1}$$

The OClO formed in the system should photolyze quite rapidly; we estimate from the extinction data for this compound[81] and our relative lamp intensity as a function of wavelength (Figure 17) that $k_{18} \cong 0.24\ min^{-1}$:

$$OClO + h\nu \rightarrow O + OCl \tag{18}$$

In a similar fashion we have estimated the rate constant for the photolysis reaction (19) for HOCl in our system using the extinction data from Molina and Molina[78]; $k_{19} \cong 4.2 \times 10^{-3}$:

$$HOCl + h\nu \rightarrow HO + Cl \tag{19}$$

54

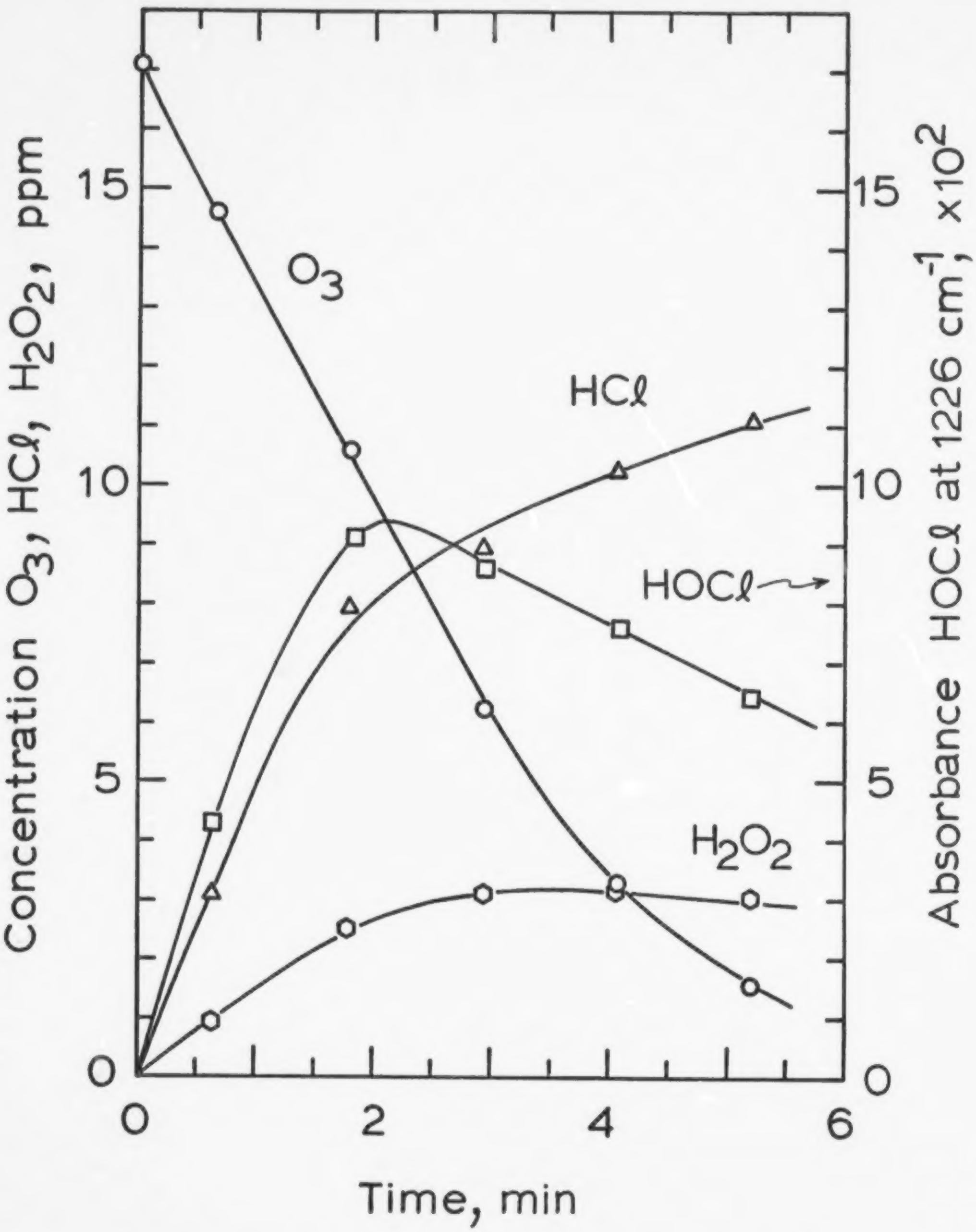

Figure 25. The concentrations of products versus time in the photolysis of Cl_2, H_2, O_3, O_2, N_2 mixture of initial composition: O_3, 17.1 ppm; Cl_2, 60 ppm; H_2, 6.20×10^4ppm; $P_{O_2} = 19.4$ torr; $P_{N_2} = 634$ torr.

TABLE 12. EXPERIMENTAL RATE DATA FROM THE PHOTOLYSIS OF Cl_2, O_3, H_2, O_2 MIXTURES[a]

Time (min)	$[H_2]/[O_3]$ ($x\ 10^{-3}$)	$-R_{O_3}$	R_{HCl} ($ppm^{-1}min^{-1}$)	$R_{H_2O_2}$	$d(Abs_{HOCl})/dt$[b] (min^{-1})
0.62	0.10	9.68	0.96	0	0.094
0.62	0.10	4.27	0.81	0	0.065
1.75	0.14	5.09	0.82	0	0.103
0.62	0.14	5.65	1.13	0	0.090
1.76	0.14	7.63	0.67	0	0.088
0.62	0.15	10.68	1.40	0	0.104
1.75	0.19	7.14	1.11	0	0.113
0.61	0.41	4.43	1.85	0	0.117
1.73	0.53	4.73	1.76	0	0.154
0.63	0.72	2.86	1.76	0	0.159
1.78	0.85	3.74	1.69	0	0.174
0.61	0.94	6.39	2.31	0	0.169
0.63	1.12	3.33	2.22	0.17	0.161
1.74	1.20	4.69	1.76	----	0.179
1.78	1.37	4.26	2.47	0.49	0.133
0.63	1.48	3.02	2.24	0.44	0.137
1.78	1.80	3.83	2.96	0.63	0.114
0.63	1.87	3.49	2.89	0.67	0.131
0.62	2.14	3.87	2.85	0.79	0.119
1.78	2.26	4.00	3.29	0.77	0.094
0.64	2.39	3.12	2.22	0.92	0.094
1.75	2.61	3.63	3.43	0.78	0.099
0.63	2.62	2.06	2.86	1.03	0.091
1.77	2.86	3.63	3.50	0.88	0.077
0.63	3.31	2.06	3.60	1.29	0.076
1.76	3.85	4.07	3.79	1.12	0.065
0.64	4.03	2.34	----	1.43	0.067
0.62	4.51	1.77	3.63	1.56	0.059
1.79	4.91	3.45	4.22	1.38	0.042
1.75	5.67	3.27	3.89	1.41	0.036
0.43	5.80	1.21	3.44	1.49	0.039
1.16	6.79	2.01	3.99	1.59	0.037

---

[a] Initial concentration of Cl_2 was 60 ppm in all experiments; the initial ozone concentrations were in the range of 18 ppm; temperature, 25 ± 3°C.

[b] Rate of change of absorbance of HOCl ($1226\ cm^{-1}$) with time.

56

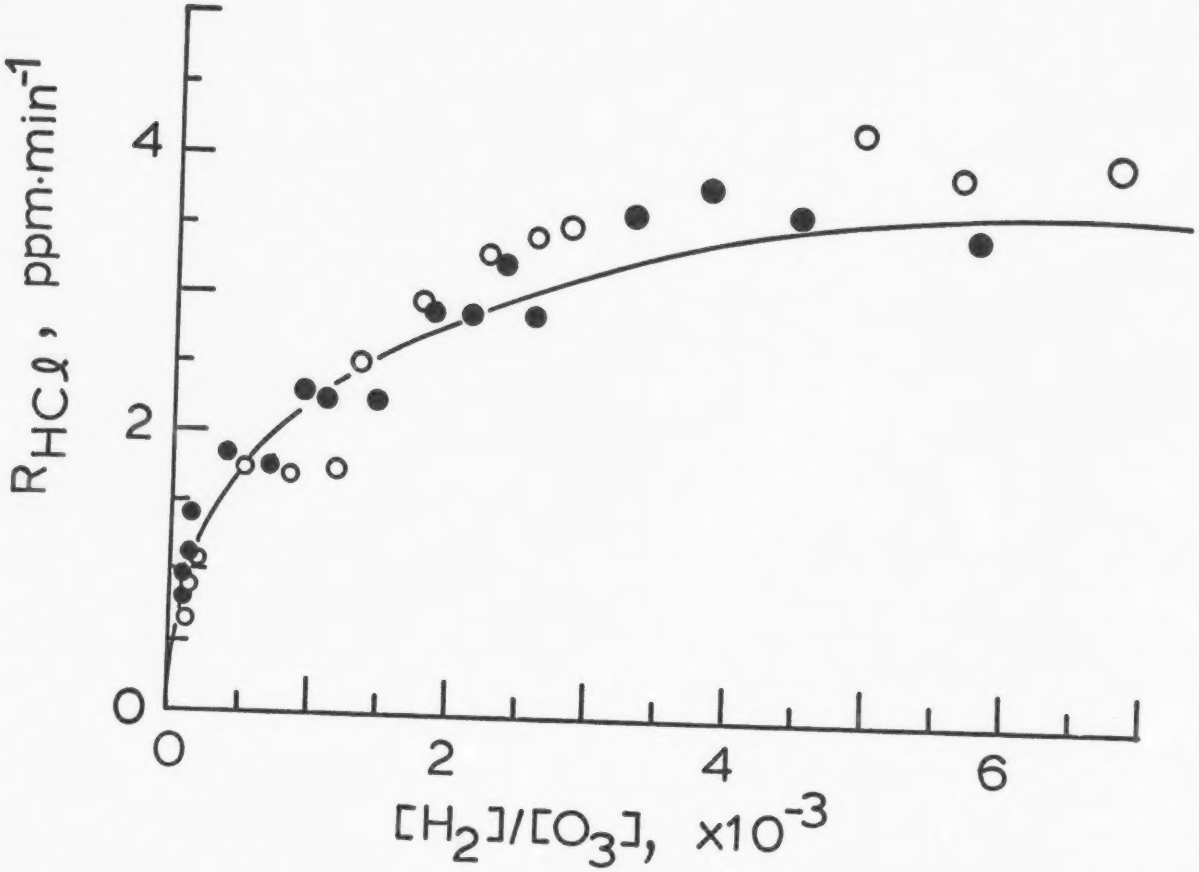

Figure 26. Rates of HCl formation in the photolysis of Cl_2, H_2, O_3, O_2, N_2 mixtures at varied $[H_2]/[O_3]$ ratios; data were estimated from the 0.62 (closed circles) and 1.74 min points (open circles); initial concentrations: Cl_2, 60 ppm; O_3, 16.1-23.5 ppm; H_2, 570-62,000 ppm; solid curve represents a computer simulation of the rates at 0.62 min based upon a complete reaction mechanism given in Table 11.

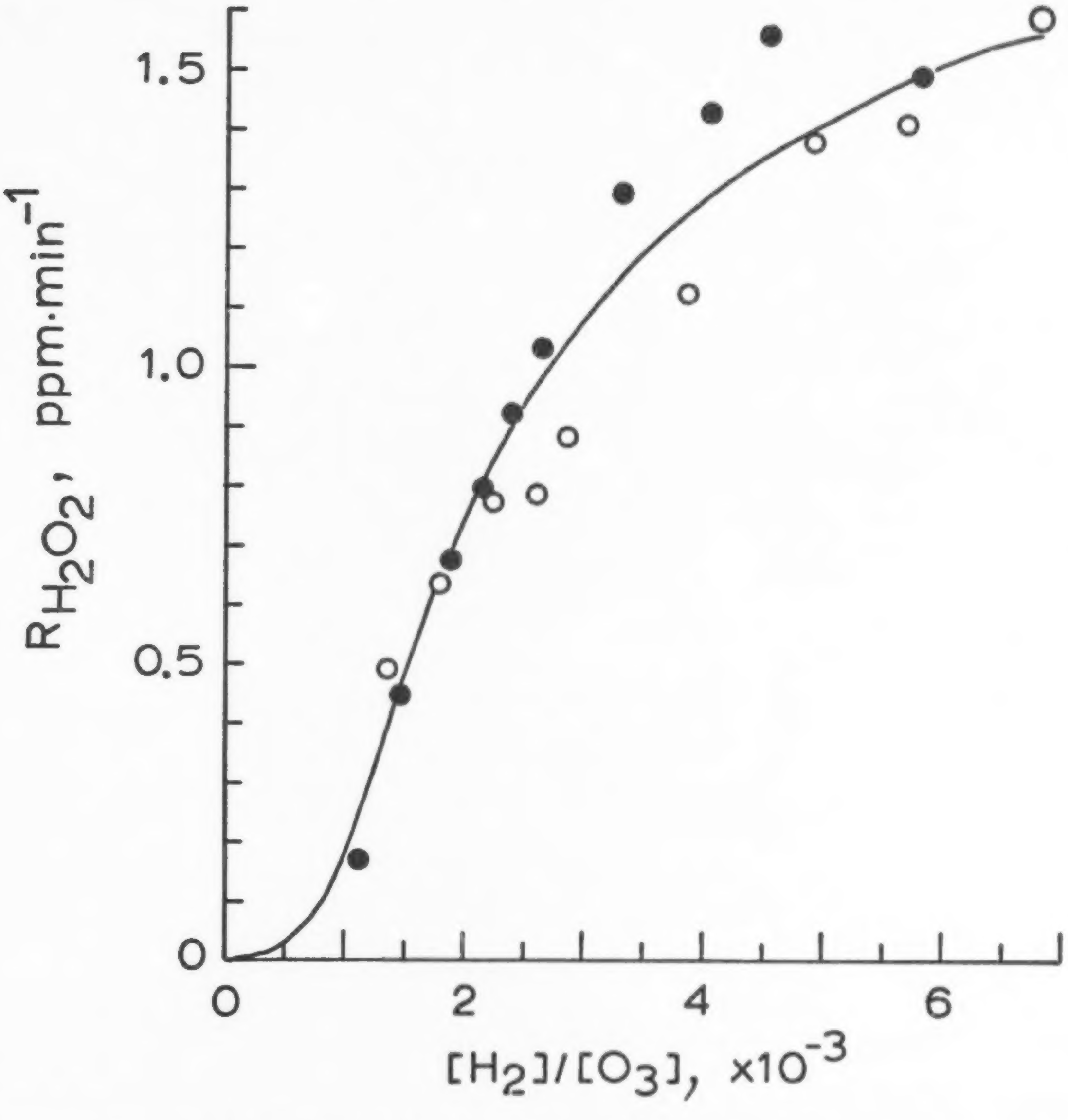

Figure 27. Rates of H_2O_2 formation in the photolysis of Cl_2, H_2, O_3, O_2, N_2 mixtures at varied $[H_2]/[O_3]$ ratios; conditions as outlined in Figure 26.

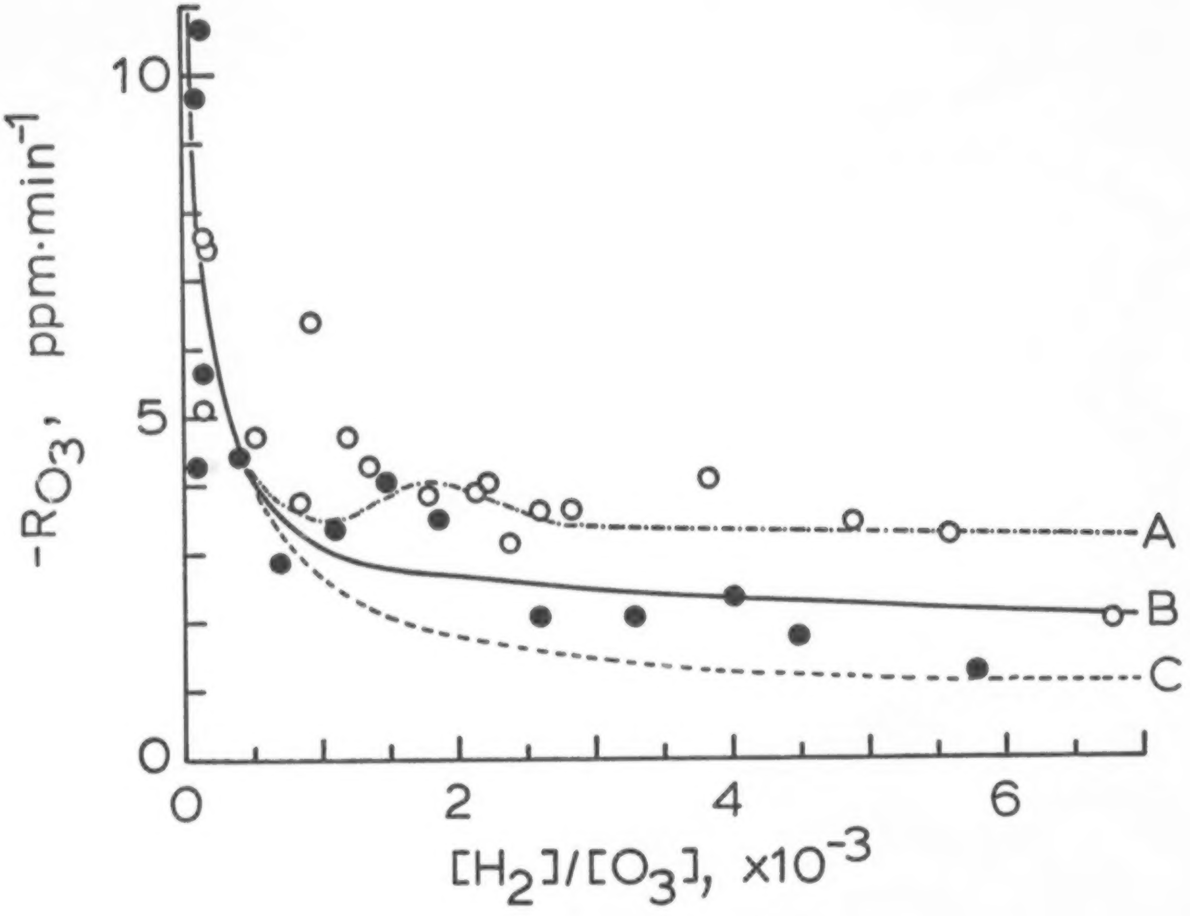

Figure 28. Rates of O_3 loss in the photolysis of Cl_2, H_2, O_3, O_2, N_2 mixtures at varied $[H_2]/[O_3]$ ratios; conditions as outlined in Figure 26; the curves shown are computer simulations of the rates at 0.62 min based upon a complete reaction mechanism given in Table 11 but with k_{14} = 6.0 (A), 3.0 (B), and 0.0 ppm^{-1}min^{-1} (C).

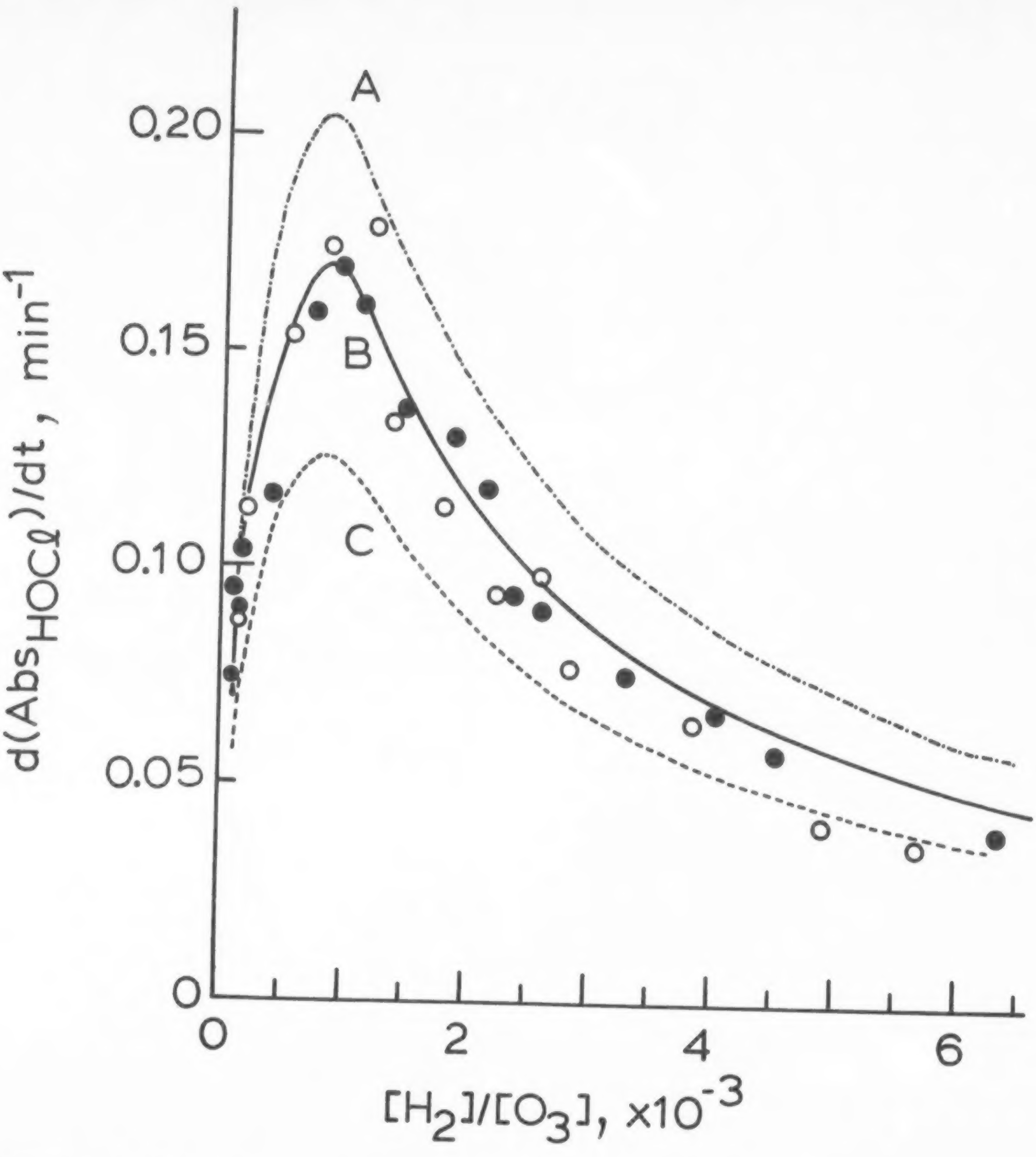

Figure 29. Rate of change of the absorbance of HOCl (1226 cm^{-1}) with time versus $[H_2]/[O_3]$ ratios from the photolysis of Cl_2, H_2, O_3, O_2, N_2 mixtures; conditions as outlined in Figure 26; the solid and dashed curves represent the results of computer simulations with various choices for the extinction coefficient of HOCl at 1226 cm^{-1}; $\epsilon = 6.50 \times 10^{-4}$ (curve A); 5.36×10^{-4} (B); $4.00 \times 10^{-4} ppm^{-1}m^{-1}$ (C); the match of these data was used to establish the extinction coefficient for HOCl.

BEGIN FIRST LINE OF TEXT HERE
TYPING GUIDE SHEET
CENTER OF PAGE
TOP OF IMAGE AREA
DROPPED HEAD; BEGIN SECTIONS HERE

Alternative sinks for Cl-atoms exist in experiments at long exposure times and for experiments at low $[O_3]$ and $[H_2]$. Thus reactions (20-24) were included in our mechanism:

$$Cl + HOCl \rightarrow HCl + OCl \tag{20}$$

$$Cl + H_2O_2 \rightarrow HCl + HO_2 \tag{21}$$

$$Cl + ClOO \rightarrow 2ClO \tag{22}$$

$$Cl + ClOO \rightarrow Cl_2 + O_2 \tag{23}$$

For the usual experimental conditions which we employed these reactions are relatively unimportant at short times.

Two other possible reactions of the OCl radical should be considered for our H_2-rich system:

$$OCl + H_2 \rightarrow HOCl + H \tag{24}$$

6-1/2"

$$OCl + H_2O_2 \rightarrow HOCl + HO_2 \tag{25}$$

Current literature sources[82] suggest $k_{24} < 1.5 \times 10^{-4}$ ppm^{-1}min^{-1}. There are no current estimates for k_{25}, although we can feel confident that $k_{25} < k_{21}$, and it will be relatively unimportant for rate data from short exposure times where $[H_2O_2]$ is low. We can use our data to define better the limits on k_{24} and k_{25}.

The reaction sequence (1-25) listed in Table 11 was used in computer simulations to test the mechanism against the experimental data summarized in Table 12. From these simulations the product rates were determined for exposure times of 0.62 min; these estimates are shown as the solid curves in Figures 26-29 where they may be compared with the experimental rate data. The filled circles represent the data for 0.62 min exposure; the open circles are from rates at 1.76 min. Obviously the theoretical dependence of initial product rates on the reactant ratio $[H_2]/[O_3]$ matches very well that observed experimentally in the case of HCl and H_2O_2 formation and O_3 loss rates, and some confidence in the mechanism choice is gained. The rate data for HOCl shown in Figure 29 are presented as rates of change of absorbance (1226 cm^{-1}) with time, since extinction data from standard samples were not available initially in this case. Different choices of this ϵ were made in attempts to match these data using the computer-generated rate data based upon the complete reaction scheme given in Table 11. Again it is clear that the mechanism outlined predicts well the shape of the experimentally observed dependence of the R_{HOCl} upon $[H_2]/[O_3]$ ratio. From the best visual match between the experimental $d(Abs_{HOCl})/dt$ versus $[H_2]/[O\ ]$ data and the simulations (solid curve in Figure 29), we estimated $\epsilon_{HOCl} \cong 5.36 \times 10^{-4}$ ppm^{-1}m^{-1} at 1226 cm^{-1} using 1 cm^{-1} resolution. This estimate was then used to calibrate the absolute extinction coefficients of HOCl within the three fundamental IR bands. The resulting ϵ versus $1/\lambda$ plots for these three regions are given in Figure 30. From the spectral data collected at 1 cm^{-1} we have estimated the more

BEGIN LAST LINE OF TEXT
BOTTOM OF IMAGE AREA; OUTSIDE DIMENSION FOR TABLES AND ILLUSTRATIONS
3/8"

EPA-287 (Cin.)
(4-76)

TYPING GUIDE SHEET

generally useful, and resolution insensitive, integrated band intensities, $\int \epsilon \, d(1/\lambda)$ where the limits on the integration include the range of the band. For ν_1, ν_2, and ν_3 regions, the integrated band intensities are 2.3×10^2, 3.0×10^2, and 4.3×10^1 $cm^{-2}atm^{-1}$, respectively (base for absorbance). Recently Marker et al.[84a] have estimated these quantities for the ν_2 and ν_3 bands by employing the thermal reactions, $HCl + Cl_2O \rightarrow HOCl + Cl_2$ and $H_2O + Cl_2O \rightleftharpoons 2HOCl$, for HOCl preparation; [HOCl] was estimated by mass balance as represented by these equations. Their preliminary estimates of the integrated band intensities for ν_2 and ν_3 regions are: 2.7×10^2 and 4.5×10^1 $cm^{-2}atm^{-1}$, respectively, in reasonable agreement with our estimates[84b] Both these experimental estimates are in qualitative accord with preliminary theoretical estimates of these quantities[85]: 5.0×10^2, 1.9×10^2, and 2.5×10^1 cm^{-2} atm^{-1} for the ν_1, ν_2, and ν_3 bands, respectively. Our present data should be accurate to about ± 20%, and it is hoped that they will provide a sound basis for the estimation of HOCl concentrations in the stratosphere.

New Kinetic Information Related to the Cl_2, O_3, H_2, O_2, System

Although the published rate constants for the reactions listed in Table 11 are in reasonable accord with our present findings, there are some refinements fo the older estimates which our data suggest. In particular the shapes of the theoretically predicted R_{HOCl} and R_{O_3} versus $[H_2]/[O_3]$ plots are somewhat sensitive to the choice of constants k_4, k_5, k_{14}, and k_{24}. In Figure 31 the experimental values of R_{HOCl} versus $[H_2]/[O_3]$ are compared with those calculated using the computer simulation and the rate constants of Table 11 but with k_4/k_5 varied: 0.69×10^3(curve A), 0.95×10^3(B), and 1.31×10^3(C).

$$Cl + O_3 \rightarrow OCl + O_2 \tag{4}$$

$$Cl + H_2 \rightarrow HCl + H \tag{5}$$

Our data favor $k_4/k_5 \simeq (9.5 \pm 1.5) \times 10^2 (25 \pm 3^\circ C)$. This is somewhat higher than the ratio of the presently preferred values of k_4 and k_5 for this temperature, but it is within the range of values which the previous data define, $(6.2 \pm 2.7) \times 10^2$. Our estimates of the integrated band intensities of HOCl are not very sensitive to the choice of k_4/k_5, although the $[H_2]/[O_3]$ ratio at which the maximum R_{HOCl} occurs in Figure 31 is shifted significantly with variation in this rate constant ratio.

Our present data provide a new estimate for the upper limit to k_{24}; in Figure 32 the comparison is given between the experimental R_{HOCl} versus $[H_2]/[O_3]$ values and the theoretical predictions for several choices of k_{24}:

$$OCl + H_2 \rightarrow HOCl + H \tag{24}$$

Observe that the use of $k_{24} = 1.5 \times 10^{-3} ppm^{-1}min^{-1}$ leads to a large mismatch of the theory and experiment. The choice of $k_{24} = 1.5 \times 10^{-4}$, the current upper limit cited in the literature, provides a better match. However taking $k_{24} = 1.5 \times 10^{-5} ppm^{-1}min^{-1}$ gives our best fit. This reaction is 10 kcal $mole^{-1}$ endothermic, and it is not surprising that k_{24} is this small. Our initial rate data are not sensitive to the choice of k_{25} since little H_2O_2 is present

EPA-287 (Cin.)
(4-76)

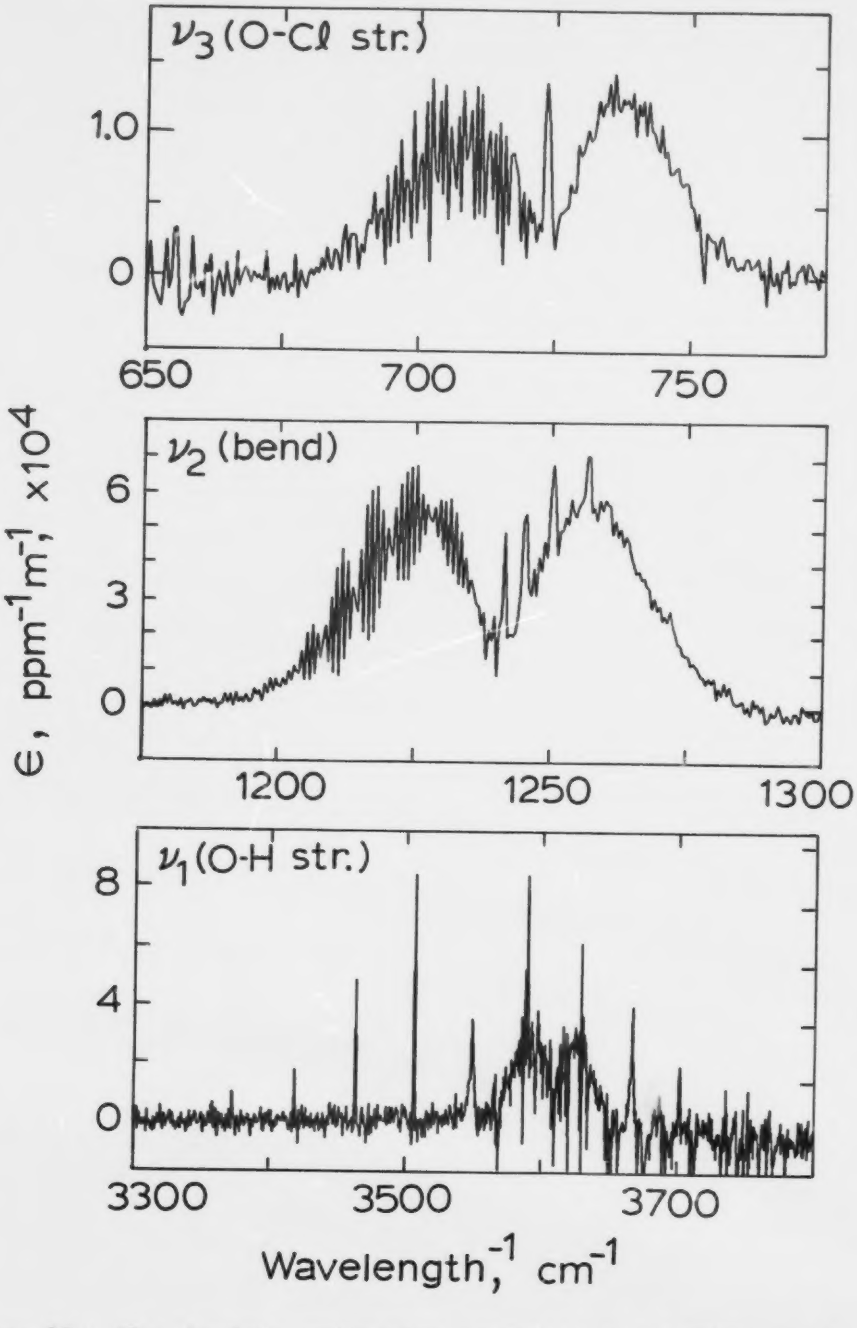

Figure 30. The absolute extinction coefficients of HOCl gas (1 cm^{-1} resolution) as a function of wavelength in the infrared, regions of the three fundamental vibrational transitions.

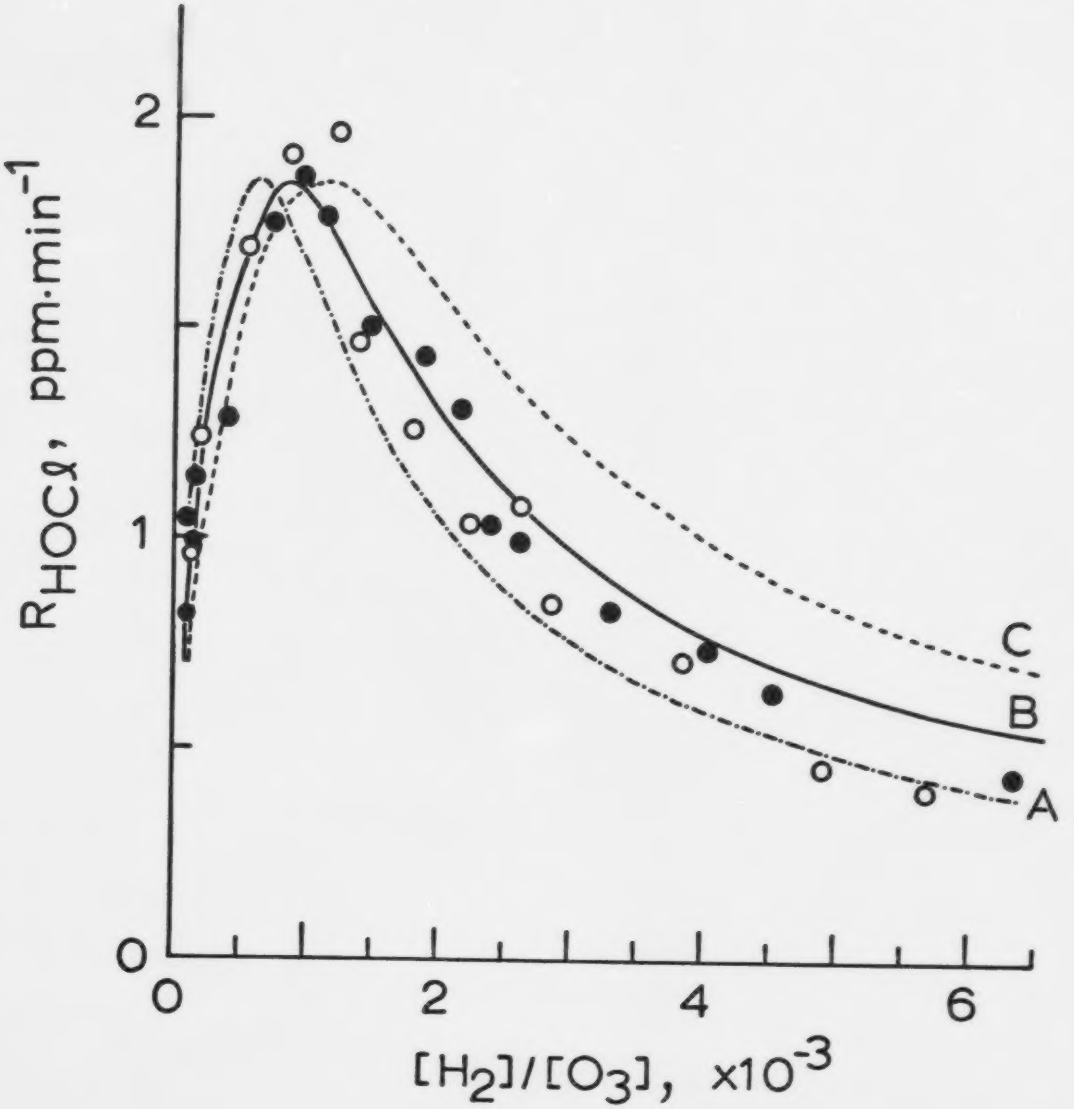

Figure 31. Rates of HOCl formation in the photolysis of Cl_2, H_2, O_3, O_2, N_2 mixtures at varied $[H_2]/[O_3]$ ratios; the curves are computer simulations of the results for various choices of the k_4/k_5 ratio: 0.69 x 10^3(curve A); 0.95 x 10^3 (B); 1.31 x 10^3 (C).

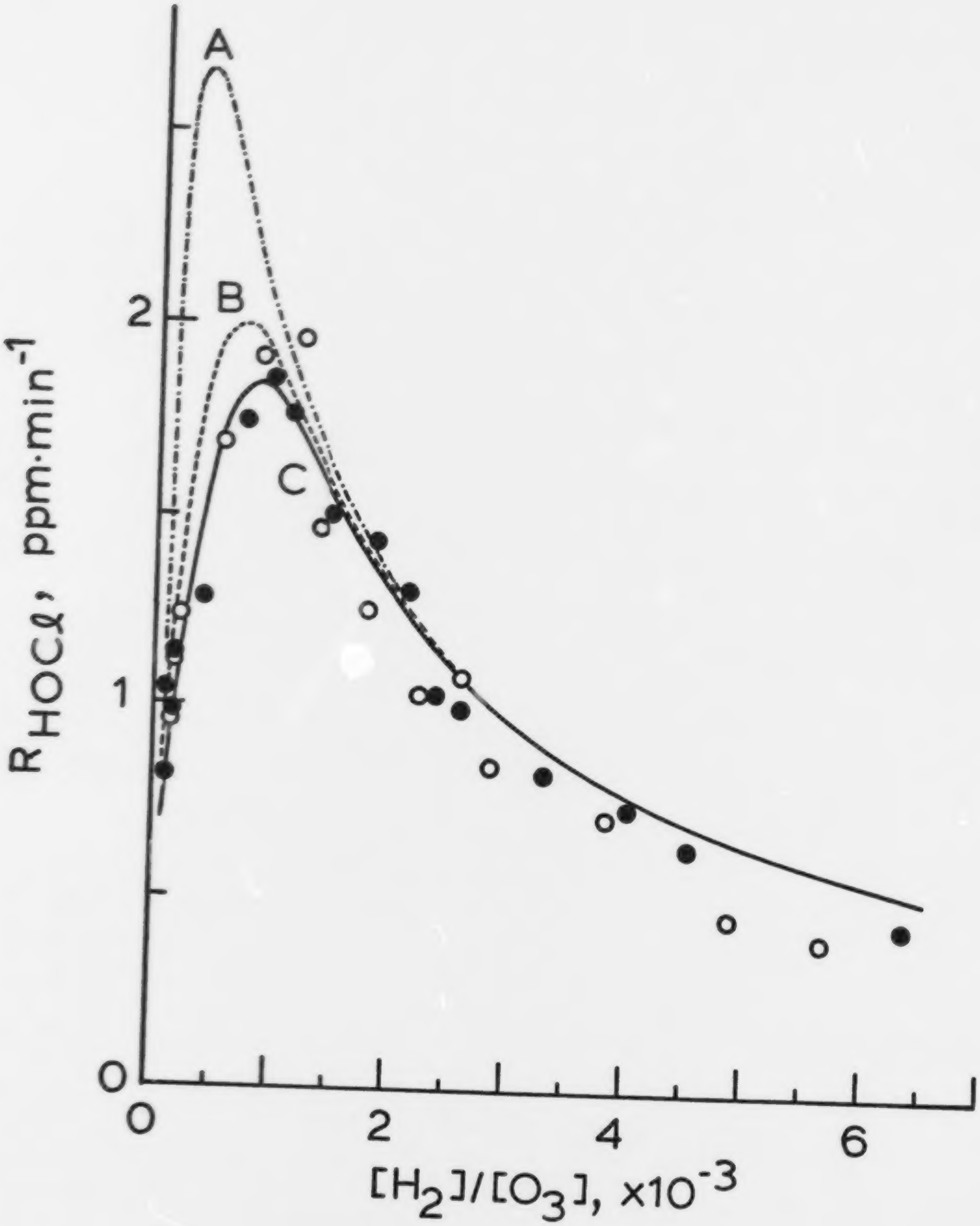

Figure 32. Rates of HOCl formation in the photolysis of Cl_2, H_2, O_3, O_2, N_2 mixtures at varied $[H_2]/[O_3]$ ratios; the curves are computer simulations of the results for various choices of the rate constant k_{24}: 1.5×10^{-3} (curve A); 1.5×10^{-4} (B); and 1.5×10^{-5} ppm^{-1}min^{-1} (C).

at early times. In Figure 33 one can see the effect of changing k_{25} from the upper limit of 6.9×10^2 set, assuming $k_{21} \geq k_{25}$, to 0. The slight displacement of the maximum in the theoretical R_{HOCl} versus $[H_2]/[O_3]$ curve tells us little about k_{25}. Since $\Delta H_{21} \simeq -13$ and $\Delta H_{25} \simeq -5$ kcal $mole^{-1}$, it is reasonable that $k_{25} < k_{21}$; in any case 25 is relatively unimportant for our conditions, and it is likely that k_{25} is much less than $6.9 \times 10^2 ppm^{-1} min^{-1}$.

Our O_3 loss rate data give some indication of the magnitude of k_{14} (see Figure 28). Simulations are shown using $k_{14} = 6.0$ (curve A), 3.0 (B), and

$$HO_2 + O_3 \rightarrow HO + 2O_2 \qquad (14)$$

0.0 $ppm^{-1}min^{-1}$(C). The O_3 data are subject to considerable scatter, but our computer fits are most consistent with the choice $k_{14} \leq 3.0 \pm 1.5$. This estimate lies within the range of values reported in recent work (1.9 ± 0.5).[82] Our estimate is expressed as a maximum value since an ill-defined O_3 loss reaction which is photochemically initiated appears in our system at long exposure times. Although O_3 (20 ppm) is very stable in the presence of 10 ppm of HCl in our unirradiated system, the decomposition of O_3 is catalyzed on irradiation when HCl or $HONO_2$ is present (10 ppm). Of course this reaction should be relatively unimportant in our experiments at short irradiation times, but we cannot rule out a small contribution (<5%) for which a correction could not be made realistically.

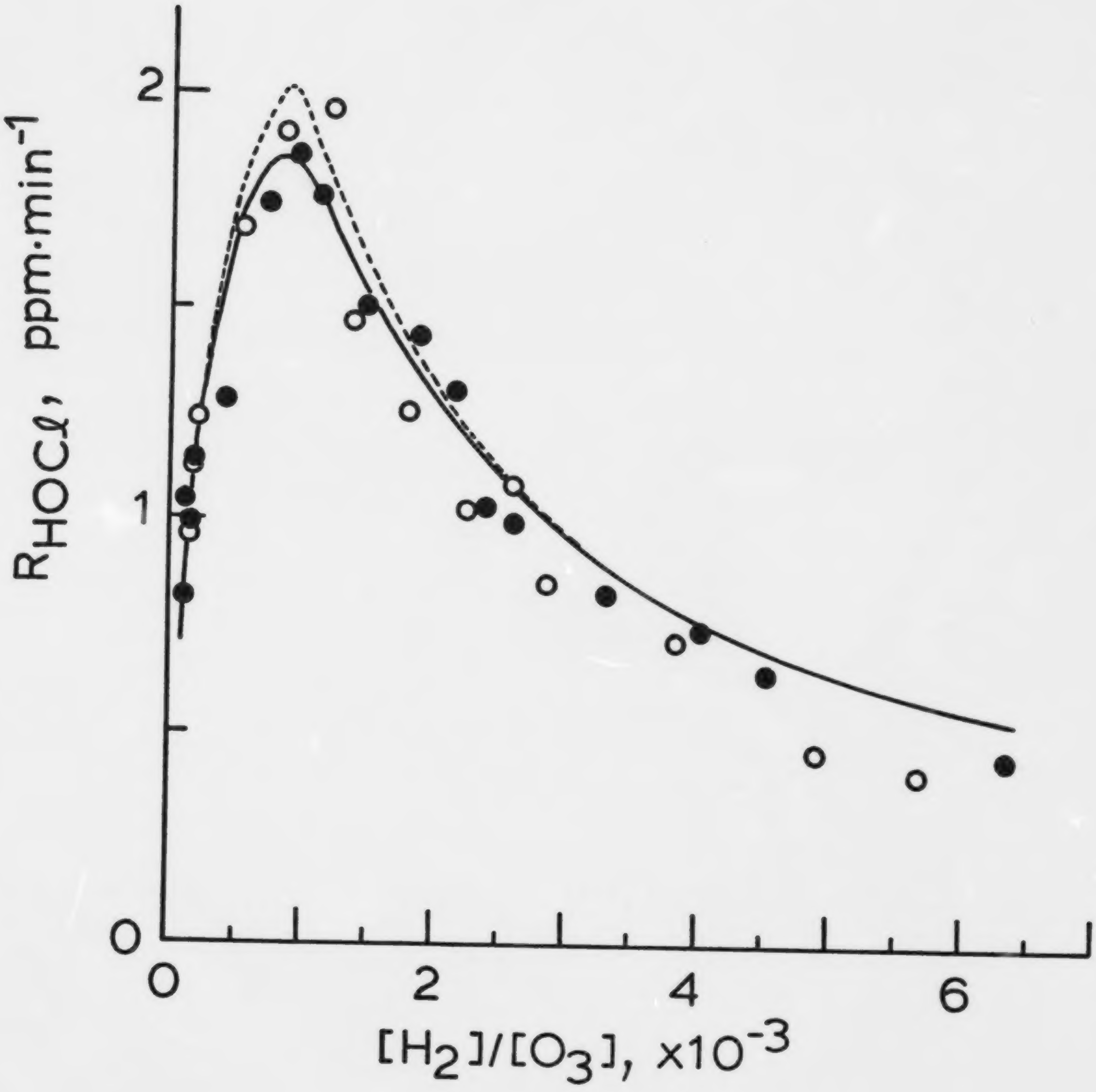

Figure 33. Rates of HOCl formation in the photolysis of Cl_2, H_2, O_3, O_2, N_2 mixtures at varied $[H_2]/[O_3]$ ratios; the curves are computer simulations of the results for two choices of the rate constant k_{25}: 6.90 x 10^2 (dashed line); 0 ppm^{-1}min^{-1} (solid line).

BEGIN FIRST LINE OF TEXT HERE
TYPING GUIDE SHEET
CENTER OF PAGE
TOP OF IMAGE AREA
DROPPED HEAD, BEGIN SECTIONS HERE

SECTION 8

RATE STUDIES OF THE REACTIONS OF THE $(CH_3)_2N$ RADICAL WITH O_2, NO, AND NO_2

INTRODUCTION

The high potency of the nitrosamines in inducing cancer in test animals has focused interest in recent years on the potential for nitrosamine formation in polluted urban atmospheres.[86] Indeed recent studies[87-90] show qualitatively that nitrosamine formation may result in simulated polluted atmospheres. The dark reaction generating $(CH_3)_2N\text{-}N{=}O$ from HONO and $(CH_3)_2NH$ vapors[87] appears to be largely heterogeneous in character, and it is probably not a significant homogeneous source of nitrosamines in the atmosphere.[88] The irradiated dilute mixtures of dimethyl or diethylamine (R_2NH), HONO, NO, and NO_2 in air lead to detectable levels of the corresponding nitrosamines ($R_2N\text{-}N{=}O$) and nitramines ($R_2N\text{-}NO_2$).[89,90] In theory these products may arise from a reaction sequence initiated by HONO photolysis, $HONO + h\nu \rightarrow HO + NO$, and subsequent HO-radical attack on the amine; e.g., the reactions (1a) and (1b) in the case of the dimethylamine reactant:

$$HO + (CH_3)_2NH \rightarrow H_2O + (CH_3)_2N \qquad (1a)$$

$$HO + (CH_3)_2NH \rightarrow H_2O + CH_2NHCH_3 \qquad (1b)$$

Recent experimental measurements[91] show that the rate constant sum, $k_{1a} + k_{1b}$ is large, 3.94×10^{10} ℓ mole^{-1} sec^{-1}; the ratio $k_{1a}/(k_{1a} + k_{1b})$ is not known. The $(CH_3)_2N$ radical product of (1a) may in theory react with the small amount of NO and NO_2 in (3) and (4), respectively, to form the observed products, provided that the reaction with the large excess of O_2 in (2) is sufficiently slow to allow this competition:

$$(CH_3)_2N + O_2 \rightarrow \text{Products} \qquad (2)$$

$$(CH_3)_2N + NO \rightarrow (CH_3)_2N\text{-}N{=}O \qquad (3)$$

$$(CH_3)_2N + NO_2 \rightarrow (CH_3)_2N\text{-}NO_2 \text{ (or other products)} \qquad (4)$$

The nitrosamine, in contrast to the nitramine, photodecomposes at the short wavelengths of sunlight present within the lower troposphere ($\lambda < 4200$ A), and hence its buildup is significantly limited by (I):

$$(CH_3)_2N\text{-}N{=}O + h\nu \rightarrow (CH_3)_2N + NO \qquad (I)$$

BEGIN LAST LINE OF TEXT
BOTTOM OF IMAGE AREA, OUTSIDE DIMENSION FOR TABLES AND ILLUSTRATIONS
3/8"

PAGE NUMBER
EPA-287 (Cin.)
(4-76)

BEGIN FIRST LINE OF TEXT HERE
TYPING GUIDE SHEET
CENTER OF PAGE
TOP OF IMAGE AREA
DROPPED HEAD. BEGIN SECTIONS HERE

Quantitative rate information on these reactions is not now available. In this work we have derived the kinetic data related to this system using long-path FT-IR spectroscopy. The nature of the reaction (2) has been determined for the first time as well as the needed rate constant data, k_I, $k_{1a}/(k_{1a} + k_{1b})$, k_2/k_3, and k_3/k_4. These results, coupled with the measured value of $k_{1a} + k_{1b}$ of Atkinson et al.,[91] make possible quantitative predictions concerning the significance of this homogeneous mechanism leading to nitrosamines and nitramines in the polluted atmosphere.

EXPERIMENTAL

A brief description of the long-path, FTS-IR equipment and large photochemical reactor employed in this work has been given previously,[92] and more detailed reports are also available.[93,94] $(CH_3)_2N$ radicals were prepared photochemically employing three different sources. In one series of experiments dilute mixtures of HONO and $(CH_3)_2NH$ were irradiated. From these studies the rate constant ratio $k_{1a}/(k_{1a} + k_{1b})$ was estimated. However the heterogeneous thermal reactions of HONO and $(CH_3)_2NH$ discouraged the use of this system as a quantitative source of $(CH_3)_2N$ radicals. The photolysis of $(CH_3)_2N\text{-}N{=}O$ and $(CH_3)_2N\text{-}N{=}N\text{-}N(CH_3)_2$ in dilute mixtures proved to be excellent homogeneous sources of the $(CH_3)_2N$ radical. The much better overlap of the ultraviolet absorption spectrum of the nitrosamine than that of the tetrazene with the emission envelope of the simulated solar spectrum of the lamps of the photochemical reactor favored the use of the nitrosamine in most of our experiments reported here. The initial products of the $(CH_3)_2N$ radical reactions in NO, NO_2, O_2 mixtures were unambiguously identified as largely $(CH_3)_2N\text{-}N{=}O$, $(CH_3)_2N\text{-}NO_2$, $CH_2{=}N\text{-}CH_3$, together with smaller amounts of HONO; formaldehyde and a trace of HCN appeared at later times. These products and reactants were determined at regular intervals during the photolysis of dilute mixtures of $(CH_3)_2N\text{-}N{=}O$ or $(CH_3)_2N\text{-}N{=}N\text{-}N(CH_3)_2$ in O_2 and N_2 mixtures (700 torr). Authentic samples of each reactant and product compound were prepared and purified using standard methods, and their IR spectra were determined at several concentrations in 700 torr N_2 and at 1 cm^{-1} nominal resolution. Concentration-absorbance plots followed Beer's law well for our conditions. The details of the preparative methods, the infrared spectra, and the extinction coefficient estimates are available elsewhere.[94]

The identification, synthesis, and calibration of the product dimethylmethyleneamine ($CH_2{=}N\text{-}CH_3$) offered a special challenge. The relatively stable trimer of this compound was prepared, purified, and introduced into the cell in weighed amount, and the spectra of the vapors were determined as a function of time. Changes in the spectrum showed the development of monomer from trimer. A plot of the absorbance at 917 cm^{-1}, attributable to trimer, versus absorbance at 1025^{-1}, attributable to monomer (each pair of values from a measurement at a given time), gave a straight line; similar absorbance data from experiments with different weighed samples of trimer gave parallel straight lines. The slope of these lines, equal in theory to $\epsilon_{trimer(917\ cm^{-1})}/3\epsilon_{monomer(1025\ cm^{-1})}$, and their intercepts could be used to derive the desired extinction coefficients of the monomer and trimer. From direct spectral observations of the trimer and monomer concentrations which were achieved at long times, the equilibrium constant for the

BEGIN LAST LINE OF TEXT
BOTTOM OF IMAGE AREA, OUTSIDE DIMENSION FOR TABLES AND ILLUSTRATIONS
3/8"

PAGE NUMBER
EPA-287 (Cin.)
(4-76)

BEGIN FIRST LINE OF TEXT HERE
TYPING GUIDE SHEET
CENTER OF PAGE
TOP OF IMAGE AREA
DROPPED HEAD; BEGIN SECTIONS HERE

dissociation of trimer to monomer was estimated at several temperatures in the range 14.5-23.3°C. These equilibrium data from direct spectroscopic observations of the reactant and product were in reasonable agreement with the data estimated by Gowenlock and Thomas[95] who used pressure measurements alone in experiments at much higher temperatures. These results certainly confirm our identification and analysis method for $CH_2=N-CH_3$.

The apparent first-order constant (k_I) for Me_2NNO photodecomposition was established to be $0.12 \pm 0.02\ min^{-1}$ for the experimental conditions employed in this work. This is also the theoretical constant for Me_2NNO decay in sunlight ($Z = 40^o$) which we estimate from our extinction data and solar irradiance estimates.

RESULTS AND DISCUSSION

Determination of Rate Constant Ratios

The present kinetic results allow a new insight into the reactions of the $(CH_3)_2N$ radicals in the atmosphere. Some typical time-concentration data obtained in an experiment with $(CH_3)_2N-N=O$ photolysis in 730 torr of O_2 are shown in Figure 34. These and other kinetic data taken from the first few minutes of the reaction in experiments at varied concentrations of NO, NO_2, and O_2 can be rationalized well in terms of the reaction sequence (I-4):

$$(CH_3)_2N-N=O + h\nu \rightarrow (CH_3)_2N + NO \qquad (I)$$

$$(CH_3)_2N + O_2 \rightarrow CH_2=N-CH \ + HO_2 \qquad (2)$$

$$(CH_3)_2N + NO \rightarrow (CH_3)_2N-N=O \qquad (3)$$

$$(CH_3)_2N + NO_2 \rightarrow (CH_3)_2N-NO_2 \qquad (4a)$$

$$(CH_3)_2N + NO_2 \rightarrow HONO + CH_2=N-CH_3 \qquad (4b)$$

For mixtures at low $[NO_2]$ this mechanism leads to the following rate functions related to the rate constant ratio k_2/k_3:

$$A = \frac{-R_{Me_2N-NO_2} - R_{Me_2N-N=O}}{k_I[Me_2N-N=O] + R_{Me_2N-N=O}} = \frac{k_2[O_2]}{k_3[NO]}$$

$$A' = \frac{R_{Me-N=CH_2}}{k_I[Me_2N-N=O] + R_{Me_2N-N=O}} = \frac{k_2[O_2]}{k_3[NO]}$$

The functions A and A' have been evaluated from the appropriate rate data from experiments over a range of $[O_2]/[NO]$ ratios. These are plotted versus the $[O_2]/[NO]$ ratio in Figure 35; the open and closed symbols represent the A and A' functions, respectively. It is clear that both functions define the same straight line and that the intercept is near zero within the error of the experiments, in agreement with theoretical expectations based upon the

BOTTOM OF IMAGE AREA; OUTSIDE DIMENSION FOR TABLES AND ILLUSTRATIONS
BEGIN LAST LINE OF TE
3/8"

PAGE NUMBER
EPA-287 (Cin.)
(4-76)

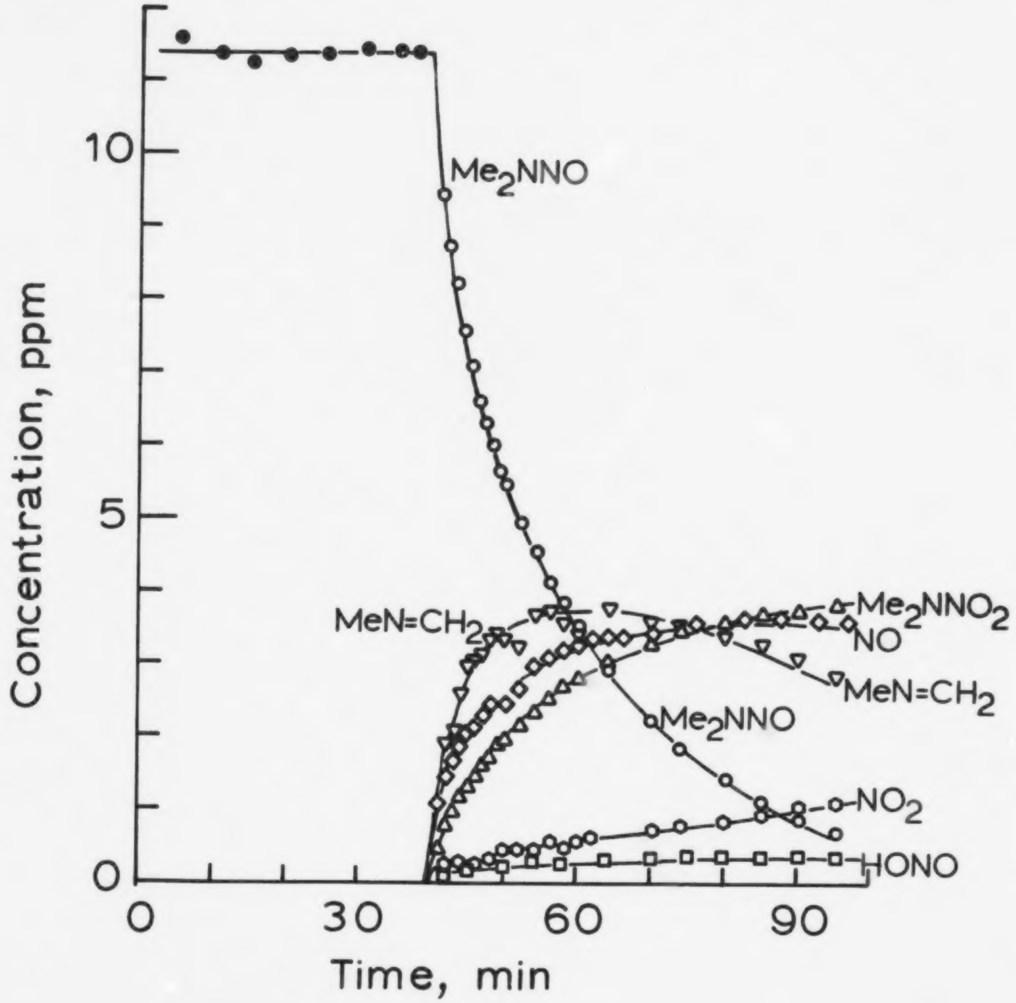

Figure 34. Concentration-time profile of the products of dimethylnitrosamine photolysis in 730 torr of O_2; illumination was initiated at 39.6 min.

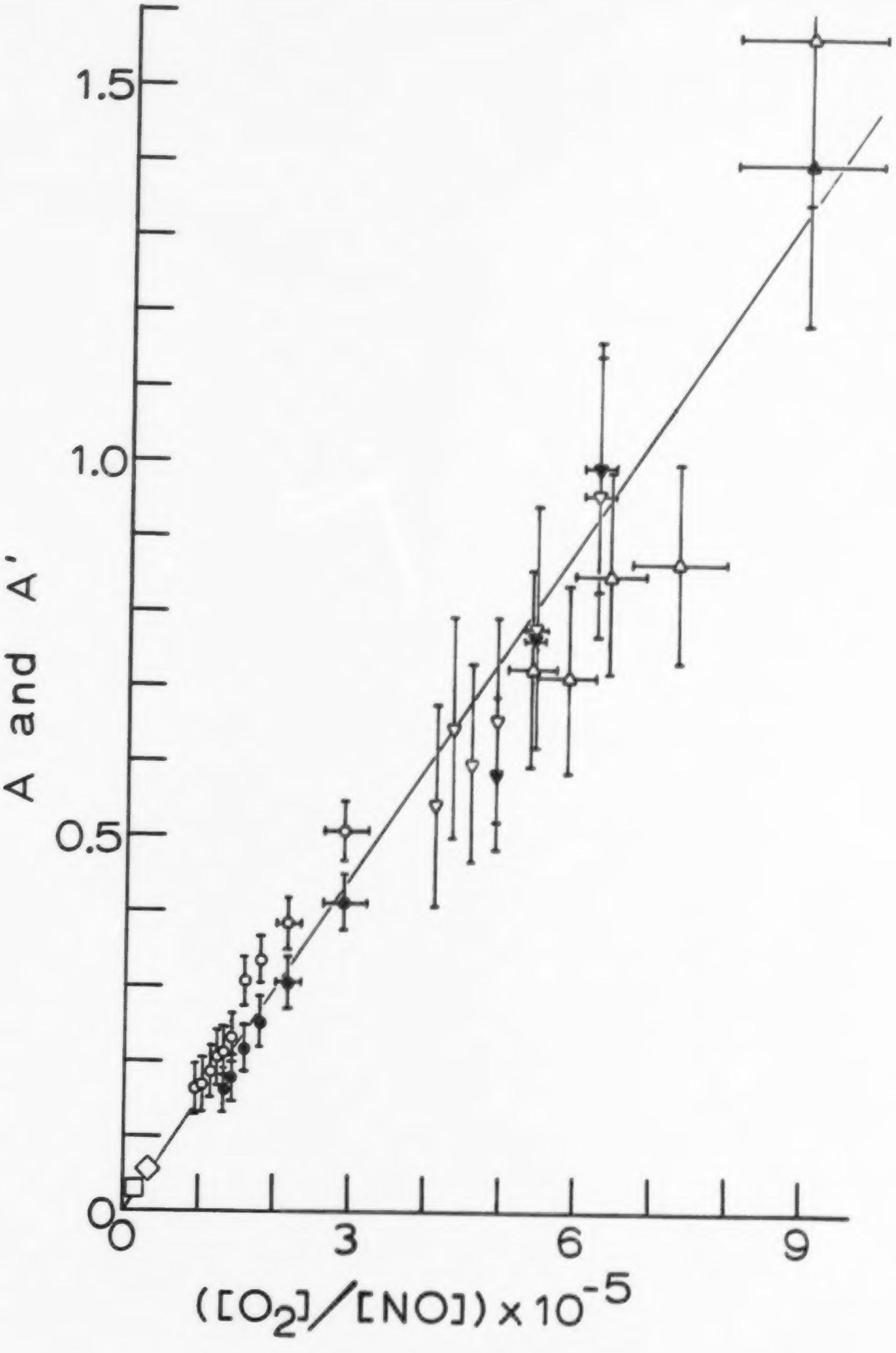

Figure 35. Plot of function A of the text (open symbols) and A' (closed symbols) versus $[O_2]/[NO]$ ratio; data were derived from a series of five dimethylnitrosamine photolyses in various O_2-NO-containing mixtures; in theory the slope of the plot gives k_2/k_3.

TYPING GUIDE SHEET

mechanism outlined. The slope of the line gives $k_2/k_3 = (1.48 \pm 0.07) \times 10^{-6}$ ($\pm 2\sigma$).

In experiments containing significant NO_2, the nitramine ($Me_2N\text{-}NO_2$) is the major product; small amounts of HONO also form. For these conditions and the operation of the above mechanism, one expects relations B and B' to hold:

$$B = \frac{-R_{Me_2N\text{-}N=O} - R_{Me_2N\text{-}NO_2}}{R_{Me_2N\text{-}NO_2}} = \frac{k_{4b}}{k_{4a}} + \frac{k_2[O_2]}{k_{4a}[NO_2]}$$

$$B' = \frac{R_{MeN=CH_2}}{R_{Me_2N\text{-}NO_2}} = \frac{k_{4a}}{k_{4b}} + \frac{k_2[O_2]}{k_{4a}[NO_2]}$$

The appropriate rate data from a series of experiments were used to evaluate B and B'; these data are plotted versus the $[O_2]/[NO_2]$ ratio in Figure 36. The slope and intercept of the plot provided the estimates $k_2/k_{4a} = (3.90 \pm 0.28) \times 10^{-7}$ and $k_{4b}/k_{4a} = 0.22 \pm 0.06$ (2σ).

The very low reactivity of the $(CH_3)_2N$ radical with O_2 compared to that with NO and NO_2 may seem surprising at first sight in view of the high reactivity of organic radicals with O_2, NO, and NO_2. However the results reported here are consistent with those observed for the unsubstituted amino radical (NH_2). Thus Lesclaux et al. found $k_5 \leq (1.2 \pm 0.6) \times 10^3$ ℓ $mole^{-1}sec^{-1}$ [96,97] and $k_6 = (1.1 \pm 0.2) \times 10^{10}$ ℓ $mole^{-1}sec^{-1}$ [98]:

$$NH_2 + O_2 \rightarrow \text{Products} \tag{5}$$

$$NH_2 + NO \rightarrow \text{Products} \tag{6}$$

The very low reactivity of NH_2 and $(CH_3)_2N$ with O_2 may reflect the thermodynamic instability of the O_2 adducts; this seems to be the case with some other electronegative species such as Cl and HO. Thus at equilibrium in air[100] at 25°C, 1 atm, the ratio $[ClOO]/[Cl] \simeq 2 \times 10^2$ [14], and $[HOOO]/[HO] \simeq 2.6 \times 10^{19}$:

$$Cl + O_2 \rightleftarrows ClOO \tag{7}$$

$$HO + O_2 \rightleftarrows HOOO \tag{8}$$

$$NH_2 + O_2 \rightleftarrows NH_2OO \tag{9}$$

$$(CH_3)_2N + O_2 \rightleftarrows (CH_3)_2NOO \tag{10}$$

One may suggest that each of the eqilibria is shifted to the left even in air at 1 atm pressure.

EPA-287 (Cin.)
(4-76)

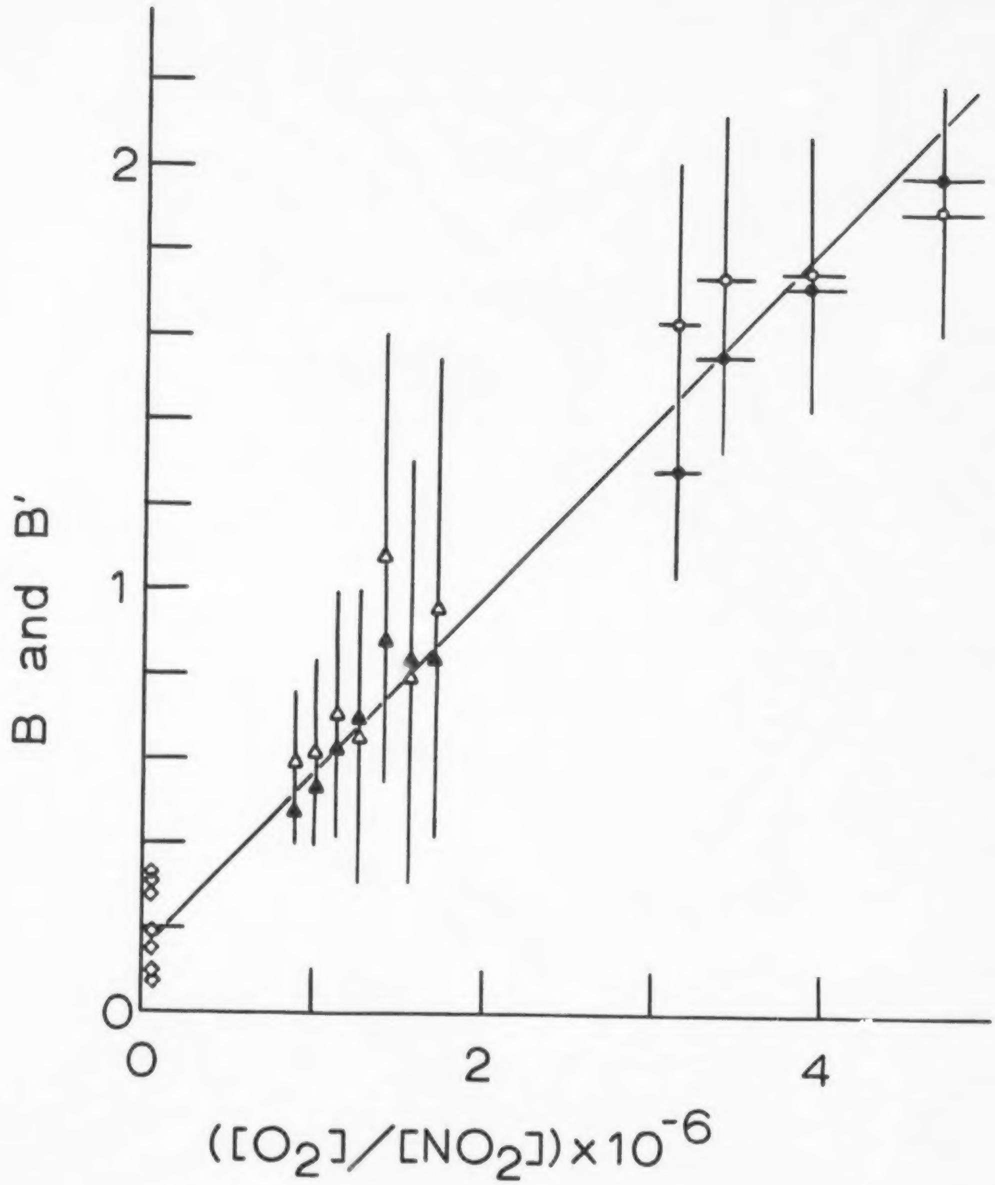

Figure 36. Plot of the function B of the text (open symbols) and B' (closed symbols) versus $[O_2]/[NO_2]$ ratio; data were derived from three dimethylnitrosamine photolyses in O_2-NO_2-containing mixtures); in theory the slope = k_2/k_{4a} and intercept = k_{4b}/k_{4a}.

TYPING GUIDE SHEET
BEGIN FIRST LINE OF TEXT HERE
CENTER OF PAGE
TOP OF IMAGE AREA
DROPPED HEAD; BEGIN SECTIONS HERE

Significance of These Results to Atmospheric Chemistry

Our results reported here have significant bearing on the possible formation of nitrosamines and nitramines in nitrogen oxide-hydrocarbon-amine-polluted atmospheres. The large reactivity difference for $(CH_3)_2N$ radicals with O_2 and NO or NO_2 which we observe here, suggests that $(CH_3)_2N$ radicals formed in the atmosphere may react to form $(CH_3)_2N\text{-}N{=}O$ and $(CH_3)_2N\text{-}NO_2$ at significant rates even when the NO and NO_2 concentrations are in the 10 pphm range commonly encountered in urban atmospheres. Furthermore the high reactivity of dimethyl amine with HO radicals[91] and the relatively high fractio fraction of the reaction that leads to dimethylamino radicals ($k_{1a}/(k_{1a} + k_{1b}) = 0.37 \pm 0.05$ derived in this work), ensure a rapid rate of $(CH_3)_2N$ radical generation in polluted atmospheres containing $(CH_3)_2NH$. If the reactivity of the $(CH_3)_2N$ radical with alkenes and alkanes follows that observed for the NH_2 radical,[101,102] then removal by reactions with hydrocarbon impurities in the polluted atmospheres will be unimportant. This result seems probable since photolyses of $Me_2N\text{-}N{=}O$(3-4 ppm) with added iso-C_4H_{10} (50 ppm) or Me_3SiH (6.4 ppm) show very little reaction of Me_2N radicals with the added species. Using our rate data, assuming a constant source of $(CH_3)_2NH$ and that the $[HO] = 1 \times 10^{-7}$ ppm, a lower limit to present experimental and theoretical estimates in the troposphere,[103] we anticipate that the steady-state level of $(CH_3)_2N\text{-}N{=}O$ which will be developed in a polluted, sunlight-irradiated atmosphere ($Z = 40°$) in about 43 min (τ 99%) should be described by relation (11):

$$[(CH_3)_2N\text{-}N{=}O]_{ss} = \frac{0.0298\ [Me_2NH]}{\frac{[NO_2]}{[NO]}\,4.6 + \frac{[O_2]}{[NO]}\,1.47 \times 10^{-6}} \qquad (11)$$

The most favorable condition for nitrosamine generation occurs at low $[NO_2]/[NO]$ ratios; a ratio less than 1 is not common except during the early morning hours. Taking $[NO_2]/[NO] = 1$ and $[NO] = 0.1$ ppm gives $[(CH_3)_2N\text{-}N{=}O]_{ss} = (4.0 \times 10^{-3})[Me_2NH]$. There are few analytical data available today which allow realistic estimates of the dimethylamine concentration in urban atmospheres. Up to 0.1 ppm of this compound has been observed in the undiluted exhaust of catalyst equipped automobiles which are operating with fuel-rich mixtures.[104] Rapid dilution of the exhaust gases may lead to maximum ambient levels of $(CH_3)_2NH$ which are < 0.1 ppb. Levels of the amine as high as 56 ppb, but more commonly < 2-11 ppb, have been detected in ambient air downwind from a dimethyl amine manufacturing plant.[105] Assuming a dimethyl amine concentration of 50, 2, and 0.1 ppb to represent these possible extremes which may be encountered in urban air, and taking $[NO] = [NO_2] = 0.1$ ppm, we calculate from relation (11) that the theoretical steady-state concentration of dimethylnitrosamine would be 200, 8, and 0.4 ppt, respectively. Bachmann and Cohen[105] found that dimethylnitrosamine concentrations were below the detection limits of their equipment in most measurements made in ambient air near a dimethylamine plant (<7 ng/m^3 or < 2 ppt). However NO and NO_2 levels were not established during these experiments and the air mass containing the amine was not followed downwind for the period required to develop the nitrosamine through the reactions outlined (about 43 min), so no direct comparison with the predictions of relation (11) are justified. Our results suggest that the maximum dimethylnitrosamine concentrations

BEGIN LAST LINE OF TEXT
BOTTOM OF IMAGE AREA; OUTSIDE DIMENSION FOR TABLES AND ILLUSTRATIONS
3/8"

PAGE NUMBER
EPA-287 (Cin.)
(4-76)

TYPING GUIDE SHEET

expected in ambient air should be below the detection limit of the most sensitive instrumentation now available provided that ambient concentrations of the dimethylamine are less than 0.1 ppb and the $[NO] \simeq [NO_2] \simeq 0.1$ ppm. One can conceive of special highly polluted conditions for which both atmospheric concentrations of amines and NO_x contaminants are very much higher where nitrosamine buildup would be significant; proper control strategy must be developed to protect against this condition.

The dimethylnitramine is not photochemically active within the wavelength range of sunlight available at the earth's surface, and as Pitts et al.[89,90] suggest, we expect this compound to be a major product of dimethylamine photooxidation in an NO_x-polluted atmosphere. Using the rate data from this study and assuming $[HO] = 1 \times 10^{-7}$ ppm, a constant source of dimethylamine, and $[(CH_3)_2N\text{-}N\text{=}O]$ at the steady-state value given by relation (11), we would predict that the rate of nitramine generation in sunlight ($Z = 40^\circ$) would be given approximately by relation (12):

$$\frac{d[(CH_3)_2N\text{-}NO_2]}{dt} = \frac{3.58 \times 10^{-3}\ \text{min}^{-1}\ [(CH_3)_2NH]}{3.9 \times 10^{-7}\dfrac{[O_2]}{[NO_2]} + 1.22} \tag{12}$$

Even at the moderate concentrations of NO_2 (0.1 ppm) the relation predicts a conversion rate of amine to nitramine of about 0.18% min^{-1}. Thus if dimethylamine is present in ambient polluted air at the 0.1 ppb level (approximate maximum expected from auto exhaust-polluted air), then after about 6 hours of sunlight irradiation (average $Z = 40^\circ$) about 65 ppt of the nitramine may develop. Since $(CH_3)_2N\text{-}NO_2$ has demonstrated carcinogenic activity in animals, these levels may be of concern.[106,107] Even higher rates of generation of the newly discovered product methylmethyleneamine ($CH_2\text{=}N\text{-}CH_3$) are expected although its buildup will be restricted by the rate of its destruction by HO radicals. We have found that O_3 attack on this species is slow, but the decay in $CH_2\text{=}N\text{-}CH_3$ seen at long times in our experiments (see Figure 34) appears to result from HO attack. In view of these findings an evaluation of the actual atmospheric levels of $(CH_3)_2N\text{-}NO_2$ and $CH_2\text{=}N\text{-}CH_3$, the major products of the dimethylamine photooxidation, and the potential for these compounds to induce cancer on inhalation by animals should be determined.

EPA-287 (Cin.)
(4-76)

TYPING GUIDE SHEET
BEGIN FIRST LINE OF TEXT HERE
CENTER OF PAGE
TOP OF IMAGE AREA
DROPPED HEAD: BEGIN SECTIONS HERE

REFERENCES

1. J.G. Calvert, W.H. Chan, E. Niple, R.J. Nordstrom, J.H. Shaw, W.R. Skinner, and W.M. Uselman, "Application of Fourier Transform Spectroscopy to Air Pollution Problems," Interim Report - 1976, U.S. E.P.A. Ecological Research Series EPA-60013-77-025 (1977).

2. Y.S. Chang, J.H. Shaw, E. Niple, J.G. Calvert, W.H. Chan, S. Levine, and W.M. Uselman, "Application of Fourier Transform Spectroscopy to Air Pollution Problems," Interim Report - 1977, U.S. E.P.A. Research and Development, EPA-60013-78-057 (1978).

3. R.J. Nordstrom, J.H. Shaw, W.R. Skinner, W.H. Chan, J.G. Calvert, and W.M. Uselman, "Application of Computer Simulated Infrared Solar Spectra to the Detection of Atmospheric Fluorocarbon-12," Appl. Spectro. 31, 224 (1977).

4. W. Skinner, "A Computer Program for Calculating Horizontal and Slant Path Infrared Spectrum Using the AFGL Line Listing," Interim Report to EPA under R 803868 (July, 1977).

5. L.S. Rothman and R.A. McClutchey, Appl. Opt. 15, 2616 (1976).

6. R.J. Nordstrom, W.R. Skinner, J.H. Shaw, W.H. Chan, J.G. Calvert, and W.M. Uselman, "Long Path Air Spectra," Appl. Opt. 16, 1477 (1977).

7. R.J. Nordstrom, J.H. Shaw, W.R. Skinner, J.G. Calvert, W.H. Chan, and W.M. Uselman, "A Comparison of High Resolution Observed and Computed Air Spectra between 700 and 2300 cm^{-1}," Interim Report to E.P.A. under R 803868 (August, 1976).

8. W.R. Skinner and R.J. Nordstrom, "Accuracy of the AFCRL Atmospheric Absorption Line Parameters Compilation in the 10-μm Atmospheric Window," Appl. Opt. 15, 2616 (1976).

9. R.J. Nordstrom, J.H. Shaw, W.R. Skinner, J.G. Calvert, W.H. Chan, and W.M. Uselman, "Application of Fourier Transform Spectroscopy to Air Pollution Problems," Interim Report - 1976, "Computer Generated Long-Path Air Spectra," U.S. E.P.A. Ecological Research Series EPA-60013-77-026 (March, 1977).

BEGIN LAST LINE OF TEXT
BOTTOM OF IMAGE AREA; OUTSIDE DIMENSION FOR TABLES AND ILLUSTRATIONS
3/8"

PAGE NUMBER
EPA-287 (Cin.)
(4-76)

10. W.H. Chan, W.M. Uselman, J.G. Calvert, and J.H. Shaw, "The Pressure Dependance of the Rate Constant for the Reaction: $HO + CO \rightarrow H + CO_2$," Chem. Phys. Lett. 45, 240 (1977).

11. S.Z. Levine, W.M. Uselman, W.H. Chan, J.G. Calvert, and J.H. Shaw, "The Kinetics and Mechanism of the HO_2-NO_2 Reactions; The Significance of Peroynitric Acid Formation in Photochemical Smog," Chem. Phys. Lett. 48, 528 (1977).

12. Y.S. Chang, J.H. Shaw, W.M. Uselman, and J.G. Calvert, "Use of the AFCRL Line Parameters Compilation to Test the Performance of an Infrared Spectrometer," Appl. Opt. 16, 2116-18 (1977).

13. Y.S. Chang, J.H. Shaw, J.G. Calvert, and W.M. Uselman, "Simultaneous Determination of the Ground Level Abundances of N_2O, CO_2, CO, and H_2O," JQSRT 18, 589 (1977).

14. A. Adel, Astrophys. J. 90, 627 (1939).

15. J.H. Shaw, G.B.B.M. Sutherland, and T.W. Wormall, Phys. Rev. 74, 978 (1948).

16. C.R. Cothern, "A Preliminary Analysis of N_2O Including a Materials Balance," EPA Report EPA 560/6-79-001 (1979).

17. E. Niple, Ph.D. Dissertation, The Ohio State University (1978).

18. E. Niple and J.H. Shaw, "Information Measures in Nonlinear Experimental Design," J. Phys, E. (submitted for publication).

19. E. Niple and J.H. Shaw, "Information in Spectra of Collision Broadened Lines", Appl. Spectros. (submitted for publication).

20. Y.S. Chang, J.H. Shaw, J.G. Calvert, and W.M. Uselman, "Retrieval of Pressure and Temperature of a Gas Sample by Analysis of its Absorption Spectrum," JQSRT 19, 103 (1978).

21. P.R. Griffiths, Appl. Spectros. 31, 497 (1977).

22. C.L. Lin, E. Niple, J.H. Shaw, and J.G. Calvert, "The Quantitative Analysis of Absorption Spectra," Appl. Spectros. 33, 481 (1979).

23. C.L. Lin, E. Niple, J.H. Shaw, and J.G. Calvert, "Retrieval of Information from an Absorption Spectrum," Appl. Spectros. 33, 487 (1979).

24. Y.S. Chang, J.H. Shaw, W.M. Uselman and J.G. Calvert, "Determination of Abundances of Gases from Solar Spectra," JQSRT 19, 599 (1978).

25. Y.S. Chang and J.H. Shaw, Appl. Spectros. 31, 213 (1977).

26. Y.S. Chang and J.H. Shaw, *Appl. Spectros.* *31*, 213 (1977).

27. C.L. Lin, W.M. Gutman, J.H. Shaw, W.M. Uselman, and J.G. Calvert, "Use of a Graphics Display Terminal to Analyze Spectral Data," *Appl. Opt.* *17*, 993 (1978).

28. C.L. Lin, E. Niple, and J.H. Shaw, "Line Parameters of HCl Obtained by Simultaneous Analysis of Spectra," *JQSRT* *20*, 581 (1978).

29. C.L. Lin and J.H. Shaw, "The Application of the IBM Library Program BMDP3R (Nonlinear Least Squares Fit) to Retrieving Parameters of Spectral Lives from Absorption Spectra," EPA Interim Report, January 1976.

30. C.L. Lin, J.H. Shaw, and J.G. Calvert, "Least Squares Analysis of Voigt-Shaped Lines," *JQSRT* *22*, 253 (1979).

31. C.L. Lin and J.H. Shaw, "The Application of the BMDP Programs BMDP3R and BMDPAR (Nonlinear Least Squares Fit) Double Precision Versions to Returning Parameters of Voigt Shaped Lines from Absorption Spectra," EPA Interim Report, November 1978.

32. C.L. Lin, J.H. Shaw, and J.G. Calvert, "Band Analysis by Spectral Curve Fitting," JQSRT (submitted for publication).

33. W.S. Benedict, R. Herman, and S. Silverman, *Astrophys. J.* *135*, 277 (1962).

34. R. Schwarz, "Uber die Peroxysalpetersaure," *Z. Anorg. Chem.* *256*, 3-9 (1948).

35. R. Simonaites and J. Heicklen, "Reactions of HO_2 with NO and NO_2 and of OH with NO," *J. Phys. Chem.* *80*, 1-7 (1976).

36. R. Simonaitis and J. Heicklen, "The Temperature Dependence of the Reactions of HO_2 with NO and NO_2," *Int. J. Chem. Kinet.* *10*, 67-87 (1978).

37. H. Niki, P.D. Maker, C.M. Savage, and L.P. Breitenbach, "Fourier Transform IR Spectroscopic Observation of Pernitric Acid Formed via $HO_2 + NO_2 \rightarrow HOONO_2$," *Chem. Phys. Lett.* *45*, 564-566 (1977).

38. B.W. Gay, Jr., R.C. Noonan, J.J. Bufalini, and P.L. Hanst, "Photochemical Synthesis of Peroxyacyl Nitrates in the Gas Phase via Chlorine-Aldehyde Reaction," *Environ. Sci. Technol.* *10*, 82-85 (1976).

39. H. Niki, P. Marker, C. Savage, and L. Breitenbach, "IR Fourier Transform Spectroscopic Studies of Atmospheric Reactions," Paper N-2, Extended Abstracts of 12th Informal Conference on Photochemistry, June 28, 1976, N.B.S., Gaithersburg, Md.

40. P.L. Hanst and B.W. Gay, Jr., "Photochemical Reactions Among Formaldehyde, Chlorine, and Nitrogen Dioxide in Air," *Environ. Sci. Technol.* *11*, 1105-1109 (1977).

BEGIN FIRST LINE OF TEXT HERE
TYPING GUIDE SHEET
CENTER OF PAGE
TOP OF IMAGE AREA
DROPPED HEAD; BEGIN SECTIONS HERE

41. S.Z. Levine, W.M. Uselman, W.H. Chan, J.G. Calvert, and J.H. Shaw, "The Kinetics and Mechanism of the HO_2-NO_2 Reactions; The Significance of Peroxynitric Acid Formation in Photochemical Smog," *Chem. Phys. Lett.* *48*, 528-535 (1977).

42. R.A. Cox and R.G. Derwent, "Significance of Peroxynitric Acid in Atmospheric Chemistry of Nitrogen Oxides," *Nature* *270*, 328-329 (1977).

43. R.A. Graham, A.M. Winer, and J.N. Pitts, Jr., "Temperature Dependence of the Unimolecular Decomposition of Pernitric Acid and Its Atmospheric Implications," *Chem. Phys. Lett.* *51*, 215-220 (1977).

44. C.J. Howard, "Kinetics of the Reaction of HO_2 with NO_2," J. Chem. Phys., in press (1978).

45. J.P. Jesson, L.C. Glasgow, D.L. Filkin, and C. Miller, "The Stratospheric Abundance of Peroxynitric Acid," *Geophys. Res. Lett.* *4*, 513-516 (1977).

46. R.A. Cox and R.G. Derwent, "Kinetics of the Chlorine-Photosensitized Oxidation of Hydrogen at 1 Atmosphere Pressure, 306 K," *J. Chem. Soc. Faraday Trans. I* *73*, 272-283 (1977).

47. P.L. Hanst, "Spectroscopic Methods for Air Pollution Measurement," *Adv. Environ. Sci. Technol.* *2*, 91-213 (1971).

48. L.T. Molina and M.J. Molina, "Ultraviolet Absorption Spectrum of Chlorine Nitrite, ClONO," *Geophys. Res. Lett.* *4*, 83-86 (1977).

49. J.N. Pitts, Jr., J.M. McAfee, W.D. Long, A.M. Winer, "Long-Path Infrared Spectroscopic Investigation at Ambient Concentrations of the 2% Neutral Buffered Potassium Iodide Method for Determination of Ozone," *Environ. Sci. Technol.* *10*, 787-793 (1976).

50. A.C. Baldwin, J.R. Barker, D.M. Golden, and D.G. Hendry, "Photochemical Smog; Rate Parameter Estimates and Computer Simulations," *J. Phys. Chem.* *81*, 2483-2492 (1977).

51. D.J. Benton and P. Moore, "Kinetics and Mechanism of the Formation and Decay of Peroxynitrous Acid in Perchloric Acid Solutions," *J. Chem. Soc. A* 3179-3182 (1970).

52. R.A. Cox, S.A. Penkett, R.G. Derwent, A.E.J. Eggleton, J.G. Calvert, and K.A. Brice, "The Mechanism of the HO_2-NO Reaction," paper in preparation.

53. R.A. Graham, A.M. Winer, and J.N. Pitts, Jr., "Pressure and Temperature Dependence of the Unimolecular Decomposition of HO_2NO_2," *J. Chem. Phys.* (submitted for publication).

BOTTOM OF IMAGE AREA; OUTSIDE DIMENSION FOR TABLES AND ILLUSTRATIONS
BEGIN LAST LINE OF TEXT

EPA-287 (Cin.)
(4-76)

BEGIN FIRST LINE OF TEXT HERE
TYPING GUIDE SHEET
CENTER OF PAGE
TOP OF IMAGE AREA
DROPPED HEAD BEGIN SECTIONS HERE

54. D.G. Hendry and R.A. Kenley, "Importance of Organic Peroxynitrates in Photochemical Smog," Division of Environmental Chemistry, Preprints of papers presented at the 175th National Meeting of the American Chemical Society, Anaheim, Calif., March 1978, p. 292.

55. E.W. Kaiser and C.H. Wu, "Measurement of the Rate Constant of the Reaction of Nitrous Acid with Nitric Acid," *J. Phys. Chem.* *81*, 187-190 (1977).

56. J.W. Bottenheim, O.P. Strausz, and J.G. Calvert, "Evaluation of Major Homogeneous Oxidation Steps of SO_2 in the Alberta Troposphere and Computer Simulation of the Homogeneous Oxidation of SO_2 in an Urban Polluted Air Parcel," Proceedings of Alberta Sulfur Gas Research Workshop III, Nov. 17-18, 1977, Edited by H.S. Sandhu and M. Nyborg, Research Secretariat, Alberta Environment, Edmonton, Alberta, p. 52.

57. J.N. Pitts, Jr., B.J. Finlayson-Pitts, and A.M. Winer, "Optical Systems Unravel Smog Chemistry," *Environ. Sci. Technol.* *11*, 568-572 (1977).

58. D.D. Davis, W. Braun, and A.M. Bass, "Reactions of $Cl^2P_{3/2}$: Absolute Rate Constants for Reaction with H_2, CH_4, C_2H_6, CH_2Cl_2, C_2Cl_4, and *c*-C_6H_{12}," *Int. J. Chem. Kinet.* *2*, 101-114 (1970).

59. R.F. Hampson, Jr., and D. Garvin, "Chemical Kinetic and Photochemical Data for Modelling Atmospheric Chemistry," N.B.S. Technical Note 866 (1975).

60. R.D. Hudson, Editor, "Chlorofluoromethanes and the Stratosphere," NASA Ref. Publication 1010, Scientific and Technical Information Office, Greenbelt, Maryland, (1977).

61. R.A. Cox, R.G. Derwent, and P.M. Holt, "Relative Rate Constants for the Reactions of OH Radicals with H_2, CH_4, CO, NO, and HONO at Atmospheric Pressure and 296 K," *J. Chem. Soc. Faraday Trans. I* *72*, 2031-2043 (1976).

62. R. Simonaitis and J. Heicklen, "Reactions of HO_2 with NO and NO_2," *J. Phys. Chem.* *78*, 653-657 (1974).

63. R.A. Cox and R.G. Derwent, "Kinetics of the Reaction of HO_2 with Nitric Oxide and Nitrogen Dioxide," *J. Photochem.* *4*, 139-153 (1975).

64. C.J. Howard and K.M. Evenson, "Kinetics of the Reaction of HO_2 with NO," *Geophys. Res. Lett.* *4*, 437-440 (1977).

65. W.H. Chan, R.J. Nordstrom, J.G. Calvert, and J.H. Shaw, "Kinetic Study of HONO Formation and Decay Reactions in Gaseous Mixtures of HONO, NO, NO_2, H_2O, and N_2," *Environ. Sci. Technol.* *10*, 674-682 (1976).

66. E.W. Kaiser and C.H. Wu, "A Kinetic Study of the Gas Phase Formation and Decomposition Reactions of Nitrous Acid," J. Phys. Chem. 81, 1701-1706 (1977).

BOTTOM OF IMAGE AREA, OUTSIDE DIMENSION FOR TABLES AND ILLUSTRATIONS
BEGIN LAST LINE OF TEXT
3/8"
PAGE NUMBER

EPA-287 (Cin.)
(4-76)

BEGIN FIRST LINE OF TEXT HERE
TYPING GUIDE SHEET
CENTER OF PAGE
TOP OF IMAGE AREA
DROPPED HEAD; BEGIN SECTIONS HERE

67. M.T. Leu and W.B. deMore, "Rate Constant for the Reaction: $ClO + NO \rightarrow Cl + NO_2$," Abstracts 13th Informal Conference on Photochemistry, paper L5, Clearwater Beach, Florida, January 1978.

68. W.H. Chan, W.M. Uselman, J.G. Calvert, and J.H. Shaw, "The Pressure Dependence of the Rate Constant for the Reaction: $HO + CO \rightarrow H + CO_2$," *Chem. Phys. Lett.* *45*, 240-244 (1977).

69. M.J. Molina and F.S. Rowland, *Nature* *249*, 810 (1974).

70. "Chlorofluoromethanes and the Stratosphere," R.D. Hudson, Editor, NASA Reference Publication 1010, Washington D.C. (1977).

71. F.S. Rowland and M.J. Molina, *Rev. Geophys. Space Phys.* *13*, 1 (1975).

72. S.S. Prasad, *Planet. Space Sci.* *24*, 1187 (1976).

73. G. Hirsch, P.J. Bruna, S.D. Peyerimhoff, and R.J. Buenker, *Chem. Phys. Lett.* *52*, 442 (1977).

74a. R.L. Jaffe and S.R. Langhoff, papers presented at the 32nd Symposium on Molecular Spectroscopy, Columbus, Ohio, June 1977.

74b. R.L. Jaffe and S.R. Langhoff, *J. Chem. Phys.* *68*, 1638 (1978).

74c. S.S. Prasad, R.L. Jaffe, R.C. Whitten and R.P. Turco, *Planet. Space* Sci. (in press).

75. R. Stimpfle, R.A. Perry, and C.J. Howard, "Laser Magnetic Resonance Spect Spectrum of ClO and the Kinetics of the Reaction $ClO + NO_2 + M \rightarrow ClONO_2 + M$," paper 35 at the 4th Biennial Rocky Mountain Regional Meeting, Amer. Chem. Soc., Boulder, Colorado, June 5-7, 1978; $k_1 = (4.5 \pm 1.5) \times 10^{-12}$ cc molec^{-1}sec^{-1} was reported here.

76. J.W. Birks, T.J. Leck, and B. Shoemaker, "Formation of HOCl in the Stratosphere," paper 36, 4th Biennial Rocky Mountain Regional Meeting, Amer. Chem. Soc., Boulder, Colorado, June 5-7, 1978; $k_1 = (3.1 \pm 0.5) \times 10^{-12}$ cc molec^{-1}sec^{-1} was reported here.

77. B. Reimann and F. Kaufman, *J. Chem. Phys.* *69*, 2925 (1978); $k_1 = (3.8 \pm 0.1) \times 10^{-12}$ cc molec^{-1}sec^{-1} was reported here.

78. L.T. Molina and M.J. Molina, "The Ultraviolet Spectrum of HOCl," *J. Phys. Chem.* (in press).

79. P.L. Hanst, *Adv. Environ. Sci. Technol.* *2*, 91 (1971).

80. W.M. Uselman, S.Z. Levine, W.H. Chan, J.G. Calvert, and J.H. Shaw, in "Nitrogenous Air Pollutants," Editor D. Grosjean, Ann Arbor Science Publishers (in press) (1978).

BEGIN LAST LINE OF TEXT
BOTTOM OF IMAGE AREA; OUTSIDE DIMENSION FOR TABLES AND ILLUSTRATIONS
6-1/2"
9-1/8"
3/8"

PAGE NUMBER
EPA-287 (Cin.)
(4-76)

BEGIN FIRST LINE OF TEXT HERE
TYPING GUIDE SHEET
CENTER OF PAGE
TOP OF IMAGE AREA
DROPPED HEAD; BEGIN SECTIONS HERE

81. R.T. Watson, *J. Phys. Chem. Ref. Data* *6*, 871 (1977).

82. R.F. Hampson, Jr., and D. Garvin, "Reaction Rate and Photochemical Data for Atmospheric Chemistry-1977," N.B.S. Special Publication 513, (May 1978).

83a. T.T. Paukert and H.S. Johnston, *J. Chem. Phys.* *56*, 2824 (1972).

83b. E.J. Hamilton, Jr., and R.-R. Lii, *Int. J. Chem. Kinet.* *9*, 875 (1977).

83c. S.N. Foner and R.L. Hudson, *Adv. Chem. Ser.* *36*, 34 (1962).

84a. P.D. Maker, H. Niki, C.M. Savage, and L.P. Breitenbach, paper 80 in the Symposium on Infrared Fourier Transform Spectroscopic Studies of Atmospheric and Interstellar Species, Phys. Div., Amer. Chem. Soc. 176th National Meeting, Miami, Florida, September 1978.

84b. P.D. Maker, private communication.

85. R.L. Jaffe, private communication.

86. U.S. Environmental Protection Agency, Scientific and Technical Assessment Report on Nitrosamines, Report No. EPA-600/6-77-001 (November 1976).

87. P.L. Hanst, J.W. Spence, and M. Miller, *Environ. Sci. Technol.* *11*, 403 (1977).

88. W.A. Glasson, private communication.

89. J.N. Pitts, Jr., D. Grosjean, K. VanCauwenberghe, J.P. Schmid, and D.R. Fitz, *Environ. Sci. Technol.* *12*, 946 (1978).

90. E.C. Tuazon, A.M. Winer, R.A. Graham, J.P. Schmid, and J.N. Pitts, Jr., *Environ. Sci. Technol.* *12*, 954 (1978).

91. R. Atkinson, R.A. Perry, and J.N. Pitts, Jr., *J. Chem. Phys.* *68*, 1850 (1978).

92. S.Z. Levine, W.M. Uselman, W.H. Chan, J.G. Calvert, and J.H. Shaw, *Chem. Phys. Lett.* *48*, 528 (1977).

93. W.M. Uselman, S.Z. Levine, W.H. Chan, J.G. Calvert, and J.H. Shaw, in *Nitrogenous Air Pollutants*, ed. D. Grosjean, Ann Arbor Science Publishers, Inc., (1979) p 17.

94. C.R.C. Lindley, "The Kinetics of Dimethylamino-radical Reactions in Simulated Atmospheres: the Formation of Dimethylnitrosamine and Dimethylnitramine," Ph.D. Thesis, The Ohio State University (1978).

BEGIN LAST LINE OF TEXT
BOTTOM OF IMAGE AREA, OUTSIDE DIMENSION FOR TABLES AND ILLUSTRATIONS
3/8"

EPA-287 (Cin.)
(4-76)

TYPING GUIDE SHEET
BEGIN FIRST LINE OF TEXT HERE
CENTER OF PAGE
TOP OF IMAGE AREA
DROPPED HEAD, BEGIN SECTIONS HERE

95. B.G. Gowenlock and K.E. Thomas, *J. Chem. Soc. B*, 409 (1966).

96. R. Lesclaux, P.V. Khe, J.C. Soulignac, and J. Joussot-Dubien, VIII International Conference Photochemistry, Edmonton, Canada, August 1975.

97. R. Lesclaux and M. Demissy, *Nouveau J. de Chimie* *1*, 443 (1977).

98. R. Lesclaux, P.V. Khe, P. Dezauzier, and J.C. Soulignac, *Chem. Phys. Lett.* *35*, 493 (1975).

99. R.F. Hampson, Jr., and D. Garvin, "Chemical kinetic and photochemical data for modeling atmospheric chemistry," U.S. National Bureau Standards Note 866 (1975).

100. S.W. Benson, Thermochemical Kinetics, 2nd Ed., John Wiley, N.Y. (1976).

101. R. Lesclaux, J.C. Soulignac, and P.V. Khe, *Chem. Phys. Lett.* *43*, 520 (1976).

102. R. Lesclaux and M. Demissy, *J. Photochem.* *9*, 110 (1978).

103. J.G. Calvert, *Environ. Sci. Technol.* *10*, 256 (1976).

104. The 1977 annual report of General Motors Company on advanced emission control systems development progress, Vol. II, 4K, p. 15-29 (obtained from the U.S. Environmental Protection Agency).

105. J.D. Bachmann and J.B. Cohen, "*In situ* investigation of atmospheric nitrosamine formation," Abstracts, 175th American Chemical Society Meeting, Anaheim, Calif., March, 1978, p. 443.

106. C.M. Goodall and T.H. Kennedy, *Cancer Lett.* *1*, 295 (1976).

107. H. Druckrey, R. Preussmann, D. Schmahl, and M. Muller, *Naturwissenschaften* *48*, 134 (1961).

BEGIN LAST LINE OF TEXT
BOTTOM OF IMAGE AREA, OUTSIDE DIMENSION FOR TABLES AND ILLUSTRATIONS
3/8"

EPA-287 (Cin.)
(4-76)

TYPING GUIDE SHEET

BEGIN FIRST LINE OF TEXT HERE

CENTER OF PAGE

TOP OF IMAGE AREA

DROPPED HEAD; BEGIN SECTIONS HERE

6-1/2"

APPENDIX A

9-1/8"

BEGIN LAST LINE OF TEXT

BOTTOM OF IMAGE AREA; OUTSIDE DIMENSION FOR TABLES AND ILLUSTRATIONS

3/8"

PAGE NUMBER

EPA-287 (Cin.)
(4-76)

BEGIN FIRST LINE OF TEXT HERE
TYPING GUIDE SHEET
CENTER OF PAGE
TOP OF IMAGE AREA
DROPPED HEAD; BEGIN SECTIONS HERE

1. J.G. Calvert, W.H. Chan, E. Niple, R.J. Nordstrom, J.H. Shaw, W.R. Skinner, and W.M. Uselman, "Application of Fourier Transform Spectroscopy to Air Pollution Problems," Interim Report - 1976, U.S. E.P.A. Ecological Research Series EPA-60013-77-025 (1977).

2. Y.S. Chang, J.H. Shaw, E. Niple, J.G. Calvert, W.H. Chan, S.Z. Levine, and W.M. Uselman, "Application of Fourier Transform Spectroscopy to Air Pollution Problems," Interim Report - 1977, U.S. E.P.A. Research and Development, EPA-60013-78-057 (1978).

3. R.J. Nordstrom, J.H. Shaw, W.R. Skinner, J.G. Calvert, W.H. Chan, and W.M. Uselman, "Application of Fourier Transform Spectroscopy to Air Pollution Problems," Interim Report - 1976, Ecological Research Series EPA-60013-77-026 (1977).

4. R.J. Nordstrom, J.H. Shaw, W.R. Skinner, J.G. Calvert, W.H. Chan, and W.M. Uselman, "A Comparison of High Resolution Observed and Computed Air Spectra Between 700 and 2300 cm^{-1}," August 1976.

5. W. Skinner, "A Computer Program for Calculating Horizontal and Slant Path Infrared Spectra Using the AFGL Line Listing," July 1977.

6. C.L. Lin and J.H. Shaw, "The Application of the IBM Library Program BMDP3R (Nonlinear Least-Squares Fit) to Retrieving Parameters of Spectral Lines from Absorption Spectra," January 1976.

7. C.L. Lin and J.H. Shaw, "The Application of the BMDP Programs BMDP3R and BMDPAR (Nonlinear Least-Squares Fit) Double Precision Versions to Retrieving Parameters of Voigt Shaped Lines from Absorption Spectra," November 1978.

BEGIN LAST LINE OF TEXT
BOTTOM OF IMAGE AREA; OUTSIDE DIMENSION FOR TABLES AND ILLUSTRATIONS
3/8"

EPA-287 (Cin.)
(4-76)

TYPING GUIDE SHEET
BEGIN FIRST LINE OF TEXT HERE
CENTER OF PAGE
TOP OF IMAGE AREA
DROPPED HEAD; BEGIN SECTIONS HERE
6-1/2''
9-1/8''
BEGIN LAST LINE OF TEXT
BOTTOM OF IMAGE AREA; OUTSIDE DIMENSION FOR TABLES AND ILLUSTRATIONS
3/8''
PAGE NUMBER
EPA-287 (Cin.)
(4-76)

APPENDIX B

BEGIN FIRST LINE OF TEXT HERE
TYPING GUIDE SHEET
CENTER OF PAGE
TOP OF IMAGE AREA
DROPPED HEAD; BEGIN SECTIONS HERE

1. W.H. Chan, R.J. Nordstrom, J.G. Calvert, and J.H. Shaw, "An IFRTS Spectroscopic Study of the Kinetics and the Mechanism of the Reactions in the Gaseous System, HONO, NO, NO_2, H_2O," *Chem. Phys. Lett. 37*, 441-446 (1976).

2. W.H. Chan, R.J. Nordstrom, J.G. Calvert, and J.H. Shaw, "A Kinetics Study of HONO Formation and Decay Reactions in Gaseous Mixtures of HONO, NO_2, NO, H_2O, and N_2," *Envir. Sci. and Techn. 10*, 674 (1976).

3. R.J. Nordstrom, J.H. Shaw, W.R. Skinner, W.H. Chan, J.G. Calvert, and W.M. Uselman, "Application of Computer Simulated Infrared Solar Spectra to the Detection of Atmospheric Fluorocarbon-12," *App. Spectros. 31*, 224-29 (1977).

4. Y.S. Chang and J.H. Shaw, "A Non-Linear Least-Squares Method of Determining Line Intensities and Half Widths," App. Spectros. 31, 213-220 (1977).

5. W.H. Chan, W.M. Uselman, J.G. Calvert, and J.H. Shaw, "The Pressure Dependence of the Rate Constant for the Reaction: $HO + CO \rightarrow H + CO_2$," *Chem. Phys. Lett. 45*, 240-244 (1977).

6. R.J. Nordstrom and W.H. Chan, "A Spectroscopic Study of the NO_2-N_2O_4 System by the Infrared Absorption Technique," *J. Phys. Chem. 80*, 847-850 (1976).

7. W.R. Skinner and R.J. Nordstrom, "Accuracy of the AFCRL Atmospheric Absorption Line Parameters Compilation in the 10-μm Atmospheric Window," *App. Opt. 15*, 2616 (1976).

8. Y.S. Chang, J.H. Shaw, J.G. Calvert and W.M. Uselman, "Simultaneous Determination of the Ground Level Abundances of N_2O, CO_2, CO and H_2O," *JQSRT 18*, 589 (1977).

9. Y.S. Chang, J.H. Shaw, J.G. Calvert and W.M. Uselman, "Retrieval of Pressure and Temperature of a Gas Sample by Analysis of its Absorption Spectrum," *JQSRT 19*, 103 (1978).

10. Y.S. Chang, J.H. Shaw, W.M. Uselman, and J.G. Calvert, "Use of the AFCRL Line Parameters Compilation to Test the Performance of an Infrared Spectrometer," *App. Opt. 16*, 2116-18 (1977).

11. Y.S. Chang and J.H. Shaw, "Intensities and Widths of H_2O Lines Between 1800 and 2100 cm^{-1}," *JQSRT 18*, 491 (1977).

12. R.J. Nordstrom, W.R. Skinner, J.H. Shaw, W.H. Chan, J.G. Calvert, and W.M. Uselman, "Long Air Path Spectra," *Appl. Opt. 16*, 1477-8 (1977).

13. Y.S. Chang, J.H. Shaw, W.M. Uselman and J.G. Calvert, "Determination of Abundances of Gases from Solar Spectra," *JQRST* 19, 599 (1978).

BEGIN LAST LINE OF TEXT
BOTTOM OF IMAGE AREA; OUTSIDE DIMENSION FOR TABLES AND ILLUSTRATIONS
3/8"

EPA-287 (Cin.)
(4-76)

TYPING GUIDE SHEET
BEGIN FIRST LINE OF TEXT HERE
CENTER OF PAGE
TOP OF IMAGE AREA
DROPPED HEAD; BEGIN SECTIONS HERE

14. C.L. Lin, W.M. Gutman, J.H. Shaw, W.M. Uselman, and J.G. Calvert, "Use of a Graphics Display Terminal to Analyze Spectral Data," App. Opt. 17, 993 (1978).

15. C.L. Lin, E. Niple, and J.H. Shaw, "Line Parameters of HCl Obtained by Simultaneous Analysis of Spectra," JQSRT 20, 581 (1978).

16. W.M. Uselman, S.Z. Levine, W.H. Chan, J.G. Calvert, and J.H. Shaw, "The Kinetics of the Decay of Gaseous Peroxynitric Acid," Chem. Phys. Lett. 58, 437 (1978).

17. F. Su, J.G. Calvert, C.R. Lindley, W.M. Uselman, and J.H. Shaw, "An FTS-IR Kinetic Study of HOCl and its Absolute Integrated IR Band Intensity," J. Phys. Chem. 83, 912 (1979).

18. C.L. Lin, J.H. Shaw, and J.G. Calvert, "Least-Squares Analysis of Voigt-Shaped Lines," JQSRT (accepted).

19. C.L. Lin, E. Niple, J.H. Shaw, and J.G. Calvert, "Retrieval of Information from an Absorption Spectrum," App. Spectros. (accepted).

20. C.L. Lin, E. Niple, J.H. Shaw, and J.G. Calvert, "The Quantitative Analysis of Absorption Spectra," App. Spectros. (submitted).

21. S.Z. Levine, W.M. Uselman, W.H. Chan, J.G. Calvert, and J.H. Shaw, "The Kinetics and Mechanism of the HO_2-NO_2 Reactions; The Significance of Peroynitric Acid Formation in Photochemical Smog," Chem. Phys. Lett. 48, 528 (1977).

22. W.M. Uselman, S.Z. Levine, W.H. Chan, J.G. Calvert and J.H. Shaw, "A Kinetic Study of the Mechanism of Peroxynitric Acid Formation in Irradiated Mixtures of Chlorine, Hydrogen, Nitrogen Dioxide, and Nitric Acid in Air," in "Nitrogenous Air Pollutants; Chemical and Biological Implications," ed., D. Grosjean, Ann Arbor Science Publishers Inc., (1979).

23. C.L. Lin, J.H. Shaw, and J.G. Calvert, "Band Analysis by Spectral Curve Fitting," JQSRT (submitted).

24. E. Niple, and J.H. Shaw, "Information in Spectra of Collision Broadened Lines," App. Spectros. (submitted).

25. F. Su, J.G. Calvert, J.H. Shaw, H. NIKI, P.D. Maker, C.M. Savage, and R.D. Breitenbach, "Spectroscopic and Kinetic Studies of a New Metastable Species in the Photooxidation of Gaseous Formaldehyde," Chem. Phys. Lett. (accepted)

26. E. Niple and J.H. Shaw, "Information Measures in Nonlinear Design," J. Phys. E. (submitted).

BEGIN LAST LINE OF TEXT
BOTTOM OF IMAGE AREA; OUTSIDE DIMENSION FOR TABLES AND ILLUSTRATIONS
3/8"
PAGE NUMBER

EPA-287 (Cin.)
(4-76)

TYPING GUIDE SHEET
BEGIN FIRST LINE OF TEXT HERE
CENTER OF PAGE
TOP OF IMAGE AREA
DROPPED HEAD; BEGIN SECTIONS HERE
6-1/2"
9-1/8"
BEGIN LAST LINE OF TEXT
BOTTOM OF IMAGE AREA; OUTSIDE DIMENSION FOR TABLES AND ILLUSTRATIONS
3/8"
PAGE NUMBER
EPA-287 (Cin.)
(4-76)

27. C.R. Lindley, J.G. Calvert, and J.H. Shaw, "Rate Studies of the Reactions of the $(CH_3)_2N$ Radical with O_2, NO, and NO_2," *Chem. Phys. Lett.* (submitted).

BEGIN FIRST LINE OF TEXT HERE
TYPING GUIDE SHEET
CENTER OF PAGE
TOP OF IMAGE AREA
DROPPED HEAD: BEGIN SECTIONS HERE
6-1/2''
9-1/8''

APPENDIX C

BEGIN LAST LINE OF TEXT
BOTTOM OF IMAGE AREA: OUTSIDE DIMENSION FOR TABLES AND ILLUSTRATIONS
3/8''

PAGE NUMBER
EPA-287 (Cin.)
(4-76)

BEGIN FIRST LINE OF TEXT HERE
TYPING GUIDE SHEET
CENTER OF PAGE
TOP OF IMAGE AREA
DROPPED HEAD; BEGIN SECTIONS HERE

1. R.J. Nordstrom, W.R. Skinner, J.H. Shaw, W.H. Chan, W.M. Uselman, and J.G. Calvert, "Infrared Spectroscopic Detection of Fluorocarbon 12 in the Atmosphere," Molecular Spectroscopy Symposium, OSU, June 1976.

2. R.J. Nordstrom, W.R. Skinner, J.H. Shaw, W.H. Chan, W.M. Uselman, and J.G. Calvert, "Comparison of Measured and Computed Spectra of Air Samples," Molecular Spectroscopy Symposium, OSU, June 1976.

3. J.H. Shaw, "Detection and Photochemistry of Selected Air Pollutants Using FT-IR Techniques," Coblentz Society Symposium, Pittsburgh Conference on Analytical Chemistry and Applied Spectroscopy, Cleveland, Ohio, March 1977.

4. Y.S. Chang, J.H. Shaw, J.G. Calvert, and W.M. Uselman, "Computer Assisted Techniques of Analyzing Spectra," Molecular Spectroscopy Symposium, OSU, June 1977.

5. J.H. Shaw, Y.S. Chang, J.G. Calvert and W.M. Uselman, "Investigations of Atmospheric Spectra," International Conference on Fourier Transform Spectroscopy, University of South Carolina, June 1977.

6. J.H. Shaw and J.G. Calvert, "FT-IR Studies of Pollutants and Photochemical Reactions," Ohio Vibrational Spectroscopists Annual Meeting, May 1976.

7. J.H. Shaw and Y.S. Chang, "Least-Squares Analysis of Spectral Data," Ohio Vibrational Spectroscopists Meeting, May 1977.

8. Y.S. Chang, J.H. Shaw, W.M. Uselman, and J.G. Calvert, "Nonlinear Analysis of Spectral Data," Opt. Soc. Amer. Ann. Meeting, Toronto, Canada, October 1977.

9. C.L. Lin and J.H. Shaw, "Line Parameters Determined by Spectral Curve Fitting," Opt. Soc. Amer. Ann. Meeting, Toronto, Canada, October 1977.

10. W.M. Uselman, J.G. Calvert, J.H. Shaw and S.Z. Levine, "Peroxynitric Acid Kinetics and HO_2 Reactions," Amer. Chem. Soc. Meeting, Anaheim, Calif., March 1978.

11. J.H. Shaw, C.L. Lin, E.R. Niple, W.M. Uselman, and J.G. Calvert, "Least-Squares Spectral Analysis," Molecular Spectroscopy Symposium, OSU, June 1978.

12. E.R. Niple, J.H. Shaw, and C.L. Lin, "On the Reliability of Line Parameters Obtained by Least Squares Analysis of Spectra," Molecular Spectroscopy Symposium, OSU, June 1978.

13. J.G. Calvert, W.M. Uselman, C.R. Lindley, F. Su, and J.H. Shaw, "The Use of Long-Path FT-IR Spectroscopy in Kinetic Studies of Gaseous Reactions of Atmospheric Interest," Amer. Chem. Soc. Meeting, Miami, Florida, September 1978.

BEGIN LAST LINE OF TEXT
BOTTOM OF IMAGE AREA; OUTSIDE DIMENSION FOR TABLES AND ILLUSTRATIONS
3/8"
PAGE NUMBER
EPA-287 (Cin.)
(4-76)

TYPING GUIDE SHEET

14. E. Niple, J.H. Shaw, and C.L. Lin, "Optimization of Experiments to Determine Parameters of Single Lines," Topical Meeting on Atmospheric Spectroscopy cosponsored by Opt. Soc. Amer. and Amer. Met. Soc., Colorado, August 1978.

15. J.H. Shaw, "Spectra and Information Content," Amer. Chem. Soc. Meeting, Miami, Florida, September 1978.

16. Symposium on Molecular Spectroscopy, OSU, June 1979.

    E. Niple and J.H. Shaw, "Spectral Analysis I: Experimental Design."

    M. Hoke, R. Hawkins and J.H. Shaw, "Spectral Analysis II: Smoothing and Interpolation of Spectral Data."

    C.L. Lin and J.H. Shaw, "Spectral Analysis III: Voigt Shaped Lines."

    J.H. Shaw and C.L. Lin, "Spectral Analysis IV: Whole Band Analysis of Rotation Bands of Diatomic Gases."

    R. Hawkins, M. Hoke, and J.H. Shaw, "Spectral Analysis V: Whole Band Analysis of Rotation Bands of Linear Molecules - N_2O."

17. W.H. Chan, R.J. Nordstrom, J.G. Calvert, and J.H. Shaw, "An IRFTS Spectroscopic Study of the Kinetics and the Mechanism of the Reactions in the Gaseous System, HONO, NO, NO_2, H_2O," Centennial ACS Meeting, New York City, April 1976.

18. W.H. Chan, C.W. Mathews, and R.J. Nordstrom, "A Partial Analysis of HONO Bands Between 750 and 1300 cm^{-1}," 31st Symposium of Molecular Structure and Spectroscopy, Columbus, Ohio, June 1976.

EPA-287 (Cin.)
(4-76)